University of Alberta

Excited-State Charge-Transfer Dynamics of Azurin From Resonance Raman Spectroscopy

By

Mark Adam Webb

A thesis submitted to the Faculty of Graduate Studies and Research in partial fulfillment of the requirements for the degree of Doctor of Philosophy.

Department of Chemistry
Edmonton, Alberta
Fall 2000

National Library of Canada

Acquisitions and Bibliographic Services

395 Wellington Street
Ottawa ON K1A 0N4
Canada

Bibliothèque nationale du Canada

Acquisitions et services bibliographiques

395, rue Wellington
Ottawa ON K1A 0N4
Canada

Your file Votre référence

Our file Notre référence

The author has granted a non-exclusive licence allowing the National Library of Canada to reproduce, loan, distribute or sell copies of this thesis in microform, paper or electronic formats.

L'auteur a accordé une licence non exclusive permettant à la Bibliothèque nationale du Canada de reproduire, prêter, distribuer ou vendre des copies de cette thèse sous la forme de microfiche/film, de reproduction sur papier ou sur format électronique.

The author retains ownership of the copyright in this thesis. Neither the thesis nor substantial extracts from it may be printed or otherwise reproduced without the author's permission.

L'auteur conserve la propriété du droit d'auteur qui protège cette thèse. Ni la thèse ni des extraits substantiels de celle-ci ne doivent être imprimés ou autrement reproduits sans son autorisation.

0-612-59696-6

Canada

University of Alberta

Library Release Form

Name of Author: Mark Adam Webb

Title of Thesis: Excited-State Charge-Transfer Dynamics of Azurin From Resonance Raman Spectroscopy

Degree: Doctor of Philosophy

Year this Degree Granted: 2000

Permission is hereby granted to the University of Alberta Library to reproduce single copies of this thesis and to lend or sell such copies for private, scholarly or scientific purposes only.

The author reserves all other publication and other rights in association with the copyright in the thesis, and except as herein provided, neither the thesis nor any substantial portion thereof may be printed or otherwise reproduced in any material form whatever without the author's prior written permission.

Adam Webb

Mark Adam Webb
5018 43 St
Stettler, Alberta
T0C 2L2

Date: July 6, 2000

University of Alberta

Faculty of Graduate Studies and Research

The undersigned certify that they have read, and recommend to the Faculty of Graduate Studies and Research for acceptance, a thesis entitled Excited-State Charge-Transfer Dynamics of Azurin From Resonance Raman Spectroscopy submitted by Mark Adam Webb in partial fulfillment of the requirements for the degree of Doctor of Philosophy.

Glen R. Loppnow

George Kotovych

Monica M. Palcic

Mark T. McDermott

Michael A. Pickard

Anne B. Myers Kelley
(External Examiner)

Date: July 5, 2000

Abstract

Azurin, a 14 kDa Type 1 blue copper protein, is involved in electron transport chains of denitrifying bacteria. Resonance Raman spectra have been measured at wavelengths throughout the S(Cys)→Cu(II) charge-transfer absorption band for azurins from *Pseudomonas aeruginosa*, *Alcaligenes denitrificans* and *Alcaligenes xylosoxidans* to examine the role of structure and environment on the excited-state charge transfer dynamics. Self-consistent analysis of the absorption spectra and the resulting resonance Raman profiles using a time-dependent wave packet formalism yields a total inner-sphere reorganization energy of 0.26 ± 0.02 eV for the four wild-type azurins. The reorganization energy is distributed along similar vibrational modes as a function of species but the individual contribution of each individual mode to the reorganization energy appears to vary by species. Comparison of spectral changes with differences in structure and environment from the known x-ray crystal structures show only a rough correlation with overall protein structure and Cu–S bond length. However, a much better correlation was revealed between the observed spectral changes and amino acid changes, indicating that coupling of the copper site to the protein environment extends at least 10 Å from the copper. An apparent anisotropic response of the resonance Raman spectrum to specific amino acid changes suggests the resonance Raman spectrum may be sensitive to long-range vibronic coupling in the protein, important for efficient electron transfer. Resonance Raman spectra of *Pseudomonas aeruginosa* azurin mutant Met121Glu were measured throughout the ca. 600 nm absorption band at pH 3.5 and 7.0 to examine the role of the axial ligand in the copper site. These results show that the replacement of Met121 with Glu results in a significant perturbation on the electronic structure and provides

evidence that the axial ligand is critical in tuning the properties of the copper metal site.

Dedicated to

my niece Brianna Lee Webb and nephew Bailey Thomas Riley Webb

God has put a secret art into the forces of Nature so as to enable it to fashion itself out of chaos into a perfect world system.

Immanual Kant (1724-1804)

Universal Natural History and Theory of the Heavens

Acknowledgments

First of all, I thank the Almighty for this life and for guidance through this world. As I journey along the path of life I am sure that you will provide all that I need even when I do not truly know where I am going.

I thank my mother Joy, father Frank, brother Paul and sister Natalie for their love and support. I also thank Joyce Sproul who believed in me and always saw more in me than I did. I thank Anna Jordan for being a good friend and generous colleague who always had advice to give and time to listen.

This work would not have been possible without the research group. I thank Dr. Glen R. Loppnow for his time as my supervisor and for providing the resources and research facilities needed to make the work possible. I also thank Dr. Ester Fraga for her help with the protein purification and for the work on plastocyanin which helped me for this thesis. I thank Musilli M. Mitambo and Lucio H. Beyere for their help, support and friendship. I thank Christine Kwong for her work on *P. aeruginosa* azurin. Finally, I thank all the summer students that made working in the lab all summer enjoyable.

I thank Dr. T. Harris, Dr. K. Michaelian, Prof. M. Palcic, Prof. H. B. Dunford, and Prof. N. Dovichi for equipment support. I also thank R. Mah and Prof. M. Pickard at the University of Alberta for the growth and harvesting of *P. aeruginosa*, *A. denitrificans* and *A. xylosoxidans*. I thank H. Gray, A. Di Bilio and C. Kiser (Cal. Tech.) for providing Met121Glu mutant azurin. I thank Linda Peteanu and Arindam Chowdury (Carnegie-Mellon) for their work using Stark spectroscopy of azurin. I would also like to acknowledge the financial support provided by NSERC, the Alberta Heritage Foundation for Medical Research and the Department of Chemistry, University of Alberta.

I thank all those I have passed in this life for many have had even some small influence on my life. After all, it is our whole environment that influences the direction we take and the decisions we make.

Table of Contents

Chapter 1: Introduction **1**

1.1 Overview 2

1.2 Background 3

1.2.1 Blue Copper Proteins *3*

1.2.2 Azurin *3*

1.2.3 Resonance Raman Spectroscopy *11*

1.2.4 Intensity Analysis *14*

1.2.5 Electron Transfer *18*

1.2.6 Solute-Solvent Interaction *22*

1.2.7 Plastocyanin Studies *22*

1.3 Summary of Chapters 23

1.4 References 25

Chapter 2: Excited-State Charge Transfer Dynamics of Azurin, a Blue Copper Protein, from Resonance Raman Intensities **27**

2.1 Introduction 28

2.2 Experimental 33

2.3 Theory 40

2.4 Results 42

2.5 Discussion 56

2.5.1 Comparison to Plastocyanin *56*

2.5.2 Reorganization Energy *59*

2.5.3 Normal Modes *63*

2.6 Conclusions 64

2.7 References 65

Chapter 3: Protein Tuning of the Excited-State Charge Transfer Dynamics in Azurin **67**

3.1 Introduction 68

3.2 Experimental 71

3.2.1 Resonance Raman Spectroscopy *71*

3.2.2 Intensity Analysis. *72*

3.2.3 Molecular Modeling *73*

3.3 Results 74

3.4 Discussion 87

3.4.1 Electronic Structure. *87*

3.4.2 Comparison of Azurins *89*

3.4.3 Proposed Model 96
3.5 Conclusions 101
3.6 References 102

Chapter 4: A Structural Basis for Long-Range Coupling in Azurins from Resonance Raman Spectroscopy **104**

4.1 Introduction 105
4.2 Experimental 106
4.3 Results and Discussion 107
4.4 Conclusion 120
4.5 References 121

Chapter 5: Evidence for Anisotropic Long-Range Coupling Between the Active Site and Protein in Four Azurins **122**

5.1 Introduction 123
5.2 Methods 125
5.2.1 Experimental *125*
5.2.2 Intensity Analysis *125*
5.3 Results and Discussion 126
5.3.1 Analysis of A. xylosoxidans I and II *126*
5.3.2 Molecular Parameters *139*
5.3.3 Electron Transfer *145*
5.4 Conclusion 147
5.5 References 149

Chapter 6: Electronic Structure of *Pseudomonas aeruginosa* M121E Mutant Azurin **151**

6.1 Introduction 152
6.2 Methods 155
6.2.1 Experimental *155*
6.2.2 Intensity Analysis. *155*
6.2.3 Molecular Modeling *156*
6.3 Results 158
6.4 Discussion 176
6.4.1 Structure *176*
6.4.2 Reorganization Energy *181*
6.5 Conclusion 183
6.6 References 184

Chapter 7: Conclusions and Future Work **186**

7.1 Conclusions and Future Work 187

7.2 References 195

List of Tables

Table 1.1: Physical properties of azurin 6
Table 2.1: Absolute resonance Raman cross sections of *P. aeruginosa* azurin 48
Table 2.2: Comparison of the excited-state charge-transfer parameters for azurin 57
Table 2.3: Mode-specific reorganization energies of azurin and plastocyanin 60
Table 3.1: Absolute resonance Raman cross sections of *A. denitrificans* azurin 84
Table 3.2: Absolute resonance Raman cross sections of the overtone and combination bands of *A. denitrificans* azurin 88
Table 3.3: Mode-specific reorganization energies of *A. denitrificans* azurin and *P. aeruginosa* azurin 94
Table 4.1: Distances around copper atom in azurins 116
Table 4.2: Amino acid differences in azurin 118
Table 5.1: Absolute resonance Raman cross sections of *A. xylosoxidans* I azurin 131
Table 5.2: Absolute resonance Raman cross sections of *A. xylosoxidans* II azurin 132
Table 5.3: Comparison of parameters for four species of azurin 143
Table 6.1: Mode specific reorganization energies of azurin 163
Table 6.2: Absolute resonance Raman cross sections of M121E at pH 3.5 167
Table 6.3: Absolute resonance Raman cross sections of M121E at pH 7.0 168

List of Figures

Figure 1.1: Amino acid sequences of four azurins 7

Figure 1.2: Ribbon drawing of azurin 9

Figure 1.3: Jablonski diagram of Raman and IR processes 12

Figure 1.4: Raman spectra of CCl_4 and toluene at 457.9 nm 15

Figure 1.5: Time-dependent picture of absorption and resonance Raman scattering 19

Figure 2.1: Copper metal center of *P. aeruginosa* azurin 29

Figure 2.2: Isolation and purification of azurin 34

Figure 2.3: Resonance Raman experimental setup 37

Figure 2.4: Resonance Raman spectra of *P. aeruginosa* azurin at excitation wavelengths throughout the 625 nm absorption band 43

Figure 2.5: Deconvolution of the 300 to 500 cm^{-1} region of *P. aeruginosa* azurin 46

Figure 2.6: Experimental and calculated absorption spectra of *P. aeruginosa* azurin 49

Figure 2.7: Resonance Raman excitation profiles of *P. aeruginosa* azurin 51

Figure 2.8: Resonance Raman of overtone/combination bands of *P. aeruginosa* using an excitation wavelength of 647.1 nm 54

Figure 3.1: Copper metal site of *A. denitrificans* and *P. aeruginosa* azurin 69

Figure 3.2: Resonance Raman spectra of *A. denitrificans* azurin polarized parallel and perpendicular at an excitation wavelength of 568.2 nm 75

Figure 3.3: Resonance Raman spectra of *A. denitrificans* azurin at excitation wavelengths throughout the absorption band 77

Figure 3.4: Experimental and calculated absorption spectra of *A. denitrificans* azurin 80

Figure 3.5: Resonance Raman excitation profiles of *A. denitrificans* azurin 82

Figure 3.6: Resonance Raman spectrum of the overtone/combination band region of *A. denitrificans* azurin excited at 568.2 nm 85

Figure 3.7: Resonance Raman spectra of *A. denitrificans* and *P. aeruginosa* azurin 90

Figure 3.8: Absorption spectra of *A. denitrificans* and *P. aeuruginosa* azurin 92

Figure 3.9: RMS histogram and plot as a function of distance 98

Figure 4.1: Partial structure of *Pseudomonas aeruginosa* azurin near the copper site 108

Figure 4.2: Resonance Raman spectra of azurins using an excitation wavelength of 568.2 nm 110

Figure 4.3: Correlations of the azurin structures and sequences with resonance Raman spectral differences 113

Figure 5.1: Resonance Raman spectra of *A. xylosoxidans* I azurin 127

Figure 5.2: Resonance Raman spectra of *A. xylosoxidans* II azurin 129

Figure 5.3: Absorption spectra of *A. xylosoxidans* I/II azurin 133

Figure 5.4: Resonance Raman excitation profiles of *A. xylosoxidans* I azurin 135

Figure 5.5: Resonance Raman excitation profiles of *A. xylosoxidans* II azurin 137

Figure 5.6: Correlations of the azurin structures and sequences with resonance Raman spectral differences 140
Figure 6.1: Copper metal site of *P. aeruginosa* azurin for wild type and M121E mutant 153
Figure 6.2: Resonance Raman spectra of M121E azurin at pH 3.5 159
Figure 6.3: Resonance Raman spectra of M121E azurin at pH 7.0 161
Figure 6.4: Comparison of absorption spectra of M121E azurin at pH 3.5 and pH 7.0 165
Figure 6.5: Absorption spectrum of M121E azurin 169
Figure 6.6: Resonance Raman excitation profiles of M121E, pH 3.5 171
Figure 6.7: Resonance Raman excitation profiles of M121E, pH 7.0 173
Figure 6.8: Structure of the copper metal site of M121E azurin at pH 3.5, pH 7.0 178
Figure 7.1: Selected azurin amino acids 188

Chapter 1: Introduction

1.1 Overview

The environment of a chemical species can be very important in determining its electronic, structural and reaction properties. The surrounding solvent can interact with a chemical species through electrostatic forces, hydrophobic interactions, hydrogen bonding or collisions. It is of great interest to understand these solvent-solute interactions.

This work examines the excited-state dynamics of the copper metal active site of azurin, a blue copper protein, using resonance Raman spectroscopy as a structural probe of the copper metal site. Resonance Raman spectroscopy allows us to directly probe the chromophore and gives information about the excited state structure and dynamics on an extremely fast time-scale.[1] The protein forms a structured, inhomogeneous microenvironment whose properties are determined by the hydrophobic and electrostatic properties of the amino acid side chains. Thus, the amino acid sequence and the x-ray crystal structure data allow us to interpret the spectroscopic data in terms of variations in protein structure and composition. An homologous series of azurins is compared in this thesis to build up a self-consistent and structurally-based model of protein-chromophore interaction.

Some blue copper proteins are involved in respiratory and photosynthetic electron transport. One goal of this work is to better understand the rapid and efficient intramolecular electron transfer of these proteins. Azurin provides a useful model of an electron transport protein due to its relatively small size, easy availability and good stability. It is hoped that the optical charge transfer, which is purported to be one step in the electron transfer pathway, may provide a model for electron transfer. The ultimate goal is to elucidate the structural determinants of long-range electron transfer. The results in this thesis suggest resonance Raman spectroscopy may be sensitive to the electronic and vibronic coupling of the copper metal ion with the protein environment. This technique, therefore, may provide insight into the role of protein structure and composition in electron transfer.

1.2 Background

1.2.1 Blue Copper Proteins

After iron and zinc, the third most abundant trace metal in the human body is copper.[2] Copper is critical to a wide range of proteins with functions such as electron transfer, oxygen transport and active chemistry.[3] Copper proteins are typically classified by their spectroscopic properties. Blue copper proteins have a Type 1 copper active site and are characterized by an intense charge transfer absorption band near 600 nm with extinction coefficients of about 2000 to 6000 $M^{-1}cm^{-1}$.[4] The electron spin resonance (ESR) spectrum of blue copper proteins exhibits an unusually narrow hyperfine splitting ($A_{\parallel}$ = 35-63 × 10^{-4} cm^{-1}) in the $g_{\parallel}$ region[4] and varying degrees of rhombicity.[5] The reduction potential is much more positive than the 115 mV for aqueous $Cu^{++/+}$ and ranges from 184 mV for *Rhus vernicifera* stellacyanin to 680 mV for *Thiobacillus ferrooxidans* rusticyanin.[5]

Blue copper proteins are electron transport proteins and are important in essential biological functions, including photosynthesis and respiration. These proteins transport electrons via redox reactions and are often associated with enzymes. Blue copper proteins are found in electron transport chains in a wide variety of species. They include proteins such as plastocyanin from green plants, stellacyanin from *Rhus vernicifera* (Japanese lacquer tree), umecyanin from horseradish root, azurin from denitrifying bacteria, and rusticyanin from *Thiobacillus ferrooxidans*. Type 1 copper sites are also found in proteins and enzymes with multiple metals such as laccase from *Trametes versicolor* (white rot fungus), ceruloplasmin from humans, and cytochrome *c* oxidase from mammals.

1.2.2 Azurin

Azurin is found in denitrifying bacteria and is a blue copper protein involved in electron transfer.[3-5] The electron transfer properties have been studied extensively by *in vitro* experiments and the redox partners were identified as cytochrome c_{551} and nitrite reductase.[3-6] However, other *in vitro* electron transfer experiments have found

that azurin can serve as an electron donor to ethanol dehydrogenase in *Pseudomonas aeruginosa*[7] and in *Pseudomonas putida*,[8] aromatic amine dehydrogenase[9] in *Alcaligenes faecalis*, methylamine dehydrogenase[10] in *Methylobacillus flagellatum* KT and amicyanin[11] in an obligate methylotroph organism 4025. It was shown that an azurin deficient mutant of *Methylobasillus flagellatum* grew much slower than the wild type.[10]

The physiological role of azurin was studied further by *in vivo* studies using mutant strains of *Pseudomonas aeruginosa* that were deficient in one or both of azurin and cytochrome c_{551}.[12] This study found that azurin did not have an obligatory role in denitrification. Azurin was also not found to be necessary for the growth of the bacteria in the presence of alcohol or tyramine as the sole carbon source. It would therefore seem that azurin is not obligatory for either alcohol dehydrogenase or aromatic amine dehydrogenase in *P. aeruginosa*. The authors found that the growth phase and conditions controlled the expression of azurin.[12] They found little azurin in aerobic conditions and large expression when conditions became semi-anaerobic. There was also increased expression of azurin during the transition from exponential to stationary growth. This suggested a role for azurin in processes related to changes in growth conditions. When an azurin deficient mutant was challenged with hydrogen peroxide or the superoxide generator paraquat, growth was inhibited twice as much as that of the wild type. The authors propose that azurin may be involved in redox processes related to cellular response to redox stress.[12]

Physical mapping of genes of *P. aeruginosa* found that the *azu* gene responsible for azurin was not linked with *nirM* or *nirS*, genes responsible for cytochrome c_{551} and nitrite reductase, respectively.[13] Although it is possible for a cell to use unlinked genes in a common process, the separation of the *azu* gene from the denitrification genes is consistent with the above hypothesis. The exact role of azurin, therefore, is somewhat unclear although it is clearly involved in redox processes. *In vitro* studies mentioned above show that azurin appears to be able to transfer electrons to and from a number of proteins. This suggests a redundant role for azurin, where azurin plays the role of a general electron transfer protein involved in several pathways. Expression of azurin may be controlled by the stresses on the

bacteria which necessitate increased electron transfer in one pathway or another. Redundancy may also be built into certain key biological pathways to ensure the success of the bacteria.

Azurin is a relatively small protein having only 129 amino acids and a molecular weight of about 14,000 Dalton. Table 1.1 lists some physical properties of the species of azurin used in this study. The wild-type proteins all exhibit properties which are diagnostic of blue copper proteins. There is a strong putative S→Cu charge transfer absorption band at ~620 nm which gives the proteins the characteristic blue color. The reduction potential is 305 mV, which is significantly higher than 115 mV for aqua $Cu^{++/+}$.[4] Figure 1.1 lists the amino acid sequences of the four azurins that are examined in the work. The amino acid sequences of the proteins show many homologies among the species with many conserved amino acids and conservative substitutions. In Figure 1.1, similar amino acids are grouped according to the properties of the amino acid side chains. Amino acids can be classified as hydrophilic, hydrophobic, aromatic, acidic and basic. A high homology between protein species aids in the interpretation of the resonance Raman spectra. For example, if there is only one amino acid difference between two species than any change in the resonance Raman spectra could be attributed to that change. In this work, it will be desirable to interpret the data in the context of the protein amino acid content. In Figure 1.1, amino acid positions where there is an amino acid change resulting in a charge change are marked. Changes in the electrostatic environment of the copper has been associated with changes in the resonance Raman spectrum of plastocyanin[14] and would be expected to be similar in azurin. Amino acid changes will be interpreted with the help of the x-ray crystal structure.

Figure 1.2 shows the overall β-barrel structure of azurin. The x-ray crystal structures for each species of azurin used in this work was obtained from the Brookhaven National Laboratory Protein Data Bank.[15] The Brookhaven PDB ceased operation on June 30, 1999. The database was moved and is now operated as the Research Collaboratory for Structural Bioinformatics PDB.[16] There is also an α-helix portion. The copper ion is shown embedded at one end of the protein and is not accessible by solvent. The copper ion is near a hydrophobic region of the protein.

Table 1.1: Physical properties of azurin.

	P. aeruginosa[a]	*A. denitrificans*[b]	*A. xylosoxidans*[c] I/II	*M121E*[d] pH 3.5/7.0	Cu^{++} *(aqua)*[e]
λ_{max} (nm)	625	619	619/622	612/572	802
ε_{max} ($mM^{-1}cm^{-1}$)	4.80	5.20	6.27/5.73	4.50/1.10	0.012
MW (Dalton)[f]	13946	13979	13886/13775	13944	---
E_{red} (mV)	305	305	305/305	220/220	115

In the Table, λ_{max} is the absorption maximum of the charge transfer band, ε_{max} is the extinction coefficient, MW is the molecular weight and E_{red} is the reduction potential.

[a]Values of λ_{max}, ε_{max}, and E_{red} at pH 7.5 from ref 4, 5 and 17, respectively.
[b]Values of λ_{max}, ε_{max}, and E_{red} at pH 7.5 from ref 4.
[c]Values of λ_{max}, ε_{max}, and E_{red} at pH 7.5 from ref 18.
[d]This is the Met121Glu mutant of *P. aeruginosa* azurin. Values of A_{max}, ε_{max}, and E_{red} at pH 4 and 7 from ref 19.
[e]Values of λ_{max} and ε_{max} were measured using solutions of $Cu(NO_3)_2$ and $CuSO_4$. E_{red} for aqua $Cu^{++/+}$ is from ref 4.
[f]Molecular weight is calculated from the amino acid sequence given in Figure 1.1.

Figure 1.1: Amino acid sequences of four azurins. Species are labeled as *Alcaligenes xylosoxidans* (AXI and AXII), *Alcaligenes denitrificans* (AD) and *Psuedomonas aeruginosa* (PA). The columns are labeled as Cu ligands (⊗), cysteine involved in disulfide bridge (§), identical residues (≡), homologous residues (≈), and residues with change of charge (±). Homologous amino acids are those with similar properties such as being hydrophobic, hydrophilic or aromatic.

										10									20
AD	A	Q	C	E	A	T	I	E	S	N	D	A	M	Q	Y	D	L	K	E	M
AXII	A	Q	C	E	A	V	I	E	S	N	D	A	M	Q	Y	N	V	K	E	I
AXI	A	E	C	C	S	V	D	I	A	G	N	D	G	M	Q	Q	F	D	K	K	E	I
PA	A	E	C	S	S	V	D	I	Q	G	N	D	Q	M	Q	F	N	T	N	A	I
	≡	±	§	±	≈	±	≈	±	≈	≡	≡		≡	≡		±	±	±	±	≈

										30									40
AD	V	V	D	K	S	C	K	Q	F	T	V	H	L	K	H	V	G	K	M	A
AXII	V	V	D	K	S	C	K	Q	F	T	M	H	L	K	H	V	G	K	M	A
AXI	T	V	S	K	S	C	K	Q	F	T	V	N	L	K	H	P	G	K	L	A
PA	T	V	D	K	S	C	K	Q	F	T	V	N	L	S	H	P	G	N	L	P
		≡	±	≡	≡	§	≡	≡	≡	≡	≈	±	≡	±	≡	≈	≡	±	≈	≈

										50									60
AD	K	S	A	M	G	H	N	W	V	L	T	K	E	A	D	K	E	G	V	A
AXII	K	V	A	M	G	H	N	L	V	L	T	K	D	A	D	K	Q	A	V	A
AXI	K	N	V	M	G	H	N	W	V	L	T	K	Q	A	D	M	Q	G	A	V
PA	K	N	V	M	G	H	N	W	V	L	S	T	A	A	D	M	Q	G	V	V
	≡		≈	≡	⊗	⊗	≡		≡	≡	≈	±	±	≡	≡	±	±		≈	≈

										70									80
AD	T	D	G	M	N	A	G	L	A	Q	D	Y	V	K	A	G	D	T	R	V
AXII	T	D	G	M	G	A	G	L	A	Q	D	Y	V	K	A	G	D	T	R	V
AXI	N	D	G	M	A	A	G	L	D	N	N	Y	V	K	K	D	D	A	R	V
PA	T	D	G	M	A	S	G	L	D	K	D	Y	L	K	P	D	D	S	R	V
	≈	≡	≡	≡			≡	≡	±	±	±	≡	≈	≡	±	±	≡		≡	≡

										90									100
AD	I	A	H	T	K	V	I	G	G	G	E	S	D	S	V	T	F	D	V	S
AXII	I	A	H	T	K	V	I	G	G	G	E	S	D	S	V	T	F	D	V	S
AXI	I	A	H	T	K	V	I	G	G	G	E	T	D	S	V	T	F	D	V	S
PA	I	A	H	T	K	L	I	G	S	G	E	K	D	S	V	T	F	D	V	S
	≡	≡	≡	≡	≡	≈	≡	≡	≈	≡	≡	±	≡	≡	≡	≡	≡	≡	≡	≡

										110									120
AD	K	L	T	P	G	E	A	Y	A	Y	F	C	S	F	P	G	H	W	A	M
AXII	K	I	A	A	G	E	N	Y	A	Y	F	C	S	F	P	G	H	W	A	M
AXI	K	L	A	A	G	E	D	Y	A	Y	F	C	S	F	P	G	H	F	A	L
PA	K	L	K	E	G	E	Q	Y	M	F	F	C	T	F	P	G	H	S	A	L
	≡	≈	±	±	≡	≡	±	≡	≈		≡	⊗	≈	≡	≡	≡	⊗		≡	≈

									129
AD	M	K	G	T	L	K	L	S	N
AXII	M	K	G	T	L	K	L	G	S
AXI	M	K	G	V	L	K	L	V	D
PA	M	K	G	T	L	T	L	K	
	⊗	≡	≡		≡	±	≡	±	±

Figure 1.2: Ribbon drawing of azurin. Azurin is primarily a β-barrel (blue) with a small section of α-helix (red). The copper active site is shown at the "north" end of the protein and the disulfide bridge is shown at the "south" end. The copper-ligating side chains shown form a distorted trigonal byramidal cage around the copper metal ion.

This hydrophobic patch is the location of electron transfer from cytochrome c_{551} to azurin and azurin to nitrite reductase.[6] The copper is strongly bound to N(His46), N(His117) and S(Cys112) in a trigonal plane and weakly bound to O(Gly45) and S(Met121) in axial positions. The structure of the protein is needed for the interpretation of the data as changes in the resonance Raman may be attributed to structural or amino acid changes. The location of amino acid changes relative to the copper can also be examined. Changes far from the copper are expected to have little or no impact on the resonance Raman spectrum.

1.2.3 Resonance Raman Spectroscopy

Vibrational transitions can be observed in either infrared (IR) or Raman spectra. To obtain an IR spectrum, a beam of broadband infrared light is shone through a sample and the absorption as a function of wavelength is measured. Photons which have the same energy as a vibrational transition, are absorbed. Figure 1.3 shows the IR absorption between vibrational levels. The absorption of IR light is given by the Beer-Lambert law: $A=\varepsilon cd$, where ε is the molecular absorption coefficient, c is the concentration and d is the path length.

The method of obtaining Raman spectra is very different. A laser with a frequency, ν_0, in the UV-visible region irradiates the sample and the scattered light is observed. Figure 1.3 illustrates the possible scattering events that are possible. Most of the scattering is elastic, in which the incident photon and the scattered photon have identical energies. Inelastic scattering can also occur and results in photons with frequencies of $\nu_0 \pm \nu_m$, where lines at $\nu_0-\nu_m$ and $\nu_0+\nu_m$ are the Stokes and anti-Stokes lines, respectively. Raman scattering is very weak and is at best only one photon per $\sim 10^5$ scattered photons; the rest being Rayleigh scattering. The anti-Stokes transitions originate from excited vibrational levels which are thermally populated. The population, N_1, of a state of energy, ε_1, relative to the ground state with population, N_0 is given by a Boltzmann distribution:

$$\frac{N_1}{N_0} = \frac{g_1}{g_0} \exp\left(\frac{-\varepsilon_1}{k_B T}\right) \qquad (1.1)$$

Figure 1.3: Jablonski diagram of Raman and IR processes. Ground (S_0) and first excited (S_1) electronic states, and associated vibrational states are shown as horizontal lines. Infrared, Raman and resonance Raman transitions are shown by vertical arrows. Transitions shown are infrared absorption (IR), and anti-Stokes (AS), Rayleigh (R) and Stokes (S) Raman scattering.

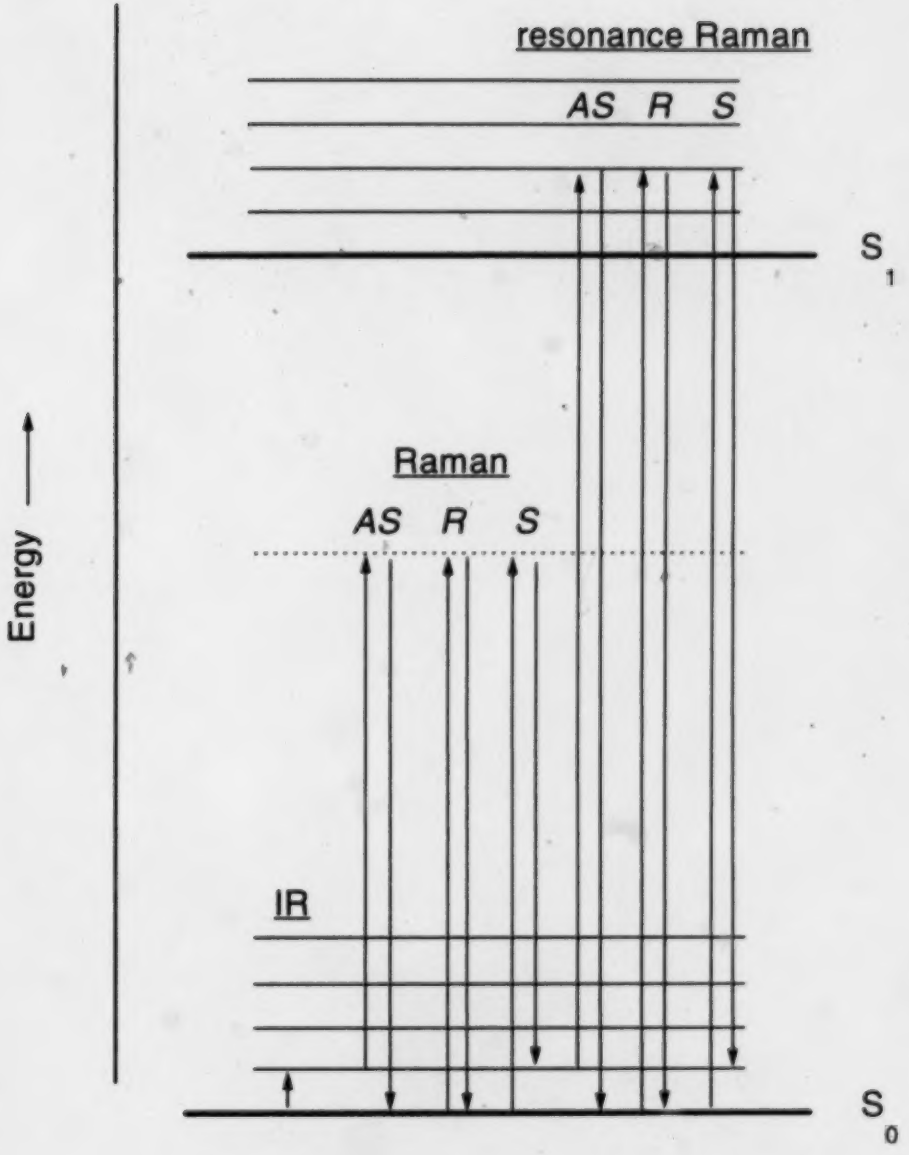
resonance Raman
AS R S
S 1
Raman
AS R S
Energy
IR
S 0

where k_B is Boltzmann's constant, T is the temperature and g_1 and g_0 are the degeneracy of the vibrational states. The low population of the excited vibrational states results in lower intensities of the anti-Stokes lines relative to the Stokes lines. For this reason, it is most common to measure the Stokes spectrum. The anti-Stokes spectra are magnified in Figure 1.4 to show them clearly compared to the Stokes spectra. The normal practice is to measure the Stokes spectrum and plot the spectrum as a difference from the Rayleigh line. The spectrum of CCl_4 (Figure 1.4A) illustrates that the anti-Stokes frequencies are the mirror image of the Stokes lines. The anti-Stokes lines of toluene (Figure 1.4B) are slightly noisier and much less intense than the Stokes lines. Interestingly, even at room temperature there is a very small population in the 1378 cm^{-1} vibration giving an anti-Stokes intensity ~4000 times smaller than the corresponding Stokes intensity.

Resonance Raman scattering occurs when the incident photon has an energy which is equal to that of an electronic transition (Figure 1.3) of a chromophore. The intensities of the Raman bands which are coupled to the electronic transition are resonantly enhanced by a factor of 10^3-10^5.[20] This allows us to selectively probe the active site copper chromophore embedded in the protein. Azurin has close to 2000 atoms which results in 6000 possible vibrations which would be far too many to interpret. Resonance Raman enhances the vibrations which are coupled to the charge transfer transition and allows us to selectively study these modes. The resonance Raman spectrum of azurin has ≤12 modes, greatly simplifying the amount of data. The Raman cross sections of azurin have been found from the relative integrated intensities of azurin and cacodylate as described in Chapter 2.

1.2.4 Intensity Analysis

One of the goals of this thesis is to examine the effect of structure and environment on the excited-state dynamics. The connection between resonance Raman intensities and excited-state dynamics becomes readily apparent in the time-domain expression for Raman cross section (Equation 1.2). The Raman cross section is dependent on a propagating wavepacket whose motion is controlled by the slope of the excited-state

Figure 1.4: Raman spectra of CCl_4 and toluene at 457.9 nm. The spectra are each a combination of two spectra taken with a holographic filter to remove the Rayleigh scattering. The x-axis is $\Delta\nu$ in cm^{-1}. Note that the y-axis scale of the anti-Stokes lines has been magnified to show anti-Stokes lines clearly. The left y-axis is for the anti-Stokes spectra and the right y-axis is for the Stokes spectra. The Rayleigh line is shown at 0 cm^{-1}, the anti-Stokes lines are shown as negative frequencies and the Stokes lines are shown as positive frequencies. The inset shows a magnified portion of the toluene anti-Stokes spectrum. The intensities of lines within ± 400 cm^{-1} of 0 cm^{-1} may be slightly attenuated due to the holographic filter used.

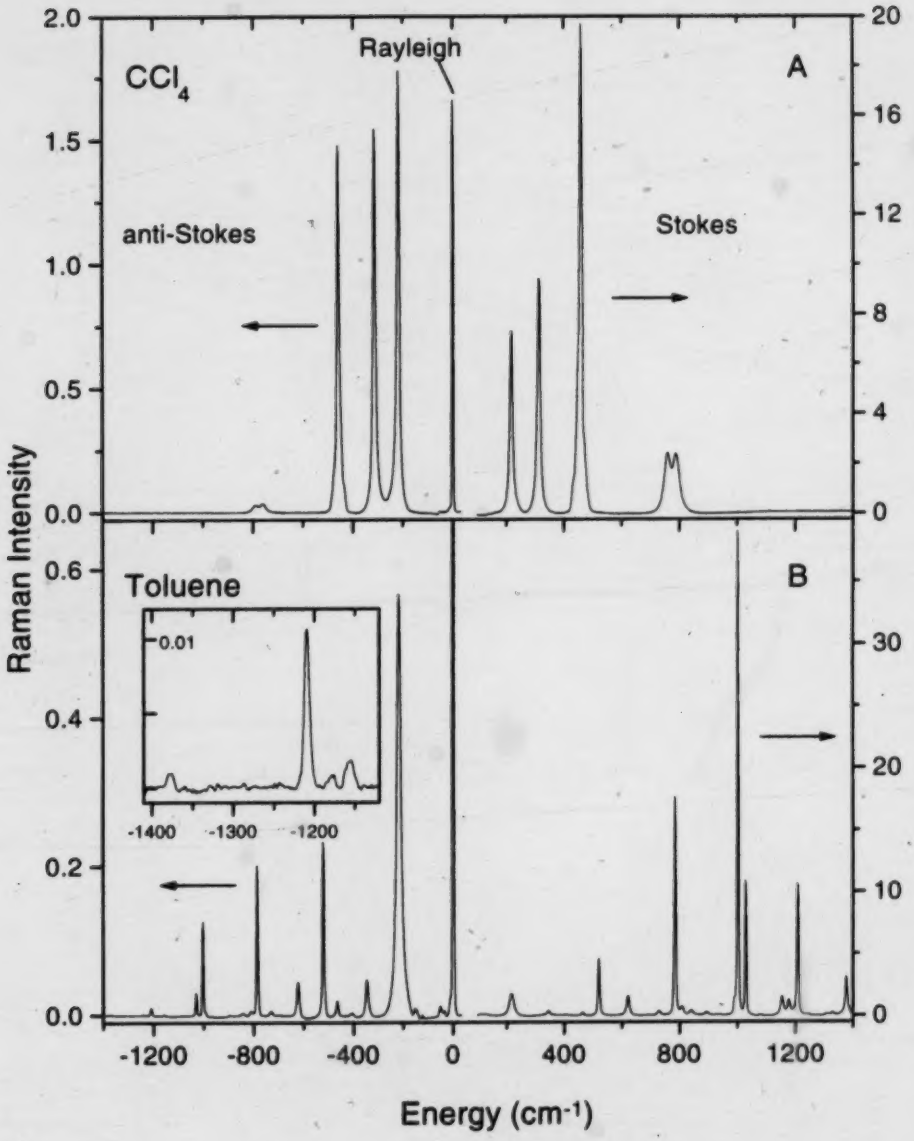
CCl4
Rayleigh
A
anti-Stokes
Stokes
Toluene
B
0.01
-1400
-1300
-1200
Raman Intensity
Energy (cm-1)
2.0
1.5
1.0
0.5
0.0
0.6
0.4
0.2
20
16
12
8
4
30
-1200
-800
-400
0
400
800
1200

potential energy surface in the Frank-Condon region.[21] The shape of the excited-state potential surface also dictates the initial dynamics of the nuclear motion on that surface.[1] Resonance Raman spectra are measured at wavelengths throughout the charge transfer absorption band to build up excitation profiles. These are analyzed using a self-consistent time-dependent wavepacket formalism developed by Lee and Heller.[22] The equations for the Raman and absorption cross sections are as follows:[1,21,22]

$$\sigma_R = \frac{8\pi E_S^3 E_L e^4 M^4}{9\hbar^6 c^4} \int_{-\infty} H(E_0)\ dE_0 \times \left| \int_0 \langle f|i(t)\rangle\ e^{\frac{i(E_L+\varepsilon_i)t}{\hbar}}\ G(t)dt \right|^2 \tag{1.2}$$

$$\sigma_A = \frac{4\pi e^2 M^2 E_L}{6\hbar^2 cn} \int_{-\infty} H(E_0)\ dE_0 \times \int_{-\infty} \langle i|i(t)\rangle\ e^{\frac{i(E_L+\varepsilon_i)t}{\hbar}}\ G(t)\ dt \tag{1.3}$$

where E_L and E_S are the energies of the incident and scattered photons, M is the transition length, $H(E_0) = (1/[\theta(2\pi)^{1/2}])\exp[-(E_0 - \overline{E_0})^2/2\theta^2]$ is a normalized Gaussian distribution of site electronic energies, n is the refractive index, ε_i is the energy of the initial vibrational state, $G(t) = \exp[-\Gamma_L t/h]\exp[-\Gamma_G^2 t^2/h^2]$ is a decay function, $|i\rangle$ and $|f\rangle$ are the initial and final vibrational wavefunctions in the resonance Raman process, and $|i(t)\rangle = e^{-iHt/\hbar}|i\rangle$ is the initial ground vibrational wavefunction propagated on the excited-state potential surface. The $\langle i|i(t)\rangle$ absorption overlap in Equation 1.3 is the product of one-dimensional $\langle i|i(t)\rangle$ overlaps for each normal mode, while the $\langle f|i(t)\rangle$ Raman overlap in Equation 1.2 is the product of $\langle f|i(t)\rangle$ along the Raman-active mode and $\langle i|i(t)\rangle$ along all other modes. In this treatment, the $\langle i|i(t)\rangle$ and $\langle f|i(t)\rangle$ overlaps are dependent only on the displacement, Δ, between ground- and excited-state equilibrium geometries along

each normal coordinate. The implementation of these equations is described in Chapter 2.

The time-dependent picture provides a pictorial interpretation shown in Figure 1.5. In absorption, an incident photon, E_L, interacts with the molecule and carries the initial vibrational function, $|i\rangle$, to the excited state. The vibrational wavepacket then propagates on the excited-state surface under the influence of the excited-state Hamiltonian. The absorption spectrum is taken from the overlap of the propagating function, $|i(t)\rangle$, and the initial function multiplied by the damping function G(t). For resonance Raman, the incident photon scatters off the excited-state surface carrying the initial wavefunction with it. The resonance Raman intensity is related to the overlap of the propagating initial wavefunction and the final wavefunction, $|f\rangle$ multiplied by the damping function G(t). Note that if the displacement along the normal coordinate is zero, the overlap is zero since the initial and final functions are orthogonal. This means that in order for there to be a significant intensity there has to be a distortion between the ground- and excited-states.

1.2.5 Electron Transfer

The rate constant of electron transfer in the Marcus normal region, k, is related to the standard free energy of reaction, $\Delta G°$, and the reorganization energy, λ, by the Marcus equation: $k \propto \exp\{-(\Delta G° + \lambda)^2/4\lambda RT\}$.[23] The reorganization energy can be divided into inner- and outer-sphere contributions ($\lambda = \lambda_i + \lambda_o$) where the inner-sphere contribution (λ_i) roughly refers to nuclear reorganizations of the donor and acceptor and the outer-sphere contribution (λ_o) roughly refers to structural reorganization of the solvent in response to the new electronic distribution.

Resonance Raman spectroscopy can be used to measure mode-specific reorganization energies in systems with optical charge transfer bands. Resonance Raman spectroscopy has been used to investigate three electron transfer systems which exhibit charge transfer absorption bands in the visible region, hexamethylbenzene/tetracyanoethylene, betaine-30 and 9,9'-bianthryl. In the first

Figure 1.5: Time-dependent picture of absorption and resonance Raman scattering. Interaction with the incident photon carries the initial vibrational wavefunction to the excited-state, where it propagates under the influence of the excited-state Hamiltonian. The absorption spectrum and the resonance Raman scattering intensity depend on the overlap of the propagating wavefunction with the initial and final wavefunctions, respectively.

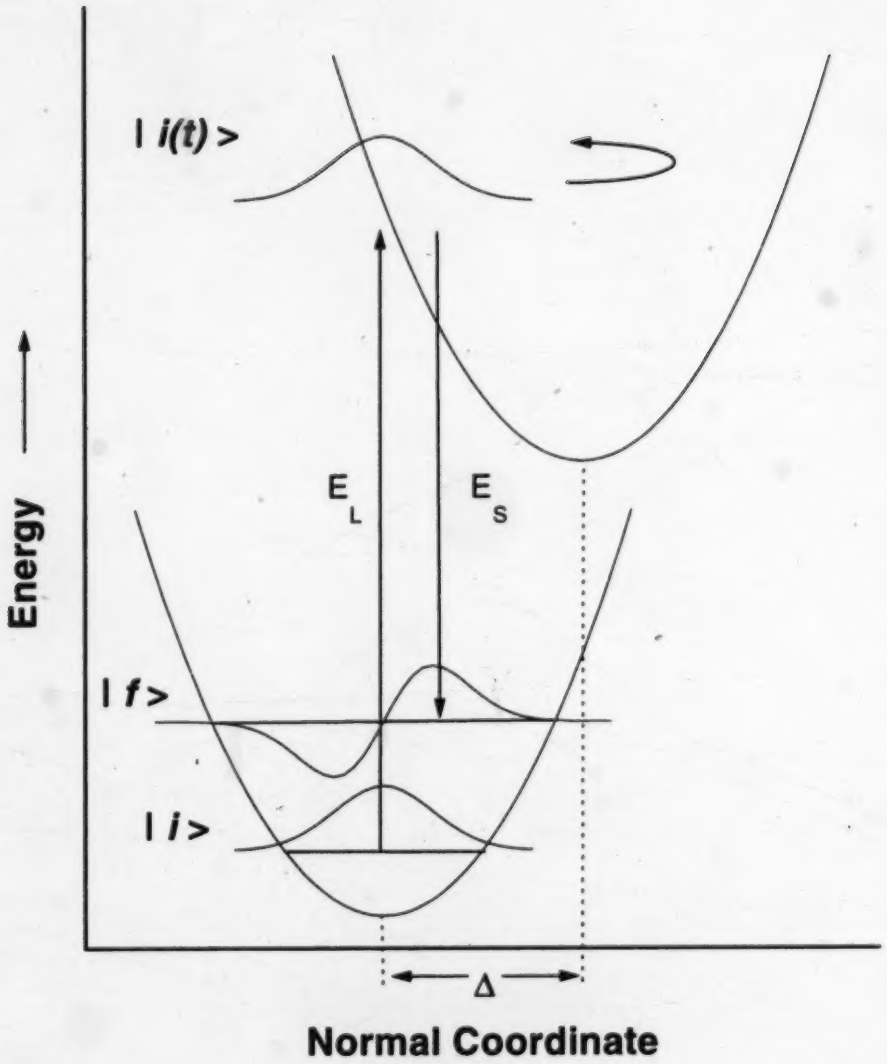
| i(t) >
E L
E S
Energy
| f >
| i >
Δ
Normal Coordinate

example, the hexamethylbenzene/tetracyanoethylene (HMB/TCNE) charge transfer complex was modeled using the eleven most intense resonance Raman bands and the solvent, treated as an overdamped Brownian oscillator.[24] The absorption spectrum, fluorescence emission, resonance Raman scattering and the electron transfer rate of HMB/TCNE in CCl_4 were simulated using one model.[24] Good fits were obtained for both the absorption and the fluorescence spectra.[24] The solvent reorganization was found to be 2450 cm^{-1} and the internal reorganization was 2266 cm^{-1} divided among HMB and TCNE vibrations.[24] However, the calculated electron transfer rate was significantly too high and was very sensitive to the solvent bandshape chosen.[24] In the second example, betaine-30 was studied in CH_3CN and CD_3CN to investigate the solvent isotope effect on electron transfer and solvent dynamics.[25] The electron transfer rate constant is longer (11.2 ps vs. 9.4 ps) and the resonance Raman cross sections are lower in the deuterated solvent.[25] This study used a modified Brownian oscillator model and a biexponential solvent relaxation for the solvent, and found a solvent reorganization energy of 6020 and 6350 cm^{-1} for protonated and deuterated solvent, respectively.[25] The internal reorganization energy was found to be mostly in low frequency modes and was 170 and 100 cm^{-1} for protonated and deuterated solvent, respectively.[25] They attribute the unexpected decrease in Raman intensity to reduced amplitude of solvent fluctuations in the deuterated solvent.[25] Finally, solvation and intramolecular reorganization was studied for 9,9'-bianthryl (BA) using resonance Raman and *ab initio* molecular orbital calculations.[26] The reorganization energy of the three most intense modes were measured for BA in several solvents and was found to be 700, 1229, 1052 and 1720 cm^{-1} in CCl_4, CH_2Cl_2, CH_3OH and CH_3CN, respectively.[26] Modeling the resonance Raman cross sections using transform theory[1,27,28] was unsuccessful, so a time-dependent approach was used.[26] It was found that although the absorption spectrum is essentially solvent independent, the fluorescence spectrum is highly solvent-dependent.[26] They propose a strong coupling between intramolecular reorganization in BA and solvation.[26] These three examples demonstrate the use of resonance Raman spectroscopy to study solvent interaction and excited-state dynamics in charge transfer systems.

1.2.6 Solute-Solvent Interaction

As mentioned above, Raman and resonance Raman can be used to investigate solute-solvent interactions. Solvent interactions of thymine and thymidine were investigated using Raman spectroscopy in ten solvents.[29] It was found that the frequency shift of modes involving NH and C=O motions correlated with donor and acceptor number of the solvents.[29] A similar study of mercury(II) thiocyanate complexes in ten aprotic solvents found a correlation between Hg-S frequency and donor number of the solvent.[30] Raman spectroscopy of ethyl 4-(dimethylamino)benzoate (DMABEE) in eighteen solvents of varying polarity and hydrogen bonding found a correlation of acceptor number and vibrational frequencies of the C=O stretching, C–O stretching and OCO bending modes.[31] DMABEE is purported to have a twisted intramolecular charge transfer (TICT) excited state which gives rise to a dual fluorescence.[32,33] Another molecule with a TICT state is the hemicyanine dye, 4-[2-(4-dimethylamino-phenyl)ethenyl]-1-methyl-pyridinium iodide.[34] This molecule has been studied in aqueous solution using resonance Raman spectroscopy.[34] The Raman cross sections are higher in D_2O than in H_2O and may reflect less solvent dephasing due to larger inertial moment and stronger hydrogen bonding in the deuterated solvent. These studies show the use of Raman and resonance Raman spectroscopy to investigate solute-solvent interactions using Raman frequency shifts and changes in Raman cross section.

1.2.7 Plastocyanin Studies

Previous resonance Raman studies have been done on the blue copper protein plastocyanin.[14,35,36] The absorption spectrum and the resulting resonance Raman excitation profiles were analyzed for parsley, spinach and poplar *a* plastocyanin.[36] It was found that the mode-specific reorganization energies were significantly different for the three species, although the total reorganization was 0.18 ± 0.01 eV for all three proteins.[36] Structures were obtained using an energy minimization of the poplar *a* x-ray crystal structure as the initial point and the electrostatic field was calculated with the linearized Poisson-Boltzmann equation.[36] A detailed comparison of the three

species suggested that the observed relative intensity changes were due to changes in the normal mode description due to differential coupling of the copper active site with the protein environment. Unfortunately, only the x-ray crystal structure of poplar *a* plastocyanin was available. An advantage with azurin and a key motivation for the thesis research is that x-ray crystal structures are available for several species and numerous mutants.[16] This should allow us to build a stronger correlation between resonance Raman intensities and protein structure and environment.

Resonance Raman spectra of poplar *a*, spinach, zucchini and cucumber plastocyanin were compared.[14] It was found that the resonance Raman spectrum was affected by changes in the amino acids within 15 Å of the copper metal ion and two mechanisms have also been proposed.[14] The first is a "through-bond" mechanism, where amino acid changes at least 8 Å from the copper along a peptide strand cause a composition-dependant rotation of the normal modes.[14] This is likely a kinetic coupling of the copper to the protein normal modes and results in a redistribution of the reorganization energy among the visible vibrational modes while retaining the total reorganization energy. The second mechanism is a "through-space" mechanism by electrostatic interactions up to 12-13 Å from the copper.[14] Charged amino acids or permanent dipoles interact with the Cu–S dipole. These mechanisms are expected to operate in azurin as well and the spectrum of azurin will be interpreted with these results as a guide.

1.3 Summary of Chapters

This work is the study of azurin using resonance Raman spectroscopy. Chapter 2 looks at the excited-state dynamics of *P. aeruginosa* azurin and compares the results to parsley plastocyanin. Differences in the excited-state are attributed to differences in geometry and hydrogen bonding. Chapter 3 continues with a study of *A. denitrificans* azurin. The results from the two azurin species are compared and an initial model is proposed. It appears that the spectral changes are due to a complex relationship between the chromophore structure and the protein environment. In Chapter 4 the model is refined as two additional azurins from *A. xylosoxidans* are

added to the study. The results demonstrate a structural basis for the correlation between protein environment and the excited-state properties of the copper metal ion. In Chapter 5, the analysis of the two azurins from *A. xylosoxidans* is completed and the qualitative conclusions of Chapter 4 are tested in a quantitative manner. The apparent anisotropic coupling of the copper metal to the protein environment is discussed in relation to electron transfer. Chapter 6 is a study of the azurin mutant Met121Glu and explores the role of the axial ligand in tuning the electronic structure of the copper metal site. Chapter 7 gives conclusions and some directions for possible future work.

1.4 References

[1] Myers, A. B.; Mathies, R. A. In *Biological Applications of Raman Spectroscopy*; T. G. Spiro, Ed.; Wiley: New York, **1988**; *Vol. 2*; pp. 1.

[2] Underwood, E. J. In *Trace Elements in Humans and Animal Nutrition*, 14 Ed. Academic Press, New York, **1977**.

[3] Adman, E. T. *Adv. Protein Chem.* **1991**, *42*, 145.

[4] Sykes, A. G. *Adv. Inorg. Chem.* **1991**, *36*, 377.

[5] Adman, E. T. In *Metalloproteins - Part 1: Metal Proteins with Redox Roles*; P. M. Harrison, Ed.; Verlag Chemie: Florida, **1985**; pp. 1.

[6] Van de Kamp, M.; Silvestrini, M. C.; Brunori, M.; Van Beeumen, J.; Hali, F. C.; Canters, G. W. *Eur. J. Biochem.* **1990**, *194*, 109.

[7] Duine, J. A. In *From Neural Networks and Biomolecular Engineering to Bioelectronics*; Nicolini, C. Ed; Plenum: New York, **1995**, pp. 87-94.

[8] Matsushita, K.; Yamashita, T. Aoki, N., Toyama, H.; Adachi, O. *Biochemistry* **1999**, *38*, 6111.

[9] Hyun, Y.-L.; Davidson, V. L. *Biochemistry* **1995**, *34*, 12249.

[10] Gak, E. R.; Chistoserdov, A. Y.; Lidstrom, M. E. *J. Bacteriol.* **1995**, *177*, 4575.

[11] Auton, K. A.; Anthony, C. J. *Gen. Microbiol.* **1998**, *135*, 1923.

[12] Vijgenboom, E.; Busch, J. E.; Canters, G. W. *Microbiology* **1997**, *143*, 2853.

[13] Vollack, K.-U.; Xie, J.; Härtig, E.; Römling, U.; Zumft, W. G. *Microbiology* **1998**, *144*, 441.

[14] Fraga, E.; Loppnow, G. R. *J. Phys. Chem. B* **1998**, *102*, 7659.

[15] Berstein, F. C.; Koetzle, T. F.; Williams, G. J.; Meyer Jr, E. E.; Brice, M. D.; Rodgers, J. R. R.; Kennard, O.; Shimanouchi, T.; Tasumi, M. *J. Mol. Biol.* **1977**, *112*, 535.

[16] Berman, H. M.; Westbrook, J.; Feng, Z.; Gilliland, G.; Bhat, T. N.; Weissig, H.; Shindyalov, I. N.; Bourne, P. E. *Nucleic Acids Research* **2000**, *28*, 235. WWW address: http://www.rcsb.org/pdb/.

[17] den Blaauwen, T.; Canters, G. W. *J. Am. Chem. Soc.* **1993**, *115*, 1121.

[18] Dodd, F. E.; Hasnain, S. S.; Hunter, W. N.; Abraham, Z. H. L.; Debenham, M.; Kanzler, H.; Eldridge, M.; Eady, R. R.; Ambler, R. P.; Smith, B. E. *Biochemistry* **1995**, *34*, 10180.

[19] Karlsson, B. G.; Tsai, L.-C.; Nar, H.; Sanders-Loehr, J.; Bonander, N.; Langer, V.; Sjölin, L. *Biochemistry* **1997**, *36*, 4089.

[20] Ferraro, J. R.; Nakamoto, K. In *Introductory Raman Spectroscopy*; Academic Press Inc: San Diego, **1994**.

[21] McHale, J. L. In *Molecular Spectroscopy*; Prentice Hall; New Jersey, **1999**.

[22] Lee, S-Y.; Heller, E. J. *J. Chem. Phys.* **1979**, *71*, 4777.

[23] Marcus, R. A.; Sutin, N. *Biochim. Biophys. Acta* **1985**, *811*, 265.

[24] Kulinowski, K.; Gould, I. R.; Myers, A. B. *J. Phys. Chem.* **1995**, *99*, 9017.

[25] Zong, Y.; McHale, J. L. *J. Chem. Phys.* **1997**, *106*, 4963.

[26] Scholes, G. D.; Fournier, T.; Parker, A. W.; Phillip, D. *J. Chem. Phys.* **1999**, *111*, 5999.

[27] Chan, C. K.; Page, J. B.; *J. Chem. Phys.* **1983**, *79*, 5234.

[28] Chan, C. K.; Page, J. B.; Tonks, D. L.; Brafman, O.; Khodadoost, B.; Walker, C. T. *J. Chem. Phys.* **1985**, *82*, 4813.

[29] Beyere, L. H. M. Sc. thesis entitled "*Nucleobase Interactions with Solvents and Sunscreens from Raman Spectroscopy*" submitted to the Department of Chemistry, University of Alberta, Edmonton, Alberta, Canada, T6G 2G2, Spring **2000**.

[30] Šašić, S.; Antić-Jovanvić, A.; Jeremić, M.; Lalić, M. *Spectrosc. Lett.* **1995**, *28*, 1217.

[31] Mitambo, M.; Loppnow, G. R. *Chem. Pys. Lett.* **1996**, *261*, 691.

[32] Rotkiewicz, K.; Rubaszewska, W. *Chem. Phys. Lett.* **1980**, *70*, 444.

[33] Lipinski, L.; Chojnacki, H.; Grabowski, Z.; Rotkiewicz, K. *Chem. Phys. Lett.* **1980**, *70*, 449.

[34] Cao, X.; McHale, J. L. *J. Chem. Phys.* **1998**, *109*, 1901.

[35] Fraga, E.; Webb, M. A.; Loppnow, G. R. *J. Phys. Chem.* **1996**, *100*, 3278.

[36] Loppnow, G. R.; Fraga, E. *J. Am. Chem. Soc.* **1997**, *119*, 896.

Chapter 2: Excited-State Charge Transfer Dynamics of Azurin, a Blue Copper Protein, from Resonance Raman Intensities

Material previously published:

M. Adam Webb, Christine M. Kwong, and Glen R. Loppnow

J. Phys. Chem. B **1997**, 101, pp. 5062-5069.

2.1 Introduction

Blue copper proteins are involved in electron transport chains in plants and bacteria.[1,2] Azurin, a 14.0 kDa blue copper protein found in the denitrifying bacterium *Pseudomonas aeruginosa*, is involved in the electron transport chain of respiratory phosphorylation. Specifically, it transports electrons from cytochrome c_{551} to nitrite reductase (formerly called cytochrome oxidase).[1-3] The structure of azurin shows one Type 1 copper[4] ion in a coordination geometry which is an elongated, distorted trigonal bipyramid, with His46, Cys112, and His117 forming the three, strongly-coordinated planar ligands, and Met121 and the carbonyl oxygen of Gly45 forming the weakly interacting axial ligands (Figure 2.1). This is in contrast to plastocyanin, which exhibits a distorted tetrahedral geometry and has only one axial ligand, the sulfur of Met92.

The axial ligands in blue copper proteins seem to be responsible for tuning the copper ion EPR parameters, even though the bonds between these ligands and copper are typically quite long, 3.12 Å for Cu–S(Met121) and 2.95 Å for Cu–O(Gly45) in azurin.[5] Research performed on mutants of azurin,[6,7] in which the methionine ligand at amino acid 121 was replaced by a variety of amino acid residues or deleted completely, shows that the weakly-bound S ligand has a significant effect on the copper coordination geometry. Replacing methionine with Leu, Ala, Val, Ile, or Trp results in an axial EPR spectrum indicating a trigonal-planar geometry, weak or absent axial coordination, and a stronger interaction with the carbonyl oxygen. Replacing methionine with Asn, Asp, Gln, Cys, or His results in a rhombic EPR spectrum indicating a more tetrahedral geometry and stronger axial coordination. In the latter mutants, the copper moves out of the NNS plane towards the now stronger axial ligand and away from the carbonyl oxygen.

The redox potential also seems to be very sensitive to the number and type of axial ligands present. At pH 7.5, the reduction potentials of the copper site are +375 and +305 mV for plastocyanin and azurin, respectively.[1] These values are high compared to the aqua Cu(II/I) couple (+115 mV) and are characteristic of Type 1 copper proteins. The protein reduction potentials are pH dependent and E° values for

Figure 2.1: Copper metal center of *P. aeruginosa* azurin. A schematic representation of the copper center with Cu–ligand bonds labeled with the length in Å.

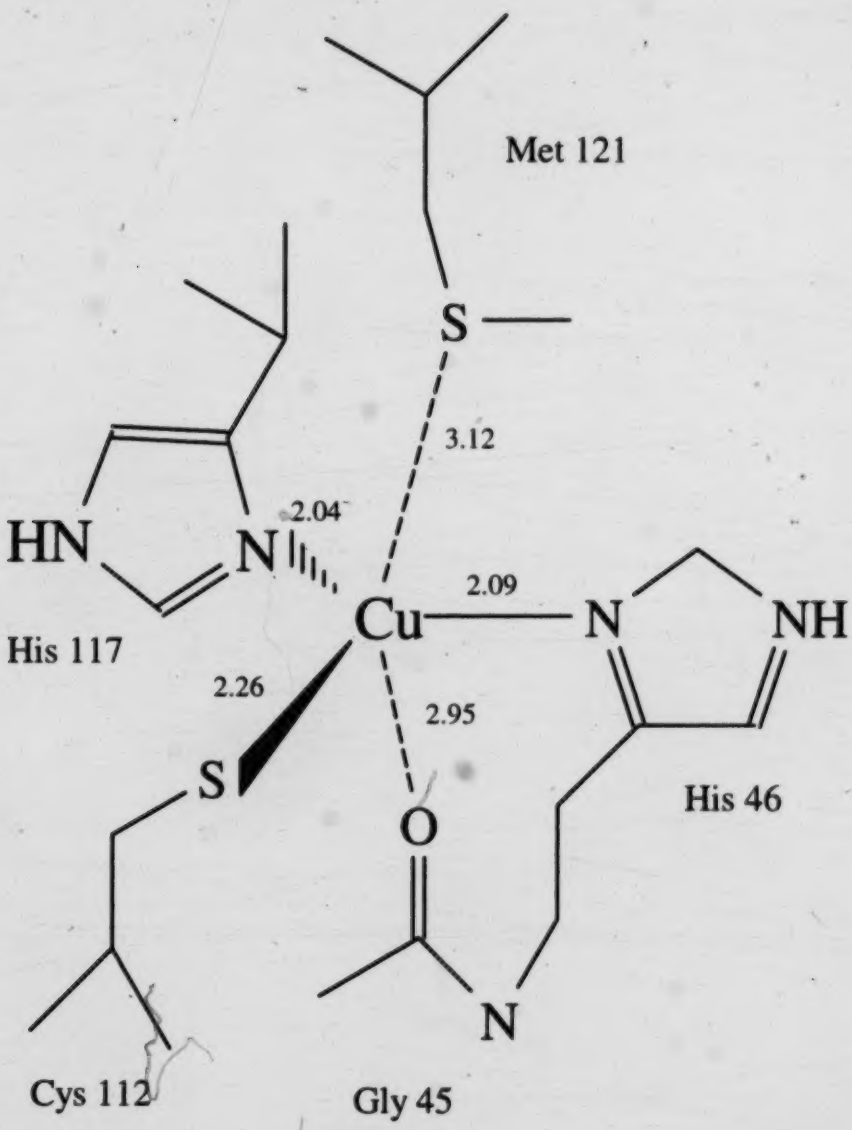
Met 121
S
3.12
2.04
HN
N
2.09
Cu
N
NH
His 117
2.26
2.95
S
O
His 46
N
Cys 112
Gly 45

all naturally-occurring azurins are lower than those of plastocyanin.[8] By comparing azurin mutants, plastocyanin and other blue copper proteins it has been shown that the reduction potential increases as the copper moves further from the NNS plane towards the axial sulfur ligand, and the reduction potential decreases when the methionine ligand is removed.[6,8] These studies indicate that the interactions of the copper ion with the three strongly bound ligands remain fairly constant among azurin species while variations in the axial ligands (distances and type) tune the reduction potential.

The electronic structure of the copper site has been studied using low temperature absorption, circular dichroism (CD), and magnetic circular dichroism (MCD) spectroscopy[8-11] which have shown at least four transitions between 400 and 1000 nm. The most intense band has been assigned to a S(Cys-π)$\rightarrow$Cu charge-transfer transition, while the other transitions have been assigned to S(Cys-σ)$\rightarrow$Cu charge-transfer, S(Met-σ)$\rightarrow$Cu charge-transfer, N(His-π)$\rightarrow$Cu charge-transfer, and ligand field transitions. Studies using mutants and the addition of exogenous ligands show that the absorption spectrum is determined by the ligands coordinated to the copper ion.[6,12,13] As the copper site is altered from an axial Type 1 to a tetragonal Type 2 coordination structure the absorption maxima at 460 and 628 nm are blue shifted and the peak at 460 nm grows in intensity at the expense of the 628 nm peak.[13] The substitution of a histidine with ligands which do not coordinate as well to the copper results in the blue shifting of the 460 nm peak and the loss of the 625 nm peak.[13] Little mention is made in these studies regarding the altered nature of the electronic transitions.

The above studies all show that the protein is a significant factor in determining ground- and excited-state properties of the copper site. In this paper, we examine the mode-specific nature of the protein's influence on the copper site properties with resonance Raman spectroscopy. Resonance Raman intensities provide detailed information about excited-state structure and dynamics on an extremely short time scale.[14] Resonant enhancement of those normal modes coupled to the electronic transition occurs when the exciting laser is tuned to a wavelength within an absorption band.[14] Measurement of the resonance Raman intensity of each

vibration as a function of excitation wavelength within an absorption band gives a set of resonance Raman excitation profiles. Self-consistent analysis of these resonance Raman excitation profiles and the absorption spectrum can yield such molecular parameters as the distortion along each normal mode upon photoexcitation, the homogeneous and inhomogeneous linewidths, and transition moment.[14] In a charge transfer absorption, resonance Raman intensities can also be used to partition the reorganization energy among the normal coordinates of the donor, acceptor, and solvent.[15-17]

In previous papers, we reported the use of resonance Raman and absorption spectroscopy to determine the mode-specific reorganization energies in a solute confined to a structurally well-defined solvent environment, specifically, the copper site in plastocyanins.[15,16] It was found that the reorganization energy of parsley plastocyanin is 0.19 eV along the resonance-enhanced Raman-active vibrations and 0.06 eV from a solvent-like dephasing component due to the protein.[15] The dephasing component was deduced from the homogeneous linewidth needed to reproduce the resonance Raman cross-section, after the term due to population relaxation was removed. The analysis indicated that the charge transfer absorption band was primarily homogeneously broadened, as a result of fast (20 fs) population relaxation and protein-induced dephasing (15 fs).[15]

A similar analysis has been done for spinach and poplar *a* plastocyanin in order to examine the role of structure and environment on the excited-state charge transfer process.[16] These two species gave values similar to parsley for many of the excited-state parameters such as the transition length, zero-zero energy, and homogeneous linewidth, reflecting the similar electronic nature of the excited-states. A surprising result was that the resonance Raman spectra of the three species show modes of similar frequency, but have significant differences in relative intensities. The experimental resonance Raman frequencies and molecular modeling indicated that the copper site environment and the ground-state geometry is similar in the two plastocyanins, but that the reorganization energy is probably distributed differently among the normal modes. Comparison of the amino acid sequence in the three

species using the experimentally-determined structure of poplar *a* plastocyanin show that these mode-specific excited-state changes occur as a result of an amino acid change ≥8 Å from the copper site.[16]

To better explore the relationship between protein composition, environment, and ground-state structure with excited-state structure and dynamics, we examine the excited-state charge transfer dynamics in azurin with resonance Raman and absorption spectroscopy in this paper. The total, mode-specific, charge transfer reorganization energy of 0.26 eV measured for azurin is significantly greater than the previously determined value of 0.19 ± 0.02 eV for the plastocyanins, probably indicating the effect of different coordination geometries in the two blue copper proteins. Partitioning of the spectral lineshape into homogeneous and inhomogeneous components is also different, with azurin having a more significant inhomogeneous contribution to the total spectral linewidth than plastocyanin. The increased inhomogeneous linewidth probably arises from hydrogen bonding at the copper site and/or conformational substates present in azurin. These results show the ability of resonance Raman spectroscopy to distinguish the important structural and environmental determinants of excited-state charge transfer dynamics.

2.2 Experimental

Preparation of azurin from *Pseudomonas aeruginosa* (ATCC 10145) was based on a modification of literature procedures.[18-20] Figure 2.2 is a flowchart showing the two preparation methods used for isolation of azurin. Briefly, cell cultures were grown anaerobically in 50-L batches and filtered. The resulting cell paste (typically 200 g) was either used immediately or frozen at -80 °C for later use. The cell paste was dried by using acetone and the resulting powder was extracted with buffer (0.1 M ammonium acetate, pH 6.5). The solids were removed by centrifugation and the supernatant was dialyzed against 0.05 M ammonium acetate (pH 4.0). The pH of the dialysate was adjusted to 4.0 and centrifuged. Azurin in the supernatant was oxidized by the addition of Na[Co(EDTA)] (~1 mg/g acetone powder) and purified by chromatography on CM-52 (Whatman), Sephadex G-50, and

Figure 2.2: Isolation and purification of azurin. The two methods are labeled by the species name; *Alcaligenes xylosoxidans* (AX), *Alcaligenes denitrificans* (AD) and *Pseudomonas aeruginosa* (PA). Columns are labeled as in text.

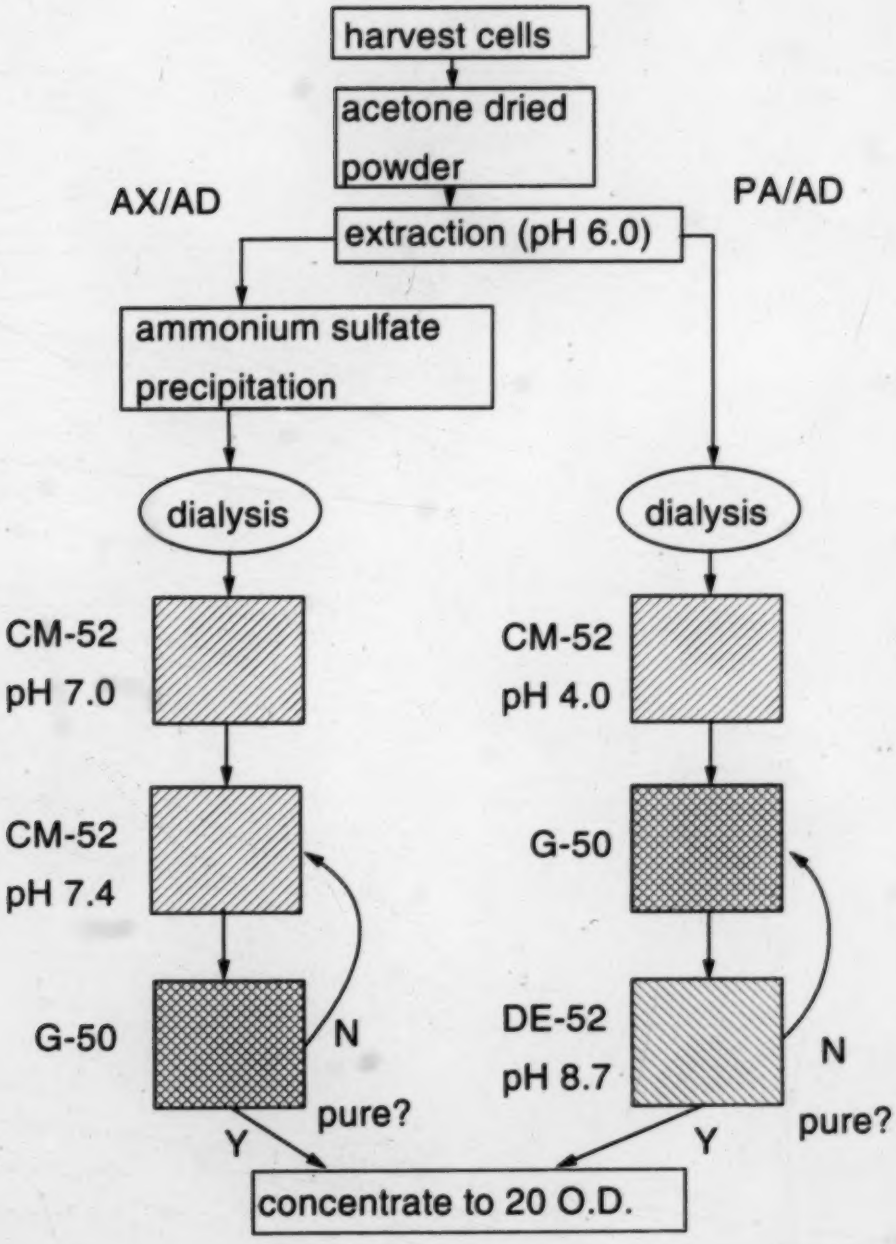
harvest cells
acetone dried powder
AX/AD
PA/AD
extraction (pH 6.0)
ammonium sulfate precipitation
dialysis
dialysis
CM-52 pH 7.0
CM-52 pH 4.0
CM-52 pH 7.4
G-50
G-50
DE-52 pH 8.7
N
N
pure?
pure?
Y
Y
concentrate to 20 O.D.

DE-52 (Whatman) columns. Additional G-50 and DE-52 columns were used to get a purity ratio (A_{280}/A_{625}) less than 2.1,close to the literature value of 1.7. A yield of 49-206 mg azurin per 100 g acetone powder was obtained using this method. The yield of azurin was found to be greatly dependent on the growth conditions of the bacteria; the yield was greatly reduced when the cells were over-grown.

Samples for the resonance Raman experiments were prepared by quantitative dilution of azurin with an internal standard, either a cacodylate/buffer solution (0.5-1.0 M cacodylic acid, 0.01 M TRIS-HCl, pH 8.7) or a nitrate/buffer solution (1.0 M potassium nitrate, 0.01 M TRIS-HCl, pH 8.7). Room-temperature resonance Raman spectra of azurin were obtained with 300 µL aqueous sample solutions (0.01 M TRIS-HCl buffer, either 0.375-0.8 M cacodylic acid or 0.8 M nitrate, pH 8.7) having an absorbance of 2.3-4.9 OD/cm at 625 nm (ε_{625} = 4800 $M^{-1}cm^{-1}$;[1,2,12] this is an average of the given literature values of 5200, 3500, 5700 $M^{-1}cm^{-1}$, respectively). The addition of cacodylic acid/cacodylate buffer did not have a noticeable effect on the absorption or resonance Raman spectra of azurin. Resonance Raman scattering was excited by spherically focusing the laser onto a spinning 5-mm o.d. NMR tube containing the sample solution in a 135° backscattering geometry (Figure 2.3). Laser excitation was obtained with Kr ion (Coherent, Santa Clara, CA), cw dye (Coherent), and HeNe lasers (PMS Electro-Optics, Boulder, Co). The wavelengths used were 530.9, 568.2, 647.1, and 676.4 nm (Kr^+), 589 and 614 nm (dye), and 594 and 612 nm (HeNe). The laser power was 100-130 mW (Kr^+, dye) or 7 mW (HeNe). Multichannel detection of resonance Raman scattering was obtained using a liquid nitrogen-cooled CCD detector (Princeton Instruments, Trenton, NJ) connected to the first half of a double monochromator (Spex Industries, Metuchen, NJ, model 1401). Frequency calibration was performed by measuring Raman scattering of solvents of known frequencies (benzene, chloroform, carbon tetrachloride and toluene). Frequencies are accurate to ±2 cm^{-1}. Absorption spectra were recorded on a diode array spectrophotometer (Hewlett Packard, Sunnyvale, CA, model 8452A). Measurement of the resonance Raman spectrum and determination of the intensities were repeated on 3-6 fresh samples of azurin for each wavelength.

Figure 2.3: Resonance Raman experimental setup.

(A) Schematic of experimental setup. Laser beams are directed to sample using mirrors.

(B) Close up of 135° backscattering geometry. Sample is in a spinning NMR tube.

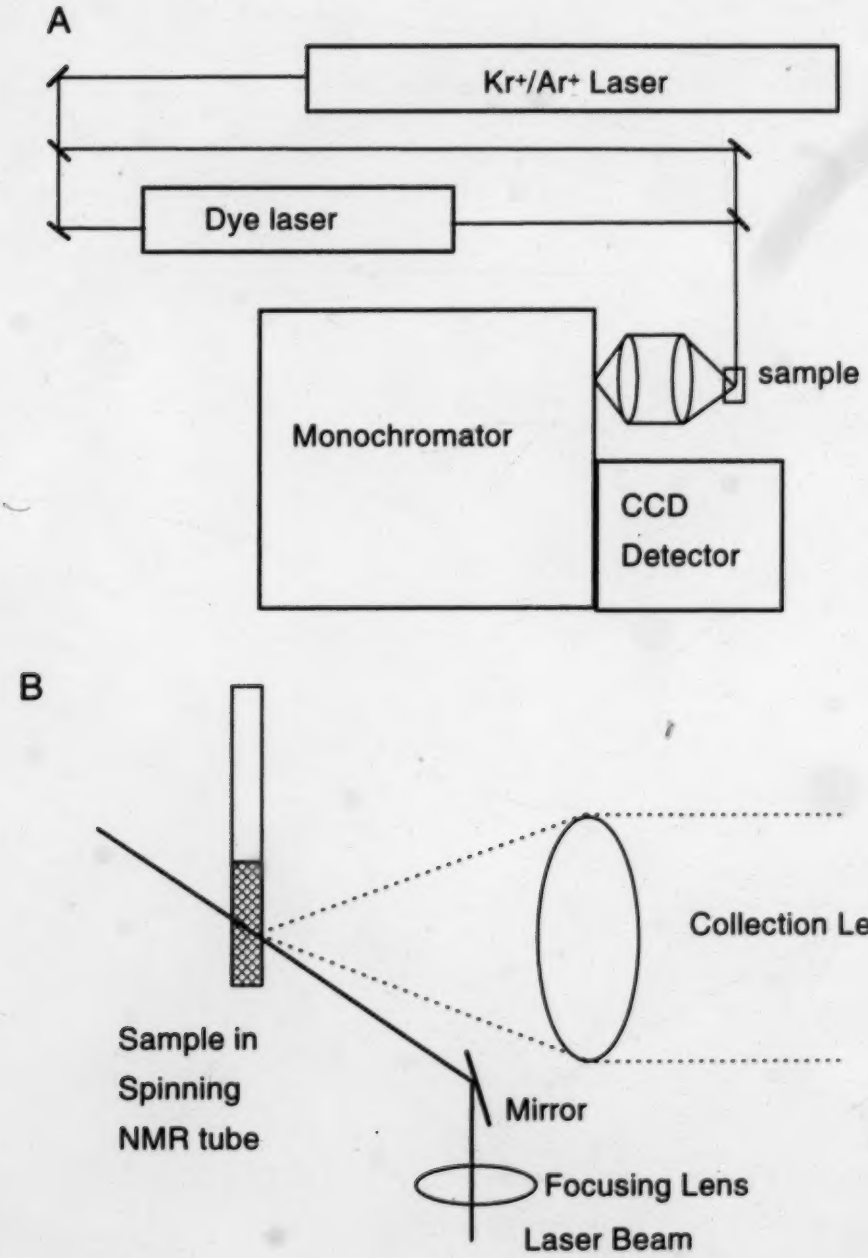
A
Kr+/Ar+ Laser
Dye laser
sample
Monochromator
CCD
Detector
B
Collection Lens
Sample in
Spinning
NMR tube
Mirror
Focusing Lens
Laser Beam

Analysis of the data was performed as previously described.[15] Bleaching of the sample was accounted for by measuring the absorbance at 580 nm (ε_{580} = 4494 $M^{-1}cm^{-1}$) before and after each scan. The absorption maximum was off-scale and so could not be measured accurately. The average absorbance was used to determine the concentration of azurin. The observed bleaching in a 90 min. scan was <3%, suggesting that the bulk photoalteration parameter[21] is small. The single-pass photoalteration parameter was estimated using the following:

$$F = \frac{2.303 \cdot 10^3 \varepsilon P \lambda t \phi}{N_A h c A} \qquad (2.1)$$

where ε is the molar extinction coefficient at the excitation wavelength, P and λ are the power and wavelength of the laser, t is the average time a molecule spends in the laser beam, ϕ is the quantum yield for the process which causes photoalteration, and A is the $1/e^2$ area of the laser beam. At a wavelength of 568 nm and typical experimental conditions, a value for ϕ of 0.014 was calculated from the average bleaching of the samples. The average time a molecule spends in the beam was estimated from the laser beam diameter (1.0 mm) and the spin rate of the sample tube (100 Hz). The single-pass photoalteration parameter, F, was found to be 0.7%, which was deemed negligible.

Absolute resonance Raman cross-sections were found from the relative integrated intensities using:[22]

$$\sigma_{az} = \frac{I_{az}\left(\frac{1+\rho}{1+2\rho}\right)_{cac}[cac]S_{cac}}{I_{cac}\left(\frac{1+\rho}{1+2\rho}\right)_{az}[az]S_{az}}\sigma_{cac} \qquad (2.2)$$

where I_{az} and I_{cac} are the integrated intensities of azurin and cacodylate, ρ is the depolarization ratio of the scattered light (ρ_{az} = 0.33 and ρ_{cac} = 0.18), [cac] and [az] are the concentrations of cacodylate and azurin, and S_{cac} and S_{az} are self absorption correction factors for cacodylate and azurin. The correction for differential self-absorption at the azurin (S_{az}) and cacodylate (S_{cac}) frequencies was calculated using[23]

$$S_i = \frac{[1-\exp\{-\ln(10)(\frac{k_0}{\cos\theta}+k_i)b\}]}{[(\ln(10)(\frac{k_0}{\cos\theta}+k_i)]} \qquad (2.3)$$

where $k_0 = \varepsilon_{laser}c$, $k_i = \varepsilon_i c$, c is the concentration of azurin, ε_{laser} and ε_i are the extinction coefficients at the laser and scattered wavelengths respectively, $\theta = 45°$ is the incident angle of the laser with respect to the sample tube, and b is the sample path length. The differential self-absorption corrections between the cacodylate line and the azurin lines were less than 15%.

Absolute total Raman cross-sections for cacodylate, the internal intensity standard used, were measured at pH 8.7 and compared to previous measurements[15] at pH 7.6 to determine their pH dependence. Cross-sections for cacodylate at pH 8.7 were measured by comparison with known values for nitrate[22] at 530.9, 568.2, 612, 647.1 and 676.4 nm, similar to that described previously.[15] The resulting experimental cacodylate cross-sections were (217 ± 2), (125 ± 6), (92.3 ± 5.5), (63.7 ± 2.4), and (68.9 ± .4) × 10^{-14} Å^2/molecule at 530.9, 568.2, 612, 647.1 and 676.4 nm, respectively. Because these experimental cross-sections obtained at pH 8.7 were identical to those obtained at pH 7.6, the cacodylate cross sections used for the determination of absolute cross sections for azurin were 168, 123, 105, 101, 88.2, 86.9, 68.8, and 56.6 × 10^{-14} Å^2/molecule at 530.9, 568.2, 589, 594, 612, 614, 647.1, and 676.4 nm, respectively, the same as those obtained previously.[15]

2.3 Theory

The resonance Raman and absorption cross sections in the Condon approximation can be written using the time dependent equations of Lee and Heller.[14,15,24]

$$\sigma_R = \frac{8\pi E_S^3 E_L e^4 M^4}{9\hbar^6 c^4} \int_{-\infty} H(E_0)\ dE_0 \times \left| \int_0^{\infty} \langle f | i(t) \rangle\ e^{\frac{i(E_L+\varepsilon_i)t}{\hbar}}\ G(t)dt \right|^2 \qquad (2.4)$$

$$\sigma_A = \frac{4\pi e^2 M^2 E_L}{6\hbar^2 cn} \int_{-\infty} H(E_0)\ dE_0 \times \int_{-\infty} \langle i|i(t)\rangle\ e^{\frac{i(E_L+\varepsilon_i)t}{\hbar}}\ G(t)\ dt \qquad (2.5)$$

where E_L and E_S are the energies of the incident and scattered photons, M is the transition length, n is the refractive index, G(t) is a decay function, $H(E_0) = (1/[\theta(2\pi)^{1/2}])\exp[-(E_0 - \overline{E_0})^2/2\theta^2]$ is a normalized Gaussian distribution of site electronic energies, ε_i is the energy of the initial vibrational state, $|i\rangle$ and $|f\rangle$ are the initial and final vibrational wavefunctions in the resonance Raman process, and $|i(t)\rangle = e^{-iHt/\hbar}|i\rangle$ is the initial ground vibrational wavefunction propagated on the excited-state potential surface. The $\langle i|i(t)\rangle$ absorption overlap in Equation 2.4 is the product of one-dimensional $\langle i|i(t)\rangle$ overlaps for each normal mode, while the $\langle f|i(t)\rangle$ Raman overlap in Equation 2.5 is the product of $\langle f|i(t)\rangle$ along the Raman-active mode and $\langle i|i(t)\rangle$ along all other modes. In this treatment, the $\langle i|i(t)\rangle$ and $\langle f|i(t)\rangle$ overlaps are dependent only on the displacement, Δ, between ground- and excited-state equilibrium geometries along each normal coordinate. The implementation of these equations has been described in detail.[14-16,22] Self-consistent analysis of the absorption spectrum and the resonance Raman excitation profiles was done in the same manner as previously described for plastocyanin.[15,16].

Resonance Raman involves scattering of the incident photon from the excited electronic state. Because this process involves the excited electronic state, the intensities are sensitive to such excited-state parameters as the homogeneous and inhomogeneous linewidths, and changes in the equilibrium structure.[14-16] The homogeneous linewidth represents contributions from excited-state population decay and dephasing which occur on the timescale of the resonance Raman scattering, ~20 fs for azurin. As the homogeneous linewidth increases, the absorption spectrum broadens and becomes more diffuse. The resonance Raman excitation profiles also broaden and become more diffuse, but they also decrease in magnitude. The

inhomogeneous linewidth is presumed to be due to probing an ensemble of molecules with different zero-zero energies which are considered to be static on the timescale of the resonance Raman scattering. The inhomogeneous linewidth affects both the absorption spectrum and the resonance Raman excitation profiles in a similar fashion: as the inhomogenous linewidth increases they both become broader and more diffuse but the integrated intensity remains constant.

2.4 Results

The resonance Raman spectra of azurin at excitation wavelengths throughout the S(Cys)→Cu absorption band are shown in Figure 2.4. No reproducible peaks were observed at frequencies of less than 200 cm^{-1}; the single monochromator used to obtain the spectra was unable to separate the Rayleigh scattering from the low frequency Raman signal. The intensity standard (cacodylate) appears at 605 and 638 cm^{-1}, marked with single asterisks in the figure. The intense bands between 340 and 440 cm^{-1} have been previously assigned to normal modes involving the Cu–S stretch mixed with other internal coordinates.[25-28] However, the exact assignments are still controversial.[25] The bands at 216 and 263 cm^{-1} have been assigned to modes involving the Cu–N stretches.[25] The broad band at about 830 cm^{-1}, marked by double asterisks in the figure, is due to combination and overtone bands of the vibrations between 340 and 440 cm^{-1}. There is also a contribution at 825 cm^{-1} from the As=O stretch of cacodylate.[29,30] Note in Figure 2.4 that the relative intensities of the azurin vibrations remain constant with respect to each other as the excitation wavelength is scanned through the absorption band. This indicates that all of the observed modes are coupled to a single electronic transition, namely the S(Cys-π)→Cu charge transfer transition.

The depolarization ratios of azurin were measured at excitation wavelengths of 647.1 nm and 568.2 nm, on the red and blue edges of the putative S(Cys-π)→Cu charge-transfer transition. The relative intensities of the azurin peaks did not change when the polarized spectra were measured, indicating that all the azurin modes have identical polarization ratios. The depolarization ratios were found to be 0. 40 ± 0.08,

Figure 2.4: Resonance Raman spectra of *P. aeruginosa* azurin at excitation wavelengths throughout the 625 nm absorption band. The spectra are the sum of three to six scans. The vibrations between 200 and 500 cm^{-1}, and the peak at 654 cm^{-1} were used in the analysis. Raman scattering of the internal intensity standard (cacodylate) is observed at 608 and 638 cm^{-1} (*). The broad band at ~820 cm^{-1} and the narrower band at 754 cm^{-1} (**) are composed of the overtones and combinations of the azurin vibrations between 350 and 500 cm^{-1} and a cacodylate peak at 825 cm^{-1}. The spectra are scaled to the intensity of the most intense azurin peak and offset for clarity.

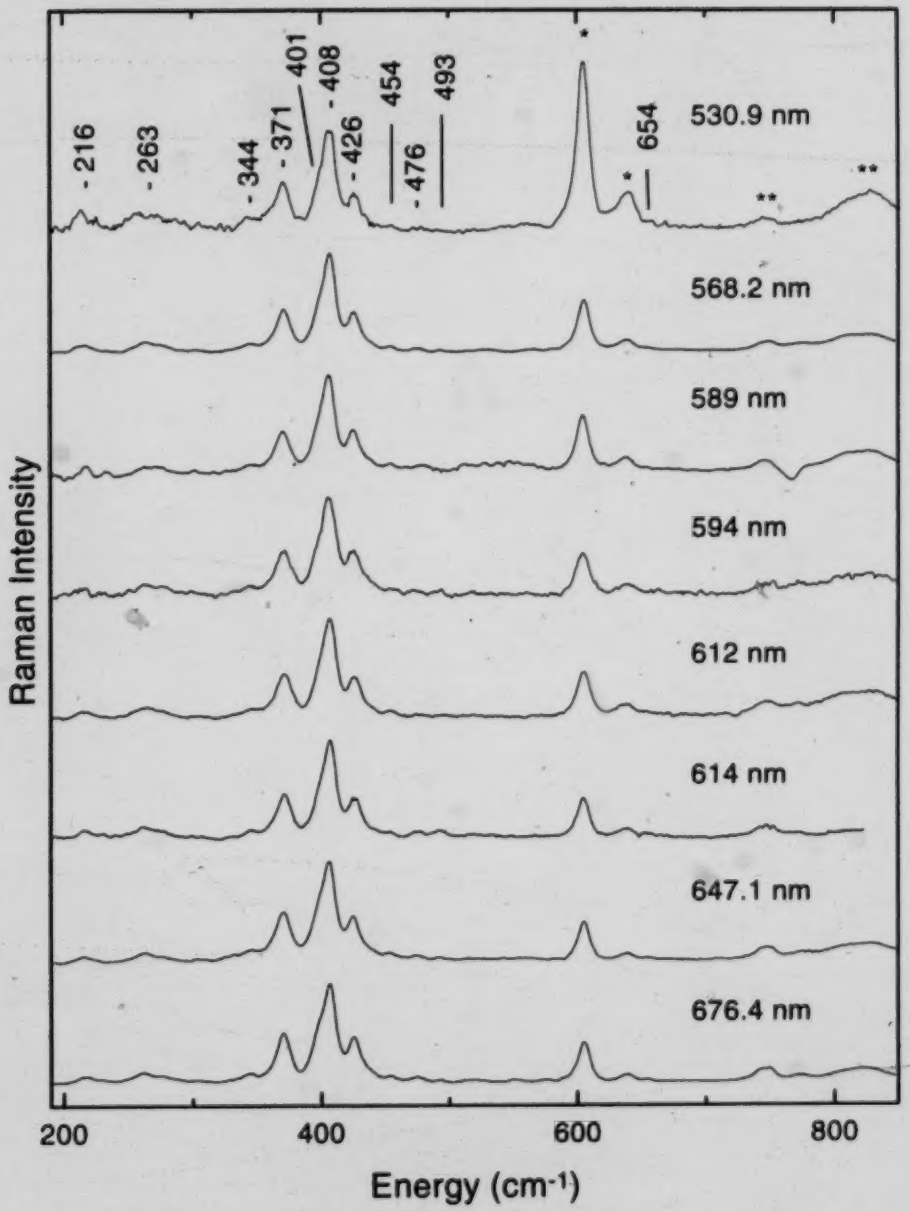
- 216
- 263
- 344
- 371
401
- 408
- 426
454
- 476
493
*
654
*
**
**
530.9 nm
568.2 nm
589 nm
594 nm
612 nm
614 nm
647.1 nm
676.4 nm
Raman Intensity
200
400
600
800
Energy (cm-1)

independent of wavelength. This is consistent with there being only a single electronic transition which enhances the Raman scattering and agrees with the expected value of 0.33 within the experimental error.

Figure 2.5 shows the deconvolution of the observed bands into individual vibrational transitions. The frequencies of the resulting peaks correspond well to those previously reported at low temperature, at which the bands are better resolved.[25] Note that the deconvolved peaks all have approximately the same linewidth, suggesting that they are an accurate reflection of the individual transitions. For the deconvolution of all spectra in this paper, the positions, widths, and shapes of the component peaks were kept constant; only the heights were allowed to vary to obtain an optimum fit to the observed spectrum.

The experimental and calculated absolute resonance Raman cross sections are summarized in Table 2.1. Figure 2.6 and Figure 2.7 show the good agreement of the experimental and calculated absorption spectra and resonance Raman excitation profiles. The parameters used for the calculated curves are given in Table 2.1. Deviations of the experimental absorption spectra from the calculated absorption spectrum at both higher and lower energies are due to the presence of other charge-transfer and ligand field transitions which were not modeled and apparently contribute no resonance enhancement to the observed normal modes (see above). The resonance Raman excitation profiles have a maximum intensity at ~610 nm which is significantly blue-shifted from the absorption maximum of 628 nm and are also narrower than the absorption band. These two results are consistent with there being more than one electronic transition within the absorption band. Due to the presence of more than one electronic transition within the charge-transfer absorption band, the resonance Raman excitation profiles provided the primary constraints on the simulated spectral bandshape and bandwidth. Thus, scaling of the Δ's was determined by the width of the resonance Raman excitation profiles. In the simulations, it was necessary to use significant amounts of inhomogeneous broadening, in addition to homogeneous broadening, to reproduce the large resonance Raman cross sections and diffuse absorption band. Figure 2.6 shows the best fit using a Gaussian (dashed line)

Figure 2.5: Deconvolution of the 300 to 500 cm^{-1} region of *P. aeruginosa* azurin. The experimental data is shown as a solid line that is very closely overlapped by the sum (dashed curve) of the individual peaks (dotted lines). The very close agreement of the experimental and calculated values results in the dashed curve being almost invisible in this figure.

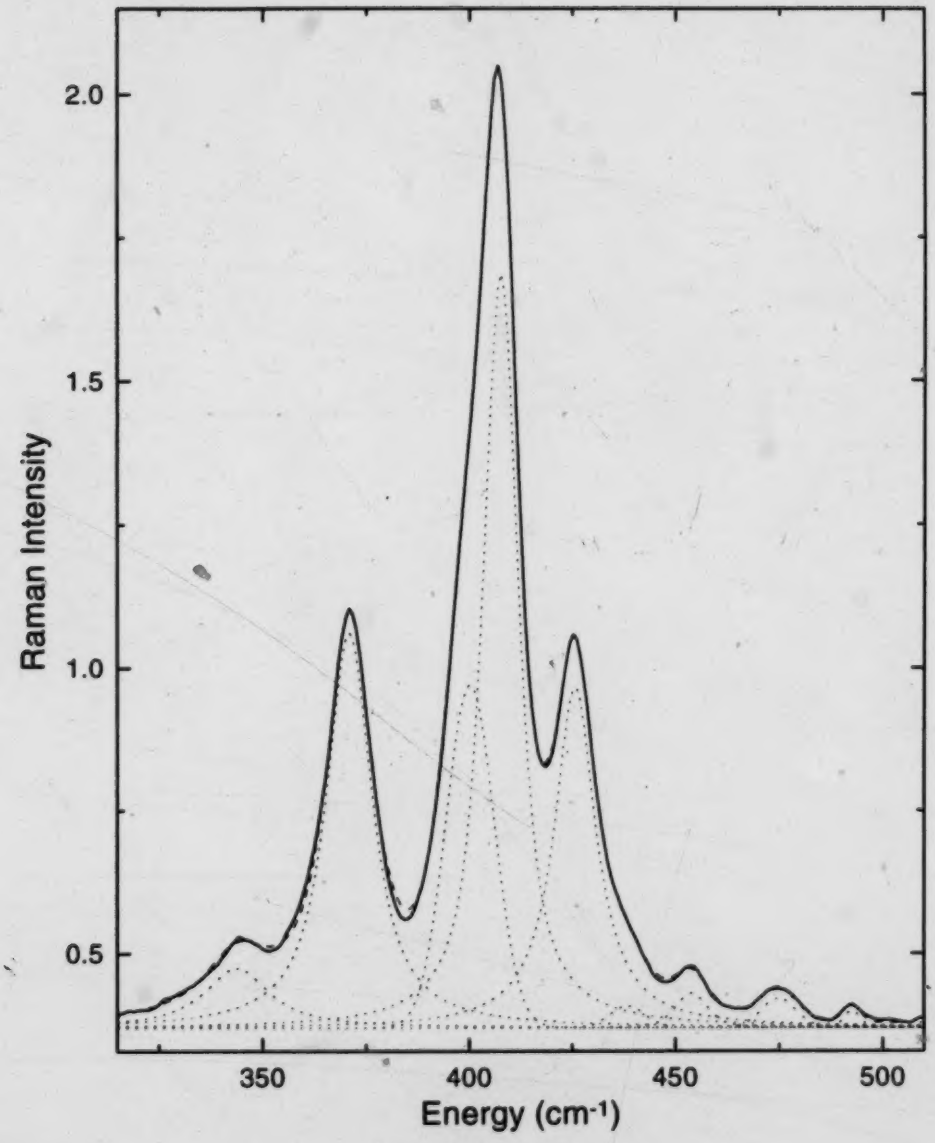
2.0
1.5
1.0
0.5
Raman Intensity
350
400
450
500
Energy (cm-1)

Table 2.1: Absolute resonance Raman cross sections of *P. aeruginosa* azurin.

		excitation wavelength/nm							
$\Delta\nu/cm^{-1}$	$\lvert\Delta\rvert$	530.9	568.2	589	594	612	614	647.1	676.4
216	0.85	0.53/0.12	0.61/0.51	0.83/0.82	---/0.88	1.22/1.03	0.63/1.04	0.68/0.78	0.47/0.34
263	1.26	1.07/0.40	1.30/1.67	1.81/2.68	3.33/2.87	2.96/3.30	2.73/3.31	1.56/2.42	1.06/1.05
344	0.75	0.50/0.26	0.99/1.04	1.37/1.63	1.86/1.74	1.90/1.95	1.93/1.95	1.42/1.36	0.95/0.57
371	1.60	1.71/1.45	4.64/5.65	7.05/8.66	9.39/9.18	9.12/10.1	10.3/10.0	6.29/6.80	4.52/2.79
401	1.22	1.04/0.96	3.08/3.81	5.89/5.90	6.87/6.26	6.33/6.94	6.95/6.92	4.53/4.71	3.28/1.94
408	1.64	2.38/1.80	6.79/7.15	9.14/11.0	12.0/11.7	12.2/13.0	13.6/12.9	7.01/8.76	4.73/3.60
426	1.26	1.18/1:17	3.91/4.63	5.03/7.12	8.36/7.54	7.39/8.30	8.24/8.29	4.98/5.57	3.54/2.27
439	0.23	0.01/0.04	0.14/0.16	0.32/0.25	---/0.27	0.24/0.29	0.29/0.29	0.18/0.20	0.14/0.08
454	0.31	0.07/0.08	0.28/0.31	0.54/0.47	0.53/0.50	0.51/0.55	0.45/0.55	0.49/0.36	0.23/0.15
476	0.27	0.06/0.07	0.21/0.27	---/0.41	0.46/0.43	---/0.47	---/0.47	0.28/0.31	0.21/0.12
493	0.13	---/0.02	0.06/0.07	---/0.10	---/0.11	---/0.12	---/0.12	0.06/0.08	0.04/0.03
654	0.18	0.14/0.06	0.19/0.24	0.05/0.34	---/0.36	0.33/0.37	0.37/0.37	0.30/0.23	0.16/0.08

The resonance Raman cross sections are shown as experimental/calculated in units of $Å^2$/molecule $\times 10^{10}$. A --- indicates no signal was observed above the baseline noise and no cross section was measured. The errors in cross sections are ±10% for strong lines and ±20% for weak lines. The Δ's are in dimensionless normal coordinates. The cross sections were calculated with Equation 2.4 using the following parameters: zero-zero energy, E_0 = 14,200 cm^{-1}, transition length, M = 0.63 Å, temperature, T = 0 K, refractive index, n = 1.33, Lorentzian homogeneous linewidth, Γ = 160 cm^{-1}, inhomogeneous linewidth, Θ = 280 cm^{-1}.

Figure 2.6: Experimental (solid line) and calculated (dashed/dotted lines) absorption spectra of *P. aeruginosa* azurin. The dotted line was calculated using a Lorenztian homogeneous lineshape and the dashed line was calculated using a Gaussian homogeneous lineshape. Deviations of the experimental absorption spectrum from the calculated absorption spectra at both higher and lower energies are due to the presence of other charge-transfer and ligand field transitions which were not modeled and apparently contribute no resonance enhancement to the observed normal modes. Note the better reproduction of the blue edge of the absorption spectrum with the Lorentzian lineshape.

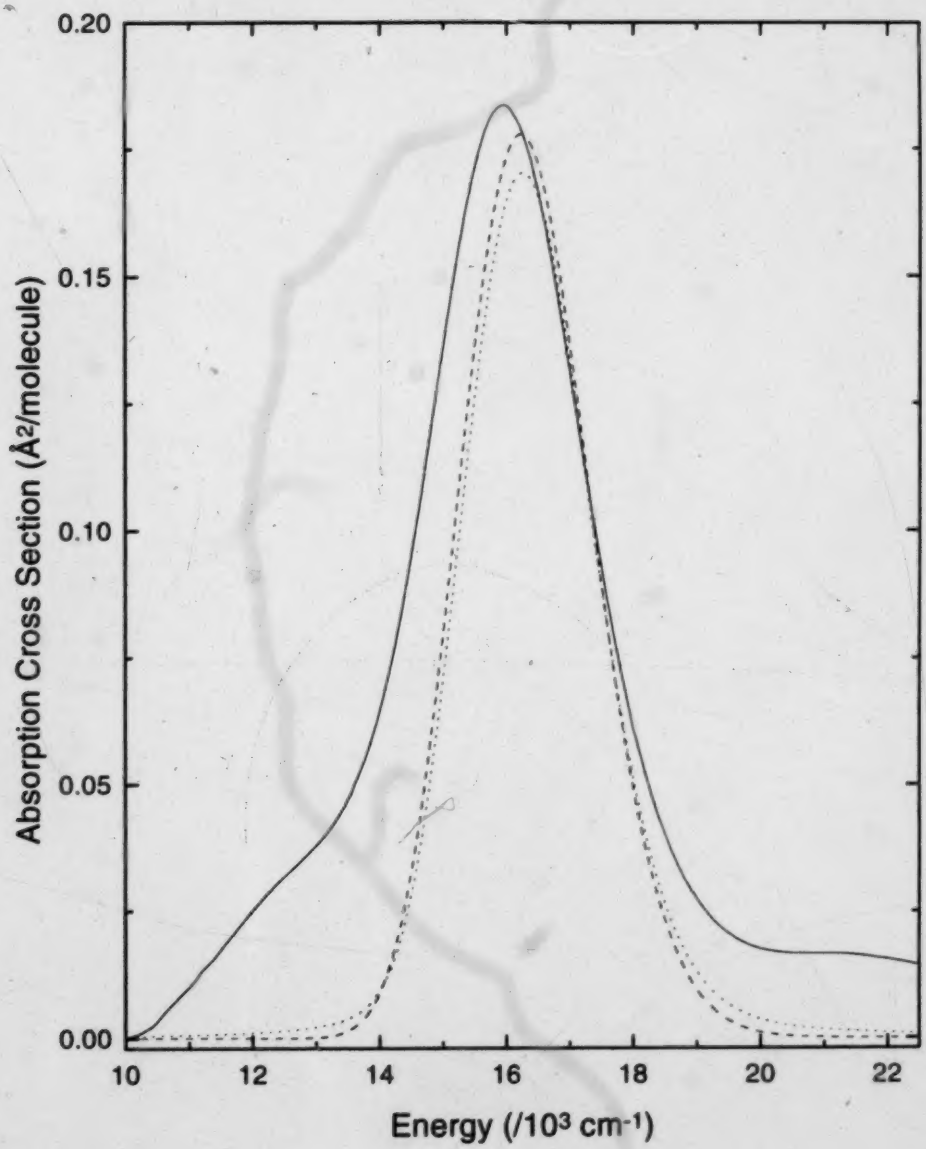
0.20
0.15
0.10
0.05
0.00
Absorption Cross Section (Å2/molecule)
10
12
14
16
18
20
22
Energy (/10³ cm⁻¹)

Figure 2.7: Resonance Raman excitation profiles. Experimental (points) and calculated (solid line) resonance Raman excitation profiles of *P. aeruginosa* azurin. The excitation profiles were calculated with Equation 2.4 using the parameters in Table 2.1.

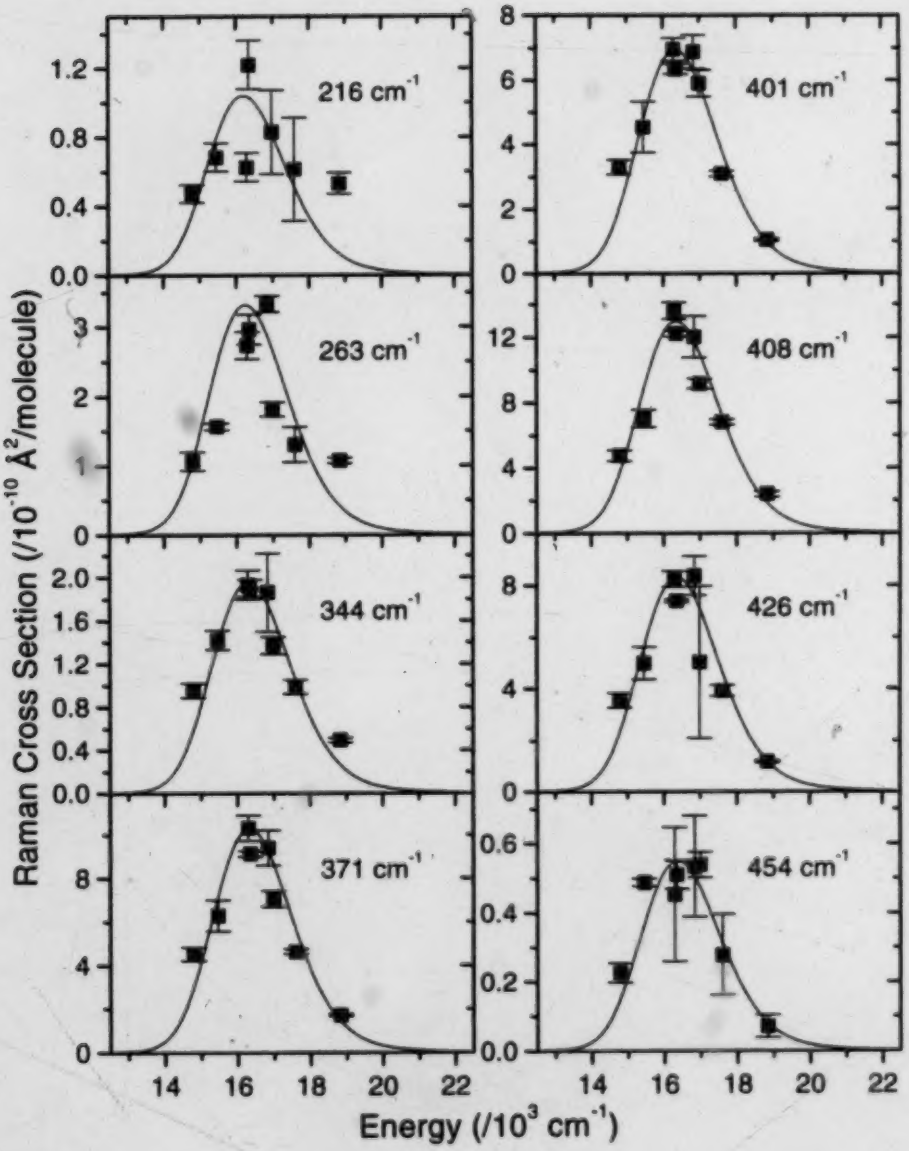
216 cm-1
401 cm-1
263 cm-1
408 cm-1
344 cm-1
426 cm-1
371 cm-1
454 cm-1
Raman Cross Section (/10-10 Å2/molecule)
Energy (/103 cm-1)

and Lorentzian (dotted line) lineshape to model the absorption spectrum. A Lorentzian homogeneous function was found to fit the shape of the absorption band better than a Gaussian function, although the bandshape was under-constrained by the experimental data. The molecular mechanism of these different lineshapes is discussed below.

The intensities of the overtone and combination bands were measured at 647.1 nm using nitrate as the internal standard (0.8 M nitrate, 0.01 M TRIS-HCl, pH 8.7) as a check on the resonance Raman intensity analysis (Figure 2.8). Measurement of the overtone and combination band intensities provide an additional constraint on the excited-state frequencies assumed in the calculations. The nitrate peak appears at 1049 cm^{-1} and is marked with an asterisk in the figure. The bands in this region have been assigned[25] to a C–S fundamental band at 753 cm^{-1} and various overtone and combination bands from 740 to 900 cm^{-1} arising from the intense mode at 408 cm^{-1}. The fundamental band at 753 cm^{-1} is overlapped by the overtone of the 371 cm^{-1} mode at 742 cm^{-1} and appears as one peak at ~749 cm^{-1}. Because the resonance Raman spectra were taken at room temperature, we were unable to resolve the overtone and combination bands into individual vibrational transitions. Small peaks were observed at frequencies greater than 900 cm^{-1} (marked with **). However, these bands were not reproducible in either intensity or position and so were not used for this analysis. The overall intensity of the overtone region from 760 to 900 cm^{-1} was calculated to be 7.58×10^{-10} cm^2/molecule, using Equation 2.4 and the parameters in Table 2.1, which is in agreement with the measured value of 5.97×10^{-10} cm^2/molecule, within experimental error. The band at ~749 cm^{-1} was not used in comparing the calculations and experimental data, as it has been assigned[25] to an overlap of an overtone (743 cm^{-1}) and a fundamental (753 cm^{-1}) and we were unable to resolve them.

Figure 2.8: Resonance Raman of overtone/combination bands using an excitation wavelength of 647.1 nm. The spectrum is the sum of three scans. Raman scattering of the internal standard (nitrate) is observed at 1049 cm^{-1} (*). Small peaks were observed at ~1150 - 1200 cm^{-1} (**) which were not reproducible. The feature at ~950 cm^{-1} (++) is an artifact of the CCD detector.

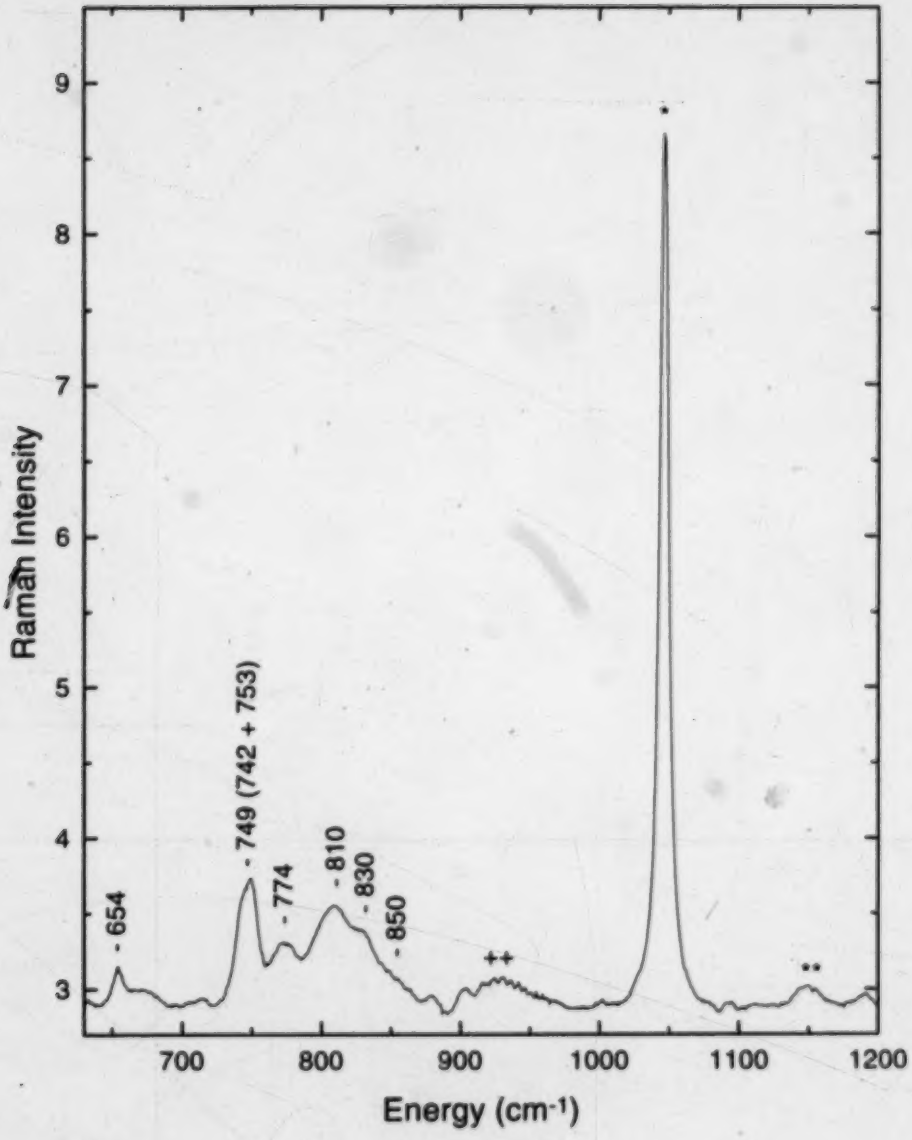
Raman Intensity
Energy (cm-1)
- 654
- 749 (742 + 753)
- 774
- 810
- 830
- 850
++
*
**

2.5 Discussion

2.5.1 Comparison to Plastocyanin

The primary goal of this work is to determine the role of structure and environment on the dynamics of excited-state charge transfer. This has been done previously for a series of plastocyanins in which the structure and environment were not significantly different near the copper site, in order to explore the effects of remote differences (i.e. at distances ≥ 8 Å).[16] In this section, a comparison of the excited-state charge transfer dynamics in plastocyanin and azurin is performed to examine the role of coordination geometry and hydrogen-bonding in the immediate vicinity of the copper site.

A comparison of the excited-state parameters of azurin and plastocyanin is shown in Table 2.2. The zero-zero energy, E_0, and the transition length, M, of azurin are both found to be different than those of plastocyanin. These differences can be easily attributed to structural differences around the copper metal center. The transition length of azurin is 0.05 Å larger than that of plastocyanin, which is somewhat close to the 0.13 Å difference in the Cu–S(Cys) bond length between the two proteins from x-ray crystallography.[5,31] This result suggests that roughly the same amount of charge is transferred in the two proteins. Apparently, the coupling between the copper and sulfur is strong enough that the transition dipole qualitatively increases with increasing distance between donor and acceptor. The zero-zero energy of azurin is found to be 1150 cm^{-1} lower than that of plastocyanin, which is consistent with the observed 750 cm^{-1} shift of the absorption band maximum of azurin to lower energy. The additional 400 cm^{-1} shift is due to the greater Δ's in azurin (see below).

The absorption band of plastocyanin was found to be primarily homogeneously broadened, in contrast to azurin which has significant inhomogeneous broadening. Plastocyanin was found to have a total phenomenological Gaussian homogeneous linewidth of 385 cm^{-1} while azurin has a mixture of Lorentzian homogeneous (160 cm^{-1}) and Gaussian inhomogeneous linewidths (280 cm^{-1}). This difference in partitioning of the broadening among homogeneous and inhomogeneous

Table 2.2: Comparison of the excited-state charge-transfer parameters for azurin.

	Azurin[a]	*Plastocyanin*[b]
E_0 (cm^{-1})	14200 ± 140	15350 ± 150
M (Å)	0.63 ± 0.01	0.581 ± 0.01
Θ (cm^{-1})	280 ± 14	0
Γ_G (cm^{-1})	0	385 ± 19
Γ_L(cm^{-1})	160 ± 8	0

In this table, E_0 is the zero-zero energy, M is the transition length, Θ is the inhomogeneous linewidth, and Γ_G and Γ_L are the Gaussian and Lorentzian homogeneous linewidths, respectively.

[a] Values from this work. [b] Values from ref. 15.

components is real and is probably due to environmental differences in the two proteins. It has been suggested that azurin has three conformational substates from the multi-exponential fluorescence decay of Trp48.[32-34] Similar studies have not been done on plastocyanin. Fluctuations between these conformational substates can contribute to the inhomogeneous and homogeneous broadening depending on the timescale of the fluctuations. The resonance Raman scattering occurs within the total optical dephasing time of ~30 fs, as determined here by the homogeneous linewidth. This is on the order of a vibrational period for a high-frequency mode (~1000 cm^{-1}), much higher than would be expected for global conformational changes in the protein. Therefore, we expect conformational substates to contribute to the inhomogeneous linewidth (i.e. the protein should be static on the timescale of resonance Ramanscattering). An additional factor in the broadening mechanism is the role of the hydrogen bonding environment. In azurin and plastocyanin the orientation of the ligands are tightly constrained by the surrounding protein structure.[4,31] In both proteins, five hydrogen bonds, including a hydrogen bond between an Asn (azurin: Asn47; plastocyanin: Asn38) and the metal-coordinating Cys, determine the shape of the protein folding in the region of the metal center and the separation of histidine and cysteine. However, azurin also contains a second hydrogen bond between the peptide NH of Phe114 and the metal-coordinating Cys, whereas this Cys in plastocyanin has only the Cys–Asn hydrogen bond. This additional hydrogen bond in azurin may increase the inhomogeneous broadening in the S(Cys-π)→Cu charge-transfer absorption. In solvents which undergo hydrogen bonding with solutes, broad bands are seen in the vibrational spectrum due to an inhomogeneous distribution of different hydrogen-bonding environments.

Although we attempted to measure the fluorescence spectrum of azurin, no detectable fluorescence was observed at energies above 13,500 cm^{-1}, the lower limit of our detection system (data not shown). Taking three times the standard deviation of the noise observed in an earlier measurement of the fluorescence of plastocyanin[15] as the minimum measurable signal, gives a lower detection limit of the fluorescence quantum yield of $\Phi_F = 1 \times 10^{-7}$. We may not have observed a fluorescence signal

because the fluorescence spectrum may be shifted to lower energies than we were able to detect. The absorption maximum of azurin is shifted 750 cm^{-1} to lower energies than that of plastocyanin. If the fluorescence maximum is shifted by the same amount from the observed fluorescence maximum of plastocyanin, the expected fluorescence maximum for azurin would be approximately 13250 cm^{-1}. If the plastocyanin fluorescence signal is shifted 750 cm^{-1} to the red, we should still be able to observe the blue edge of the fluorescence band, within the noise limit described above. However, this assumes the Stokes shifts in the two proteins are the same. The Stokes shift for azurin is expected to be larger due to the larger Δ's, resulting in the fluorescence being shifted to even lower energies than predicted from the observed absorption band shift. By comparing the difference in the zero-zero energy (1150 cm^{-1}) of the two proteins, the increase in Stokes shift is about 400 cm^{-1} in azurin. This would shift the fluorescence maximum of azurin to 12,800 cm^{-1}, compared to ~14,000 for plastocyanin. With the fluorescence shifted so far to the red, we would not expect to see any fluorescence from azurin within our experimental detection limit.

2.5.2 Reorganization Energy

Comparison of the mode-specific reorganization energies in azurin and plastocyanin reveals some interesting similarities and differences. Table 2.3 compares the resonance Raman frequencies and mode-specific reorganization energies, as calculated from the observed Δ's, of azurin and plastocyanin. In both proteins the majority of the resonance Raman intensity is in bands between 300 and 450 cm^{-1}. These bands have been assigned to the Cu–S(Cys) stretch coupled to other internal coordinates.[25] Most (85%) of the reorganization energy in azurin occurs in modes between 300 and 500 cm^{-1}. This is similar to plastocyanin, in which modes between 350 and 500 cm^{-1} contribute 90% of the reorganization energy, although it appears to be spread over fewer modes in plastocyanin. Smaller contributions (15%) to the reorganization energy in azurin are made by the modes at 216, 263 and 654 cm^{-1}. A number of modes of azurin and plastocyanin have similar frequencies (Table 2.3). This is expected, since the resonance Raman spectra of eleven blue copper

Table 2.3: Mode-specific reorganization energies of azurin and plastocyanin.

Azurin[a]			Plastocyanin[b]		
$\Delta\nu/cm^{-1}$	$\lvert\Delta\rvert$	λ/cm^{-1}	$\Delta\nu/cm^{-1}$	$\lvert\Delta\rvert$	λ/cm^{-1}
216	0.85	78			
263	1.30	220	266	0.98	130
344	0.75	100			
371	1.60	470	376	1.40	370
401	1.20	290	390	1.20	280
408	1.60	520	403	0.49	48
426	1.30	360	421	1.40	410
439	0.23	12	436	0.98	210
454	0.31	22			
476	0.27	17	473	0.24	14
493	0.13	4			
654	0.18	11			
			759	0.35	46
Total		2100 cm^{-1}			1500 cm^{-1}

Δ's are in dimensionless normal coordinates. The reorganization energy in a particular mode, λ_i, is related to Δ_i by $\lambda_i = (\Delta_i^2\omega_i)/2$ where ω_i is the frequency in cm^{-1}.
[a] Values for azurin from this work. [b] Values for plastocyanin from ref 15.

proteins all show vibrational modes between 350 and 500 cm^{-1}, albeit with different relative intensities.[2] However, the reorganization energy in the two proteins is significantly different along modes with similar frequencies, reflected in the very different absolute resonance Raman cross sections, with those of azurin often being substantially higher than those of plastocyanin. The total reorganization energy from all of the observed Raman modes is significantly larger in azurin than in plastocyanin (0.26 eV compared to 0.19 eV). For modes of similar frequency, azurin generally has greater reorganization energy. For example, the reorganization energy for the 408 (403) cm^{-1} mode of azurin (plastocyanin) is 520 (48) cm^{-1}. An exception to this observation is the 439 (436) cm^{-1} mode of azurin (plastocyanin) in which the reorganization energy is 12 (210) cm^{-1} for azurin (plastocyanin). The greater total reorganization energy in azurin is expected, as there is an additional ligand bound to the copper in azurin. Increasing the number of atoms in the coordination sphere is expected to increase the number of vibrational modes and the total reorganization energy, since it generally takes more energy to reorganize the nuclei of five ligands than four upon charge transfer. If we assume that the reorganization energy is proportional to the number of atoms directly ligated to the copper ion, we would predict that azurin would have a reorganization energy of 0.19 eV × 5/4 = 0.24 eV compared to plastocyanin. This is close to the value of 0.26 eV that is observed experimentally.

Increased reorganization in azurin may also indicate that the vibrational modes are more strongly coupled to the charge transfer than those of plastocyanin. Stronger coupling would result in larger displacements of the modes in the charge-transfer excited state and therefore a higher reorganization energy. A possible explanation of stronger coupling in azurin is the stiffness of the copper site. Studies of the x-ray crystal structure of the apoprotein suggests that the protein determines the coordination geometry at the copper site.[35-37] Structural changes at the copper site could induce structural changes to the protein backbone and affect side-chain vibrations coupled to the local motions. The metal center of azurin is expected to be more rigid than that of plastocyanin due to an additional copper coordination bond to

a carbonyl group and an additional hydrogen bond between Cys and the backbone NH of Phe114. Increased rigidity of the copper site would increase the mechanical coupling to the protein backbone and increase coupling to local motions.

The calculated reorganization energy can be compared to the upper limit reorganization enthalpy at the copper site of 0.3 eV measured for electron transport,[38] corresponding to a reorganization energy of 1.2 eV. However, this reorganization energy is measured for the process in which one electron is transferred. Assuming that the reorganization energy scales approximately linearly with the amount of charge transferred and using the value of ~25% of a charge shift between the ground and excited state,[39] we suggest that the total, mode-specific reorganization energy measured here of 0.26 eV is in good agreement with the upper limit value of 0.3 eV.[38]

In plastocyanin, a Brownian oscillator model was used to represent the contribution of the solvent environment to the homogeneous linewidth[40,41] where G(t) = exp{-g(t)}, g(t) = $g_R(t) + ig_I(t)$, and

$$g_R(t) = \left(D^2/\Lambda^2\right)\left[\exp(-\Lambda t/\hbar) - 1 + \Lambda t/\hbar\right] \qquad (2.6)$$

$$g_I(t) = \left(D^2/2kT\Lambda\right)\left[1 - \exp(-\Lambda t/\hbar)\right] \qquad (2.7)$$

In this model D is the coupling strength between the electronic and solvation coordinates, $\hbar/\Lambda$ is the characteristic time of the solvation modulation, and the solvent reorganization energy is $D^2/2kT$. A Lorenztian linewidth of 160 cm^{-1} can be approximately modeled using Equation 2.6 and Equation 2.7 with D = 630 cm^{-1} and Λ = 2400 cm^{-1}, yielding a solvent reorganization energy of 0.12 eV. This is twice the 0.06 eV which was determined for plastocyanin.[15] This suggests that the solvent reorganization energy of azurin may be greater than that of plastocyanin. However, the above calculation neglects population decay and assumes that the entire linewidth is due to solvent-induced dephasing. Because the population decay rate has not been measured for azurin, a direct comparison is difficult.

2.5.3 Normal Modes

This analysis provides a quantitative measurement of the reorganization energy along each resonance Raman active mode. A normal coordinate analysis is necessary to determine the contributions of each internal coordinate (i.e. stretch, bend, etc., of individual bonds) to the reorganization energy. This analysis is important to perform since the observed differences in the resonance Raman intensity pattern and mode-specific reorganization energies of the two proteins may be due to differences in the normal mode descriptions. A normal coordinate analysis is difficult to complete for azurin and plastocyanin due to the difficulty in preparing isotopic derivatives and the lack of model compounds that have similar electronic and vibrational properties. However, some information has recently become available for the normal mode description of blue copper proteins. Recently, some resonance Raman spectra have been reported for isotopically-substituted azurin,[26] plastocyanin,[28] and a model compound[42] with similar electronic and vibrational properties to blue copper proteins. These studies suggest that the Cu–S internal coordinate is highly coupled to bending coordinates of Cys112 to form the normal modes grouped between 340 and 500 cm^{-1}. In this picture, the resonance-enhanced normal modes arise from internal coordinates localized on the immediate coordination ligands. However, a normal coordinate analysis based on the crystallographic structure with a number of simplifications has been done on 169 atoms around the copper metal site in three Type 1 copper proteins[43] and predicts that protein motions far from the copper site may be coupled to the resonance-enhanced normal modes. This theoretical model was supported by a recent study of the resonance Raman intensities for a homologous series of plastocyanins[16] that found that significant changes in reorganization energy along specific normal modes occur for plastocyanins which have identical structures and amino acid compositions up to 8 Å from the copper site. This study suggests that protein vibrations far from the copper site are coupled to the local motions such as the Cu–S(Cys) stretch in plastocyanin. If this is the case, the normal mode descriptions of azurin and

plastocyanin are expected to be quite different as the amino acid compositions differ significantly further from the copper center.

2.6 Conclusions

There are two main results of this work. First, the resonance Raman spectrum and charge transfer reorganization energies of azurin have some qualitative similarities to plastocyanin. In the photoexcited charge transfer process, most of the reorganization energy occurs along the putative Cu–S(Cys) stretch, and the frequencies of the modes are similar in the two proteins. The absorption spectra are also similar in shape, although the absorption maximum of azurin is shifted to lower energy. Second, the structure and environment around the copper metal ion have a significant and quantitative role in determining the electronic structure and excited-state dynamics. Differences in the excited-state photophysical charge-transfer parameters of plastocyanin and azurin, such as the homogeneous and inhomogeneous linewidths, zero-zero energy, transition moment, and reorganization energy, can be related to specific structural factors such as the coordination geometry of the copper center and the hydrogen bonding environment.

2.7 References

[1] Sykes, A. G. *Adv. Inorg. Chem.* **1991**, *36*, 377.

[2] Adman, E. T. In *Metalloproteins - Part 1: Metal Proteins with Redox Roles*; P. M. Harrison, Ed.; Verlag Chemie: Florida, **1985**; pp 1.

[3] Adman, E. T. *Adv. Protein Chem.* **1991**, *42*, 145.

[4] Baker, E. N. *J. Mol. Biol.* **1988**, *203*, 1071.

[5] Nar, H.; Messerschmidt, A.; Huber, R.; van de Kamp, M.; Canters, G. W. *J. Mol. Biol.* **1991**, *221*, 765.

[6] Murphy, L. M.; Strange, R. W.; Karlsson, B. G.; Lungburg, L. G.; Pascher, T.; Reinhammar, B.; Hasnain, S. S. *Biochemistry* **1993**, *32*, 1965.

[7] Karlsson, B. G.; Nordling, M.; Pascher, T.; Tsai, L-C.; Sjölin, L.; Lundberg, L. G. *Protein Eng.* **1991**, *4*, 343.

[8] Ainscough, E. W.; Bingham, A. G.; Brodie, A. M.; Ellis, W. R.; Gray, H. B.; Loehr, T. M.; Plowman, J. E.; Norris, G. E.; Baker, E. N. *Biochemistry* **1987**, *26*, 71.

[9] Solomon, E. I.; Hare, J. W.; Gray, H. B. *Proc. Natl. Acad. Sci. USA* **1976**, *73*, 1389.

[10] Solomon, E. I.; Hare, J. W.; Dooley, D. M.; Dawson, J. H.; Stephens, P. J.; Gray, H. B. *J. Am. Chem. Soc.* **1980**, *102*, 168.

[11] Tang, S.-P. W.; Coleman, J. E.; Myer, Y. P. *J. Biol. Chem.* **1968**, *243*, 4286.

[12] den Blaauwen, T.; Canters, G. W. *J. Am. Chem. Soc.* **1993**, *115*, 1121.

[13] Andrew, C. R.; Yeom, H.; Valentine, J. S.; Karlsson, B. G.; Bonander, N.; van Pouderoyen, G.; Canters, G. W.; Loehr, T. M.; Sanders-Loehr, J. *J. Am. Chem. Soc.* **1994**, *116*, 11489.

[14] Myers, A. B.; Mathies, R. A. In *Biological Applications of Raman Spectroscopy*; T. G. Spiro, Ed.; Wiley: New York, **1988**; *Vol. 2*; pp 1.

[15] Fraga, E.; Webb, M. A.; Loppnow, G. R. *J. Phys. Chem.* **1996**, *100*, 3278.

[16] Loppnow, G. R.; Fraga, E. *J. Am. Chem. Soc.* **1997**, *119*, 896.

[17] Myers, A. B. *Chem. Rev.* **1996**, *96*, 911.

[18] St. Clair, C. S.; Ellis, W. R. J.; Gray, H. B. *Inorganic. Chim. Acta* **1992**, *191*, 149.

[19] Ambler, R. P. *Biochem. J.* **1963**, *89*, 341.

[20] Ambler, R. P.; Wynn, M. *Biochem. J.* **1973**, *131*, 485.

[21] Mathies, R. A.; Oseroff, A. R.; Stryer, L. *Proc. Natl. Acad. Sci. USA* **1976**, *73*, 1.

[22] Loppnow, G. R.; Mathies, R. A. *Biophys. J.* **1988**, *54*, 35.

[23] Womack, J. D.; Mann, C. K.; Vickers, T. J. *J. Appl. Spectrosc.* **1989**, *43*, 527.

[24] Lee, S-Y.; Heller, E. J. *J. Chem. Phys.* **1979**, *71*, 4777.

[25] Blair, D. F.; Campbell, G. W.; Schoonover, J. R.; Chan, S. I.; Gray, H. B.; Malmstrom, B. G.; Pecht, I.; Swanson, B. I.; Woodruff, W. H.; Cho, W. K.; English, A. M.; Fry, H. A.; Lum, V.; Norton, K. A. *J. Am. Chem. Soc.* **1985**, *107*, 5755.

[26] Dave, B. C.; Germanas, J. P.; Czernuszewicz, R. S. *J. Am. Chem. Soc.* **1993**, *115*, 12175.

[27] Han, J.; Loehr, T. M.; Lu, Y.; Valentine, J. S.; Averill, B. A.; Sanders-Loehr, J. *J. Am. Chem. Soc.* **1993**, *115*, 4256.

[28] Qiu, D.; Dong, S.; Ybe, J. A.; Hecht, M. H.; Spiro, T. G. *J. Am. Chem. Soc.* **1995**, *117*, 6443.

[29] Grundler, H.; Schumann, H. D.; Steger, E. *J. Mol. Struct.* **1974**, *21*, 149.

[30] Vansant, F. K.; van der Veken, B. J.; Herman, M. A. *Spectrochim. Acta A* **1974**, *30A*, 69.

[31] Guss, J. M.; Freeman, H. C. *J. Mol. Biol.* **1983**, *169*, 521.

[32] Ehrenstein, D.; Nienhaus, G. U. *Proc. Natl. Acad. Sci. USA* **1992**, *89*, 9681.

[33] Hutnik, C. M.; Szabo, A. G. *Biochemistry* **1989**, *28*, 3923.

[34] Hutnik, C. M.; Szabo, A. G. *Biochemistry* **1989**, *28*, 3935.

[35] Garrett, T. P. J.; Clingeleffer, D. J.; Guss, J. M.; Rogers, S. J.; Freeman, H. C. *J. Biol. Chem.* **1984**, *259*, 2822.

[36] Nar, H.; Messerschmidt, A.; Huber, R.; van de Kamp, M.; Canters, G. W. *FEBS Lett.* **1992**, *306*, 119.

[37] Shepard, W. E. B.; Kingston, R. L.; Anderson, B. F.; Baker, E. N. *Acta Cryst.* **1993**, *49D*, 331.

[38] Solomon, E. I.; Lowery, M. D. *Science* **1993**, *259*, 1575.

[39] Margalit, R.; Kostic, N. M.; Che, C.-M.; Blair, D. F.; Chiang, H.-J.; Pecht, I.; Shelton, J. B.; Shelton, J. R.; Schroeder, W. A.; Gray, H. B. *Proc. Natl. Acad. Sci. USA* **1984**, *81*, 6554.

[40] Bosma, W. B.; Yan, Y. J.; Mukamel, S. *Phys. Rev. A* **1990**, *42*, 6920.

[41] Mukamel, S. *Annu. Rev. Phys. Chem.* **1990**, *41*, 647.

[42] Qiu, D.; Kilpatrick, L.; Kitajima, N.; Spiro, T. G. *J. Am. Chem. Soc.* **1994**, *116*, 2585.

[43] Urushiyama, A.; Tobari, J. *Bull. Chem. Soc. Jpn.* **1990**, *63*, 1563.

Chapter 3: Protein Tuning of the Excited-State Charge Transfer Dynamics in Azurin

Material previously published:

M. Adam Webb and Glen R. Loppnow

J. Phys. Chem. B **1998**, 102, pp. 8923-8929.

3.1 Introduction

Blue copper proteins are involved in electron transport processes in photosynthesis and respiration.[1,2] Azurin, a 14.0 kDa blue copper protein found in denitrifying bacteria, transports electrons from aromatic amine dehydrogenase to cytochrome c and/or nitrite reductase.[3-5] It has an unusual copper coordination geometry, a high reduction potential, and unusual spectral properties[1,2,6] The copper ion cofactor of azurin adopts a distorted trigonal bipyramidal coordination geometry;[6] the copper sits slightly above the trigonal plane formed by two strongly-bound histidines and a strongly-bound cysteine and is weakly bound axially to a methionine S and glycine O (Figure 3.1). The reduction potential is higher for azurin than aqueous Cu^{2+} (305 mV vs. 115 mV).[1] The EPR spectrum of azurin shows an unusually narrow hyperfine splitting coupling[1], with $A_{\parallel} = 0.0060$ cm^{-1}. The absorption spectra of azurins have a strong S→Cu charge-transfer transition at ~620 nm which give them their characteristic blue color. It appears that the unusual properties of the copper metal ion are due to the unique coordination geometry and protein environment.[1,2]

Resonance Raman spectroscopy is a sensitive probe of ground- and excited-state structure and dynamics. Previous resonance Raman studies of blue copper proteins have shown the ability of this technique to discriminate different ground-state active site structures in these proteins.[7-9] We have extended this work in our lab, by using resonance Raman intensities as a probe of the excited-state charge transfer dynamics and the modulation of these ultrafast dynamics by the protein environment.[10-12] The exquisite sensitivity of the resonance Raman intensities to small changes in structure and environment coupled with the well-characterized structures of these proteins, provides a sensitive probe of the factors which control charge transfer and electron transfer in these proteins.

In this work, we use resonance Raman intensities to measure the excited-state dynamics of azurin from *Alcaligenes denitrificans* (AD) and compare them to those in *Pseudomonas aeruginosa* (PA). The absorption spectrum and the resulting resonance Raman excitation profiles are analyzed using a self-consistent time-dependent

Figure 3.1: Copper metal site of *A. denitrificans* and *P. aeruginosa* azurin. Schematic representation of the copper metal centers taken from the x-ray crystal structures.[6,20]

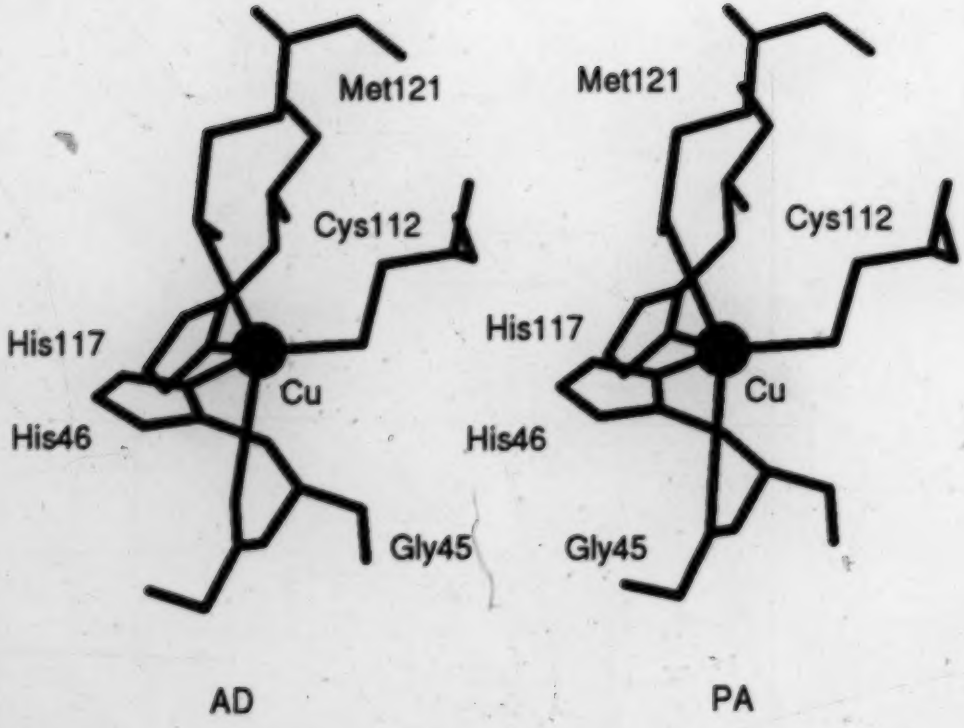
Met121
Cys112
His117
Cu
His46
Gly45
Met121
Cys112
His117
Cu
His46
Gly45

AD PA

wavepacket propagation formalism. The total inner-sphere reorganization energy is found to be the same (0.26 ± 0.02 eV) for both species and distributed along similar vibrational modes, although the contribution from each mode is different for the two species. Correlation of the experimentally-determined structures with the observed spectroscopic differences suggests that small differences in the protein can affect the excited-state dynamics through both structural and electrostatic mechanisms.

3.2 Experimental

Azurin from *Alcaligenes denitrificans* (ACTT 15173) was isolated and purified by methods described previously.[12] Column chromatography was used to obtain a purity ratio $A_{280}/A_{625} \leq 3.7$ (literature value[13] 3.6). A yield of 46-58 mg azurin per 100 g of cell paste was obtained. Azurin from *Pseudomonas aeruginosa* was isolated and purified by methods described previously.[12]

3.2.1 Resonance Raman Spectroscopy

Samples for the resonance Raman experiments were prepared by quantitative dilution of azurin with either a cacodylate buffer solution (0.5-1.0 M cacodylic acid, 0.01 M TRIS-HCl, pH 8.7) or a nitrate buffer solution (1.0 M potassium nitrate, 0.01 M TRIS-HCl, pH 8.7). Room-temperature resonance Raman spectra of azurin were obtained with 300 µL aqueous sample solutions (0.01 M TRIS-HCl buffer, either 0.25-0.84 M cacodylic acid or 0.9 M nitrate, pH 8.7) having an absorbance of 1.9-5.9 OD/cm at 619 nm (ε_{619} = 5200 $M^{-1}cm^{-1}$). The addition of cacodylate/cacodylic acid buffer did not have a noticeable effect on the absorption or resonance Raman spectra of azurin. Resonance Raman spectra were collected using a single monochromator with a CCD detector.[10,12] Frequencies are accurate to ±2 cm^{-1}. Absorption spectra were recorded on a diode array spectrophotometer (Hewlett Packard, Sunnyvale, CA, model 8452A). Measurement of the resonance Raman spectra and determination of the intensities were repeated on 3-6 fresh samples of azurin for each wavelength.

Analysis of the data was performed as previously described.[10,12] Bleaching of the sample was accounted for by measuring the absorbance at 580 nm (ε_{580} = 3562

$M^{-1}cm^{-1}$) before and after each scan. The absorbance at 580 nm was used because at the absorption maximum of this band, the absorbance is too large. The average absorbance was used to determine the concentration of azurin.

Absolute Raman cross sections of cacodylate and nitrate were calculated from the A-term expression.[10,14,15] The calculated Raman cross sections for cacodylate are 168, 126, 123, 106, 95.7, 88.2, 68.8 and 56.6 × 10^{-14} $Å^2$/molecule at 530.9, 565, 568.2, 588, 601, 612, 647.1 and 676.4 nm, respectively. The calculated Raman cross sections for nitrate are 6.40, 5.73, 4.55 and 3.40 × 10^{-13} $Å^2$/molecule at 568.2, 581, 609, and 647.1 nm, respectively.

Depolarization ratios were measured using excitation wavelengths of 568.2, 581, 612 and 647.1 nm. The spectrum was measured with the polarizer set at 0° ($I_\parallel$) and then with the polarizer at 90° ($I_\perp$) at each wavelength. The depolarization ratio is equal to the ratio of the intensities ($I_\parallel$/ $I_\perp$) for each band. The position of the polarizer was determined using the 459.7 cm^{-1} mode of CCl_4 which has a depolarization ratio of 0.02.[16] The 0° ($I_\parallel$) position of the polarizer is determined by a minimum in intensity and the 90° ($I_\perp$) position by a maximum intensity of this band. Cacodylate was added as a check on the accuracy of the depolarization ratio. Its depolarization ratio was found to be 0.14 ± 0.08 which agrees with the literature value[10] of 0.18.

3.2.2 Intensity Analysis.

The resonance Raman and absorption cross sections in the Condon approximation can be written using the time dependent equations of Lee and Heller.[10,17,18]

$$\sigma_R = \frac{8\pi E_S^3 E_L e^4 M^4}{9\hbar^6 c^4} \int_{-\infty} H(E_0)\ dE_0 \times \left| \int_0^{\infty} \langle f | i(t) \rangle\ e^{\frac{i(E_L + \varepsilon_i)t}{\hbar}}\ G(t) dt \right|^2 \tag{3.1}$$

$$\sigma_A = \frac{4\pi e^2 M^2 E_L}{6\hbar^2 cn} \int_{-\infty} H(E_0)\ dE_0 \times \int_{-\infty} \langle i | i(t) \rangle\ e^{\frac{i(E_L + \varepsilon_i)t}{\hbar}}\ G(t)\ dt \tag{3.2}$$

where E_L and E_S are the energies of the incident and scattered photons, M is the transition length, n is the refractive index, G(t) is a decay function, $H(E_0) = (1/\theta(2\pi)^{1/2})\exp[-(E_0 - \overline{E_0})^2/2\theta^2]$ is a normalized Gaussian distribution of site electronic energies centered at a mean 0–0 energy $\overline{E}_0$ and having a width of θ, ε_i is the energy of the initial vibrational state, $|i\rangle$ and $|f\rangle$ are the initial and final vibrational wavefunctions in the resonance Raman process, and $|i(t)\rangle = e^{-iHt/\hbar}|i\rangle$ is the initial ground-state vibrational wavefunction propagated on the excited-state potential surface. Significantly, the $\langle i|i(t)\rangle$ and $\langle f|i(t)\rangle$ overlaps are only sensitive to Δ, the difference in ground- and excited-state equilibrium geometries along each normal mode, within the separable harmonic oscillator approximation. Thus, the resonance Raman intensities directly reflect the dynamics of the excited state. The implementation of these equations has been described in detail.[10,11,15,17] Self-consistent analysis of the absorption spectrum and the resonance Raman excitation profiles was done in the same manner as previously described for plastocyanin[10,11] and azurin.[12]

3.2.3 Molecular Modeling.

The structures of the proteins were obtained from the Brookhaven protein data bank[19] (5azu[20] and 2aza[6] for PA and AD, respectively) and compared by calculating the Cartesian Root Mean Square deviation:

$$CartesianRMS = \left[\sum\left(\Delta X^2 + \Delta Y^2 + \Delta Z^2\right)/N\right]^{1/2} \qquad (3.3)$$

where the sum is carried over all N atoms (hydrogen atoms were not included). The Brookhaven files contain more than one molecule of azurin per unit cell. For the RMS calculations and Cu-C_α distances, the A structure was selected; no significant differences were found by using other structures. All other distances and angles are averages of the reported x-ray structures for each azurin. The RMS per residue was calculated by neglecting the side chains of the amino acids as they are different for many residues; the two proteins have 48 different amino acids and a resulting

homology of 63%. The two structures were then spatially overlapped using the remaining backbone structure and the copper metal, minimizing the overall RMS (1026 atoms, RMS = 0.827). The RMS for each residue was then calculated separately using only its backbone atoms (N, C_α, C and O). These residue RMS values were then compared as a function of distance from the copper ion, using the C_α–Cu distance.

3.3 Results

The resonance Raman spectra of AD azurin were measured using excitation wavelengths throughout the S(Cys)→Cu absorption band. Figure 3.2 shows the resonance Raman spectrum taken at an excitation wavelength of 568.2 nm. The spectra at other wavelengths have similar relative intensities, indicating resonance enhancement occurs for a single electronic state (Figure 3.3). No reproducible peaks were observed at frequencies of less than 200 cm^{-1} because the single monochromator used to obtain the spectra was unable to separate the Rayleigh scattering from the low frequency Raman signal. The cacodylate intensity standard appears at 605 and 638 cm^{-1}, marked with single asterisks in the figure. The intense bands between 300 and 500 cm^{-1} have been previously assigned to normal modes involving the Cu–S stretch mixed with other internal coordinates.[21-24] However, the exact assignments are still controversial.[21] The bands at 212, 251 and 274 cm^{-1} have been assigned to modes involving the Cu–N stretches.[21] The broad band at about 830 cm^{-1}, marked by double asterisks in the figure, is due to combination and overtone bands of the vibrations between 300 and 500 cm^{-1}. There is also a contribution at 825 cm^{-1} from the As=O stretch of cacodylate.[25,26]

The depolarization ratio of AD azurin was measured at 568.2, 581, 612, and 647.1 nm in order to determine if there is only one electronic transition which gives resonance enhancement. Figure 3.2 shows the parallel and perpendicular polarized spectra taken at an excitation wavelength of 568.2 nm; spectra at other wavelengths are similar. The relative intensities of the peaks do not change when different polarization components are detected, indicating that the depolarization ratio is the

Figure 3.2: Resonance Raman spectra of *A. denitrificans* azurin polarized parallel (dashed) and perpendicular (solid) at an excitation wavelength of 568.2 nm. The spectrum is the sum of two scans. The fundamental vibrations between 200 and 500 cm^{-1}, and the shoulder at 654 cm^{-1} were used in the analysis. Raman scattering of the internal intensity standard (cacodylate) is observed at 608 and 638 cm^{-1} (*). The broad band at ~820 cm^{-1} and the narrower band at ~750 cm^{-1} (**) are composed of the overtone and combination bands of the vibrations between 350 and 500 cm^{-1} and a cacodylate peak at 825 cm^{-1}.

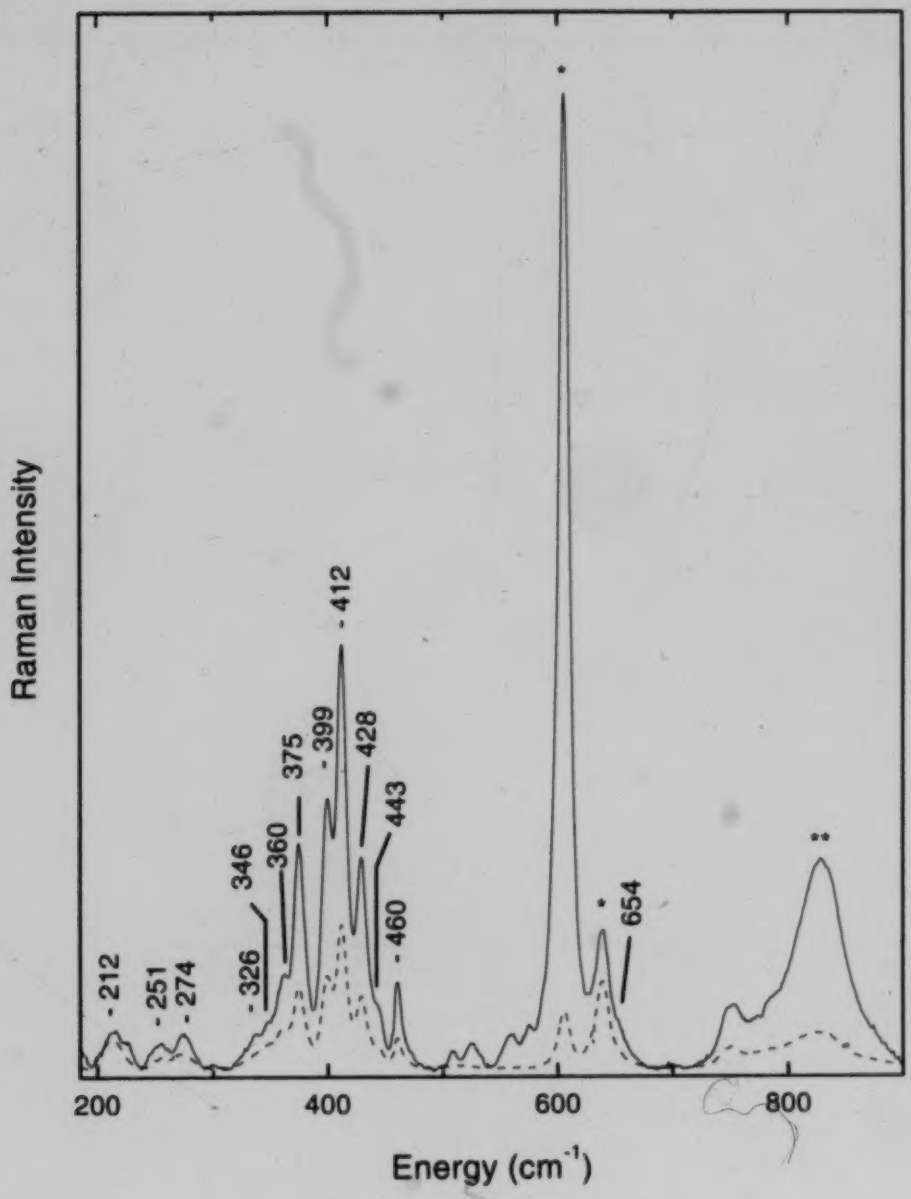
Raman Intensity
Energy (cm-1)
200
400
600
800
212
251
274
326
346
360
375
399
412
428
443
460
654

Figure 3.3: Resonance Raman spectra of *A. denitrificans* azurin at excitation wavelengths throughout the absorption band. The spectra are the sum of three to five scans. The vibrations between 200 and 500 cm^{-1}, and the peak at 654 cm^{-1} were used in the analysis. Raman scattering of the internal intensity standard (cacodylate) is observed at 608 and 638 cm^{-1} (*). The broad band at ~820 cm^{-1} and the narrower band at ~755 cm^{-1} (**) are composed of the overtones and combinations of the azurin vibrations between 350 and 500 cm^{-1} and a cacodylate peak at 825 cm^{-1}.

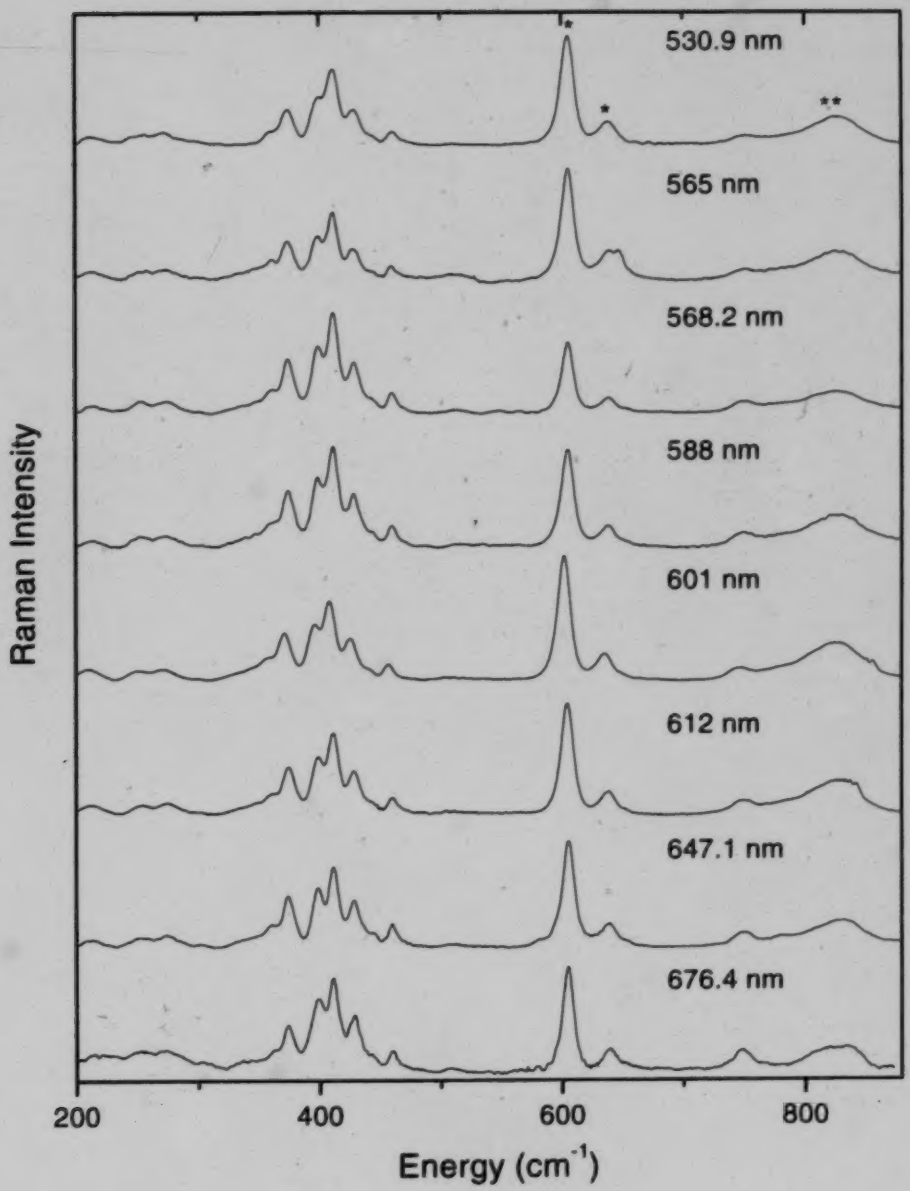
530.9 nm
565 nm
568.2 nm
588 nm
601 nm
612 nm
647.1 nm
676.4 nm
*
*
**
Raman Intensity
200
400
600
800
Energy (cm-1)

same for all modes. The depolarization ratio averaged over all modes at the four wavelengths was measured to be 0.41 ± 0.05. Figure 3.4 shows the measured depolarization ratios as a function of excitation wavelength for the strongest peaks. Within experimental error, the depolarization ratio of each band remains constant as the excitation wavelength is tuned throughout the absorption band. Additionally, the depolarization ratios of different bands are the same within experimental error. The slight increase in the depolarization ratios at 647.1 nm are probably due to a lower spectral signal-to-noise ratio at this wavelength, although it may also indicate that a second electronic transition is contributing to resonance enhancement of the Raman modes at this wavelength.

Figure 3.4 shows the experimental and calculated absorption spectra. Deviations of the experimental absorption spectrum from the calculated spectrum at both higher and lower energies are due to the presence of other charge-transfer and ligand field transitions[27] which were not modeled and apparently contribute little or no resonance enhancement to the observed normal modes. Figure 3.5 shows the good agreement of the experimental and calculated resonance Raman excitation profiles. Table 3.1 summarizes the experimental and calculated resonance Raman excitation profiles. Due to the presence of more than one electronic transition within the charge-transfer absorption band, the resonance Raman excitation profiles provided the primary constraints on the simulated spectral bandshape, position and bandwidth. Thus, scaling of the Δ's was determined by the width of the resonance Raman excitation profiles. Partitioning of the broadening into homogeneous and inhomogeneous components was primarily determined by the intensity of the resonance Raman excitation profiles.

The overtone and combination bands of AD azurin were measured at excitation wavelengths of 568.2, 581, 609 and 647.1 nm using nitrate as the internal standard, as a check on the self-consistency of the resonance Raman analysis and to test the presence of Duschinsky rotation.[28,29] Figure 3.6 shows the spectrum at an excitation wavelength of 568.2 nm. The spectra at other wavelengths exhibit similar spectral frequencies and intensities. The nitrate band appears at 1049 cm^{-1} and a

Figure 3.4: Experimental (solid line) and calculated (dashed lines) absorption spectra of *A. denitrificans* azurin (scale on left side). Deviations of the experimental absorption spectrum from the calculated absorption spectrum at both higher and lower energies are due to the presence of other charge-transfer and ligand field transitions which were not modeled and apparently contribute no resonance enhancement to the observed normal modes. Points are the depolarization measurements of azurin using four excitation wavelengths (scale on right side) for the most intense vibrational modes. The legend is as follows: ■ = 360 cm^{-1}, ● = 375 cm^{-1}, □ = 399 cm^{-1}, ○ = 412 cm^{-1}, ◆ = 428 cm^{-1}, + = 460 cm^{-1}). The error in the depolarization ratios are 0.02, 0.01, 0.03 and 0.13 at 568.2, 581, 612 and 647.1 nm, respectively. Representative error bars are indicated for the 399 cm^{-1} mode.

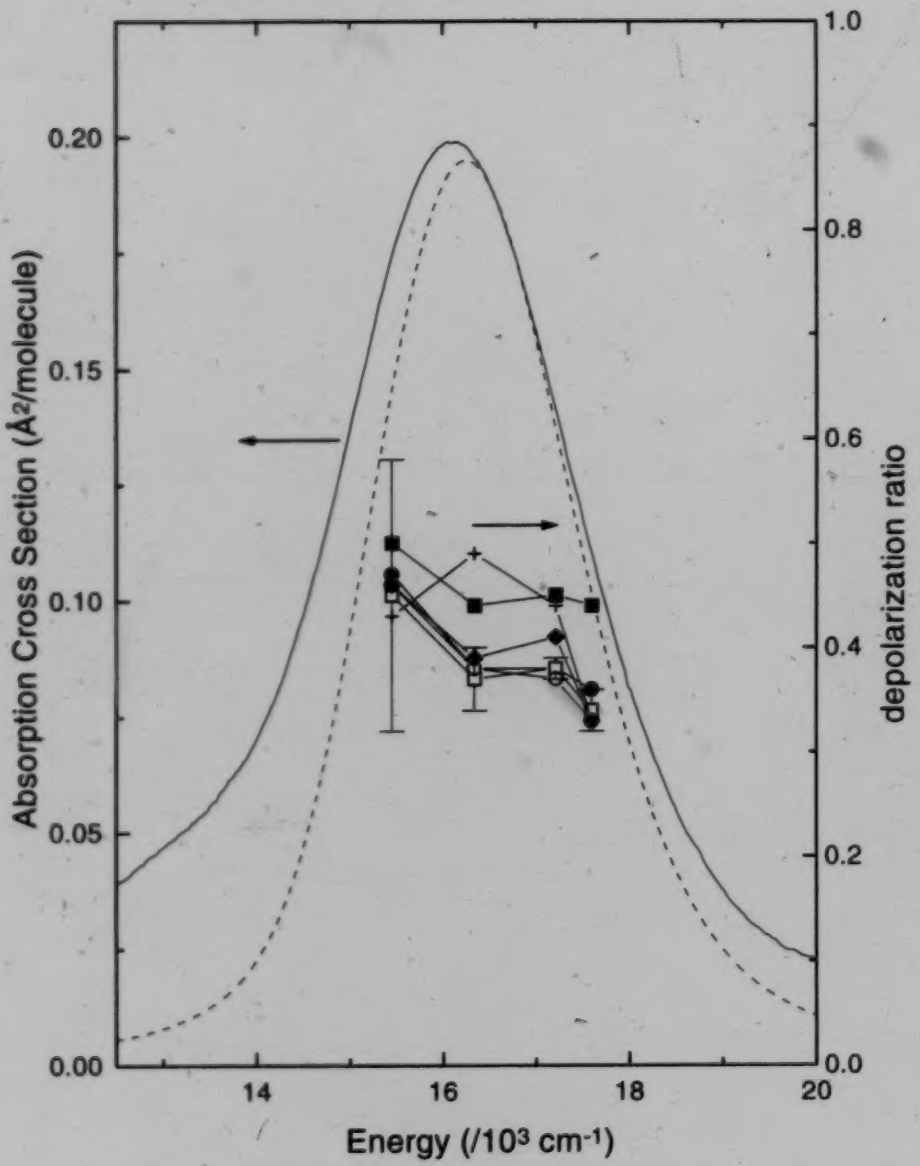
Absorption Cross Section (Å²/molecule)
depolarization ratio
Energy (/10³ cm⁻¹)
0.00
0.05
0.10
0.15
0.20
0.0
0.2
0.4
0.6
0.8
1.0
14
16
18
20

Figure 3.5: Resonance Raman excitation profiles of *A. denitrificans* azurin. Experimental (points) and calculated (solid line) resonance Raman excitation profiles of *A. denitrificans* azurin. The excitation profiles were calculated with Equation 3.1 using the parameters in Table 3.1.

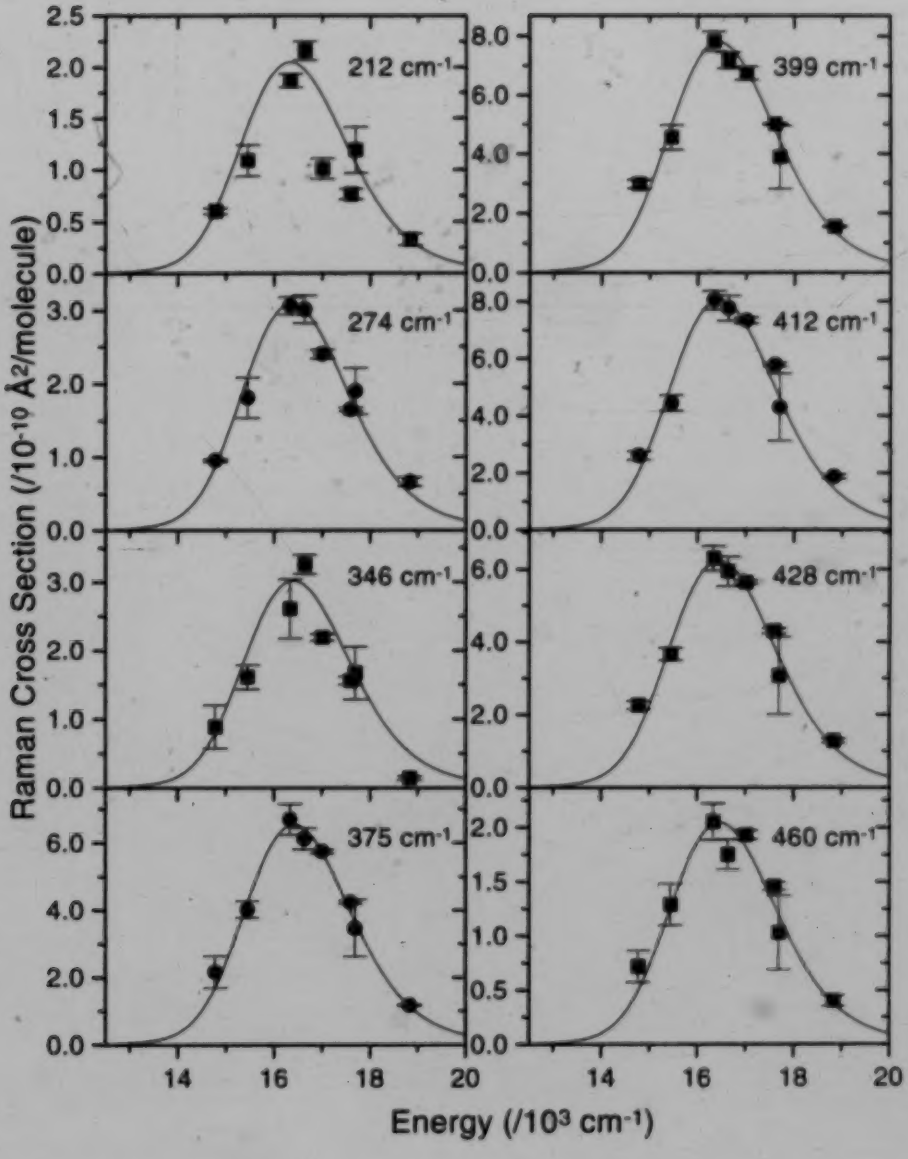
212 cm-1
399 cm-1
274 cm-1
412 cm-1
346 cm-1
428 cm-1
375 cm-1
460 cm-1
Raman Cross Section (/10-10 Å2/molecule)
Energy (/10³ cm-1)

Table 3.1: Absolute resonance Raman cross sections of *A. denitrificans* azurin.

		excitation wavelength/nm							
$\Delta\nu/cm^{-1}$	$\lvert\Delta\rvert$	530.9	566	568.2	588	601	612	647.1	676.4
212	1.24	0.33/0.31	1.19/1.05	0.77/1.14	1.01/1.72	2.16/1.97	1.87/2.03	1.09/1.03	0.60/0.60
251	0.69	0.19/0.14	0.47/0.47	0.53/0.51	0.88/0.76	0.87/0.87	0.88/0.90	0.64/0.44	0.26/0.26
274	1.18	0.66/0.49	1.90/1.63	1.65/1.78	2.40/2.63	3.01/3.00	3.06/3.09	1.81/1.49	0.95/0.87
326	0.43	---/0.09	0.32/0.31	0.42/0.34	0.42/0.49	0.65/0.56	0.47/0.57	0.25/0.27	0.18/0.15
346	0.93	0.14/0.51	1.67/1.65	1.56/1.80	2.19/2.62	3.26/2.95	2.61/3.02	1.61/1.39	0.89/0.80
360	0.60	0.26/0.23	0.83/0.74	0.87/0.80	1.25/1.16	1.09/1.31	1.39/1.33	0.91/0.61	0.45/0.35
375	1.27	1.17/1.12	3.47/3.63	4.24/3.93	5.74/5.71	6.12/6.40	6.69/6.51	4.02/2.95	2.16/1.68
399	1.30	1.55/1.36	3.89/4.38	5.01/4.75	6.74/6.86	7.18/7.67	7.83/7.77	4.56/4.47	2.98/1.97
412	1.28	1.87/1.42	4.30/4.56	5.78/4.94	7.33/7.11	7.76/7.93	8.04/8.03	4.45/3.56	2.60/2.01
428	1.08	1.29/1.11	3.07/3.55	4.30/3.85	5.64/5.52	5.94/6.14	6.30/6.20	3.66/2.72	2.26/1.53
443	0.43	0.19/0.19	0.48/0.59	0.76/0.64	1.01/0.92	0.74/1.02	1.05/1.02	0.62/0.45	0.36/0.25
460	0.58	0.40/0.37	1.03/1.18	1.46/1.28	1.93/1.82	1.75/2.02	2.05/2.03	1.29/0.87	0.72/0.49
654	0.22	0.18/0.12	0.55/0.37	0.24/0.40	0.30/0.54	0.53/0.58	0.58/0.57	0.34/0.22	0.19/0.12

The resonance Raman cross sections are shown as experimental/calculated in units of $Å^2$/molecule /10^{-10}. A --- indicates no cross section was measured. The errors in cross sections are ±10% for strong lines and ±20% for weak lines. The Δ's are in dimensionless normal coordinates. The cross sections were calculated with Equation 3.1 using the following parameters: zero-zero energy, E_0 = 14,300 cm^{-1}, transition length, M = 0.73 Å, temperature, T = 0 K, refractive index, n = 1.33, Lorentzian homogeneous linewidth, Γ_L = 450 cm^{-1}, Gaussian homogeneous linewidth, Γ_G = 75 cm^{-1} inhomogeneous linewidth, Θ = 150 cm^{-1}.

Figure 3.6: Resonance Raman spectrum of the overtone/combination band region of *A. denitrificans* azurin excited at 568.2 nm. Peak at 1049 cm^{-1} (*) is from the nitrate internal standard. The marked feature (**) is a detector artifact. The spectrum is the sum of three scans.

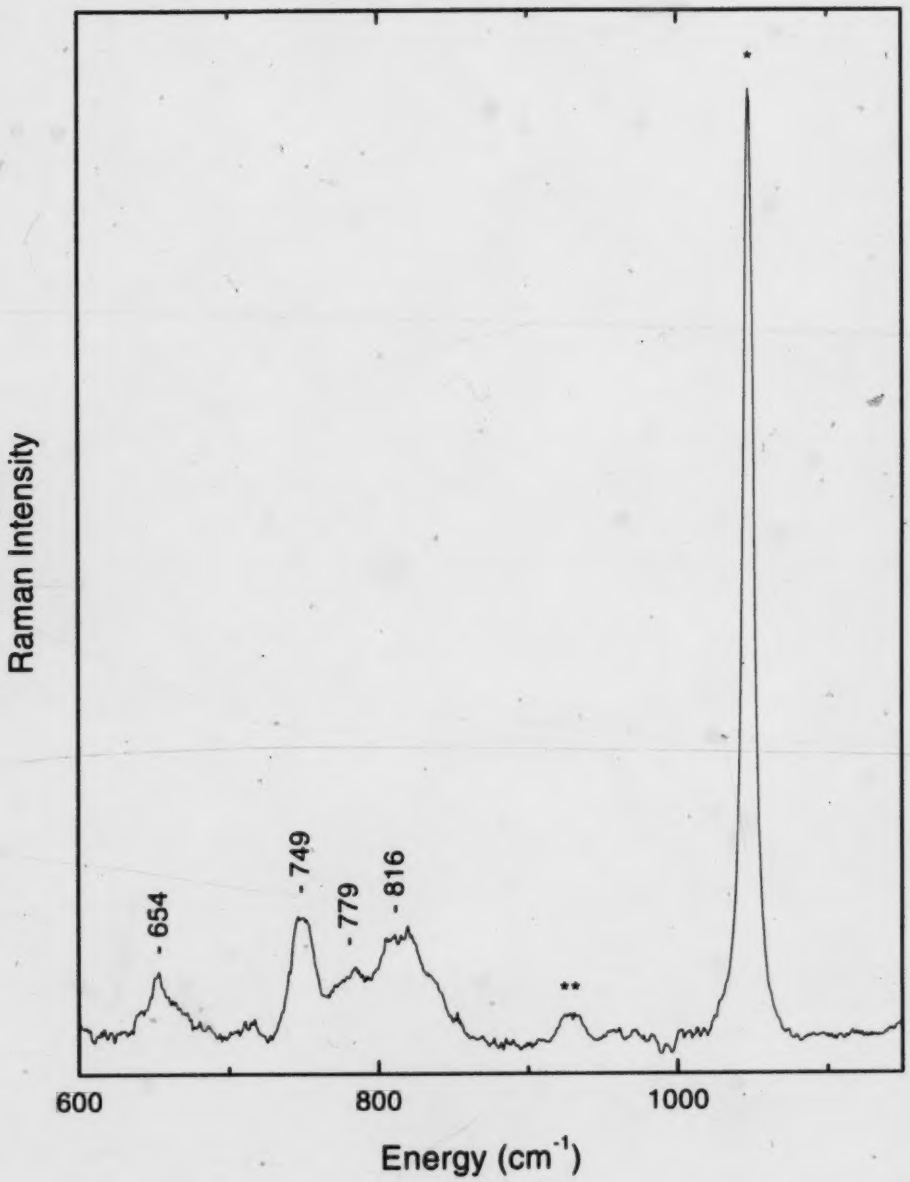
Raman Intensity
- 654
- 749
- 779
- 816
*
**
600
800
1000
Energy (cm-1)

small peak between 900 and 1000 cm^{-1} is a detector artifact. The bands in this region have been assigned for *P. aeruginosa*[21] to a C–S fundamental mode at ~750 cm^{-1} and various overtones and combination bands from the modes at 300-500 cm^{-1}. The assignment of these bands is expected to be similar for *A. denitrificans*. In analogy to *P. aeruginosa*, the peak at 749 cm^{-1} is probably due to the overlap of a fundamental band and a combination band. Because the resonance Raman spectra were taken at room temperature, we were unable to resolve the individual bands which had been observed in previous low-temperature resonance Raman spectra of *P. aeruginosa* azurin.[21] Table 3.2 lists the overall intensity of the overtone region from 774-875 cm^{-1}. These values were compared to the values calculated using Equation 3.1 and the parameters in Table 3.1. The band at ~750 cm^{-1} was not used due to the ambiguity in the assignment. The calculated overtone and combination band intensities agree with the experimental intensities within experimental error.

3.4 Discussion

3.4.1 Electronic Structure.

The resonance Raman intensities are sensitive to the electronic properties of the excited charge-transfer state. The depolarization ratios and the overtone and combination band intensities were measured in an attempt to elucidate the electronic structure of this excited state. The depolarization ratios are found to be 0.41 for all the modes across the absorption band. The lack of dispersion in the depolarization ratios and the similarity in the values of the depolarization ratios of all the modes argues that the observed Raman scattering arises from a single electronic transition. However, the mean depolarization ratio of 0.41 ± 0.05 is slightly higher than the value of 0.33 expected for totally symmetric modes on resonance, and may indicate that the charge-transfer state is partially mixed with another electronic state.

As a further constraint on the parameters of the excited-state, the overtone and combination band intensities were measured. A previous resonance Raman study of azurin, plastocyanin, and the multicopper oxidases laccase, ascorbate oxidase and ceruloplasmin[21] has suggested that the high intensity of the overtone and combination

Table 3.2: Absolute resonance Raman cross sections of the overtone and combination bands of *A. denitrificans* azurin.[a]

Excitation wavelength (nm)	Experimental Cross Section ($Å^2$/molecule)[b]	Calculated Cross Section ($Å^2$/molecule)[c]
568.2	3.04×10^{-10}	2.85×10^{-10}
581.0	3.82×10^{-10}	3.90×10^{-10}
609.0	5.54×10^{-10}	5.19×10^{-10}
647.1	3.35×10^{-10}	3.94×10^{-10}

[a]The combination and overtone modes between 774 and 875 cm^{-1} were used. These modes are: 774 (L+M), 787 (L+N), 798 (2M), 803 (L+O), 811 (M+N), 818 (L+P), 824 (2N), 827 (M+O), 835 (L+Q), 840 (N+O), 842 (M+P), 855 (N+P), 856 (2O), 859 (M+Q), 871 (O+P) and 872 (N+Q) cm^{-1}, in the notations of ref. 21.

[b]The resonance Raman spectra were measured at each wavelength using nitrate as an internal intensity standard. Cross sections were obtained from the intensities in the manner described in the text.

[c] The cross sections were calculated with Equation 3.1 using the parameters from Table 3.1.

bands between 700 and 900 cm^{-1} arises from different excited-state frequencies and/or Duschinsky rotation, a rotation of the ground-state normal modes in the excited electronic state. For the analysis performed here, it was not necessary to use Duschinsky rotation or changes of excited-state frequencies to obtain a self-consistent fit of the data.

3.4.2 Comparison of Azurins.

The primary goal of this work is to model how the coordination geometry and protein environment modulates the excited-state properties of the copper center as probed by resonance Raman spectroscopy. A comparison of the results obtained from resonance Raman experiments on azurin from *A. denitrificans* (AD) and *P. aeruginosa* (PA), both of which have a known x-ray crystal structure, provides a unique opportunity to correlate differences in the observed resonance Raman spectrum and derived excited-state parameters with structure.

Figure 3.7 and Figure 3.8 compare the resonance Raman and absorption spectra of azurin from *A. denitrificans* and *P. aeruginosa*. Table 3.3 lists the mode frequencies and mode-specific reorganization energies for both species. There are a number of similarities in the spectral properties of the two species. Many of the Raman frequencies are similar for the two species of azurin. The resonance Raman excitation profiles have similar shapes, reaching a maximum at the same energy. Self-consistent analysis of the absorption spectra and resonance Raman excitation profiles suggests the S→Cu charge transfer transition occurs at a similar energy, even though the absorption band has a different λ_{max} in the two species (619 and 625 nm for AD and PA azurin, respectively). Finally the two species have a similar total inner-sphere reorganization energy. All of these results suggest a similar nature of the charge transfer process in the two azurins.

A closer inspection of the data in Figure 3.7 and Figure 3.8, however, reveals some significant differences. There are differences in the frequencies for a few of the modes. For example, there are two overlapping modes at ca. 263 cm^{-1} for PA which are more well-resolved at 251 and 274 cm^{-1} in AD. PA has a weak mode at 344 cm^{-1},

Figure 3.7: Resonance Raman spectra of *A. denitrificans* and *P. aeruginosa* azurin. Comparison of resonance Raman spectra of *Pseudomonas aeruginosa* (upper spectrum) and *Alcaligenes denitrificans* (lower spectrum) azurins. Raman scattering of the internal intensity standard (cacodylate) is observed at 608 and 638 cm^{-1} (*). The broad band at ~820 cm^{-1} and the narrower band at ~750 cm^{-1} (**) are composed of the overtones and combinations of the azurin vibrations between 350 and 500 cm^{-1} and a cacodylate peak at 825 cm^{-1}. The spectra are the sum of three scans.

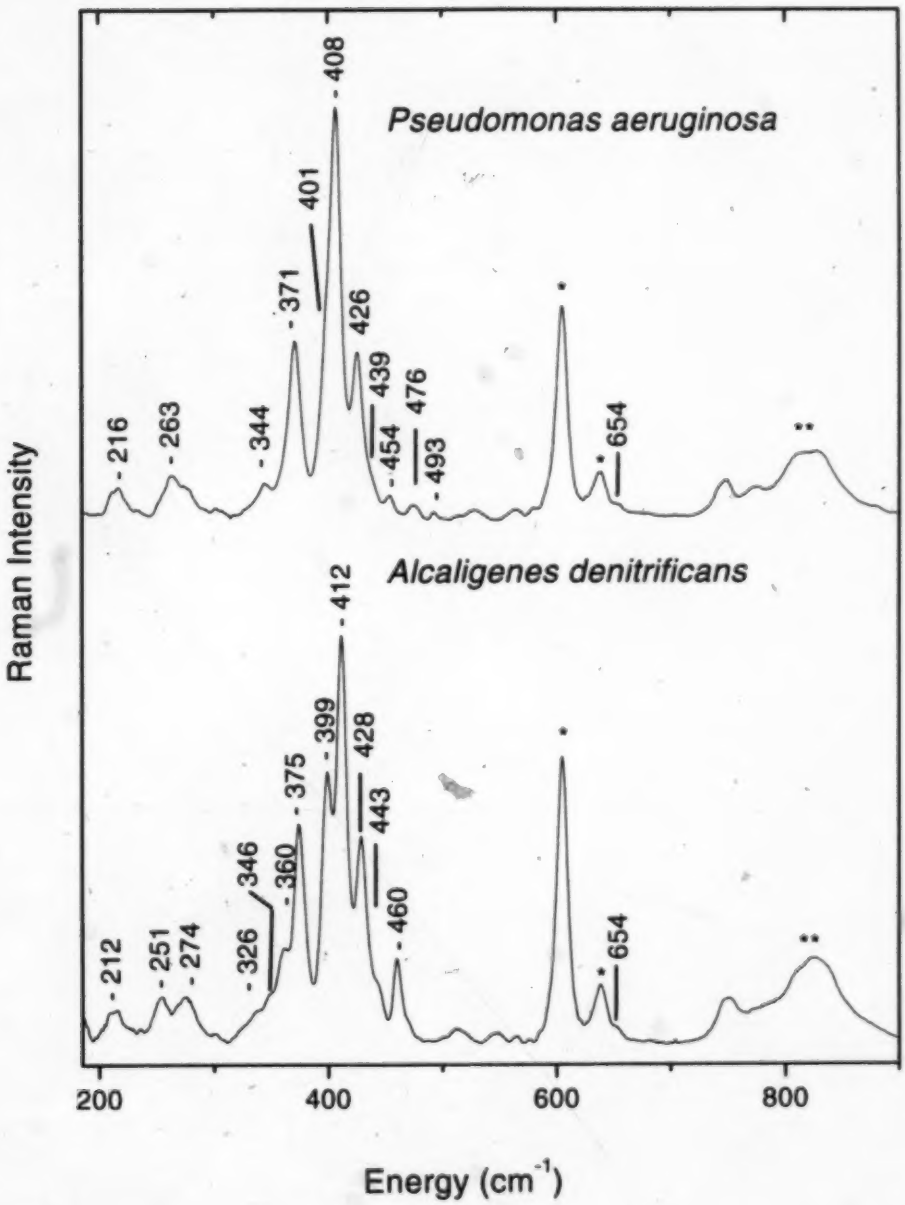
Pseudomonas aeruginosa
- 216
- 263
- 344
- 371
401
- 408
426
439
476
- 454
- 493
654
Alcaligenes denitrificans
- 212
- 251
- 274
- 326
346
- 360
- 375
- 399
- 412
428
443
- 460
654
Raman Intensity
200
400
600
800
Energy (cm-1)

Figure 3.8: Absorption spectra of *A. denitrificans* and *P. aeuruginosa* azurin. Experimental (solid) and calculated (dashed) absorption spectra of azurin from *A. denitrificans* (A) and *P. aeruginosa* (B).

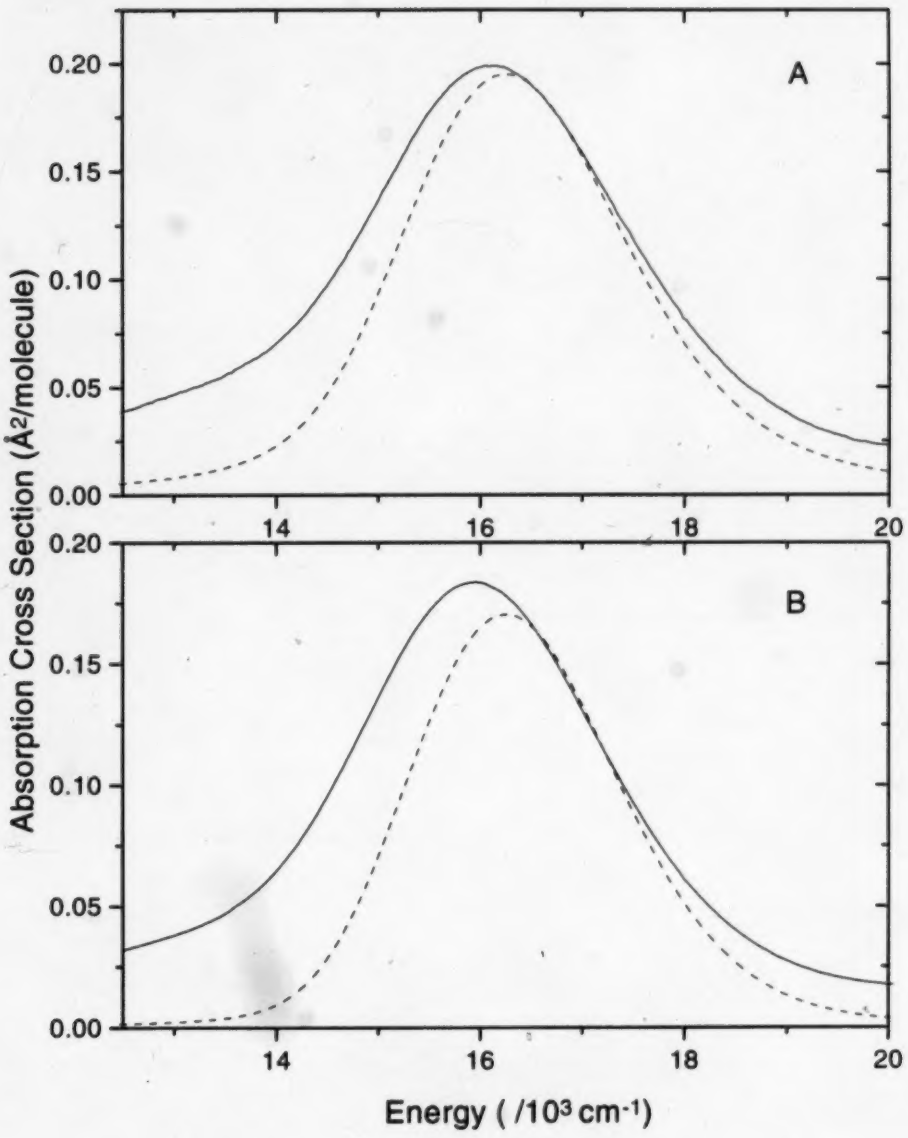
A
B
0.20
0.15
0.10
0.05
0.00
14
16
18
20
Absorption Cross Section (Å²/molecule)
Energy (/10³ cm⁻¹)

Table 3.3: Mode-specific reorganization energies of *A. denitrificans* azurin and *P. aeruginosa* azurin.

Azurin(AD)[a]			Azurin(PA)[b]		
$\Delta\nu/cm^{-1}$	$\lvert\Delta\rvert$	λ/cm^{-1}	$\Delta\nu/cm^{-1}$	$\lvert\Delta\rvert$	λ/cm^{-1}
212	1.24	160	216	0.85	78
251	0.69	60	263	1.30	220
274	1.18	190			
326	0.43	30			
346	0.93	150	344	0.75	100
360	0.60	65			
375	1.26	300	371	1.60	470
399	1.30	340	401	1.20	290
412	1.28	340	408	1.60	520
428	1.09	250	426	1.30	360
443	0.43	40	439	0.23	12
460	0.58	80	454	0.31	22
			476	0.27	17
			493	0.13	4
654	0.22	16	654	0.18	11
Total		$2020\ cm^{-1}$			$2100\ cm^{-1}$

Δ's are in dimensionless normal coordinates. The reorganization energy in a particular mode, λ_i, is related to Δ_i by $\lambda_i = (\Delta_i^2\omega_i)/2$ where ω_i is the frequency in cm^{-1}.

[a]Values for AD azurin from this work.

[b]Values for PA azurin from ref. 12.

while AD has a more intense mode at 360 cm^{-1} and a shoulder at 326 cm^{-1}. At higher frequencies, PA has several modes with low intensity (454, 476 and 493 cm^{-1}) which are not visible in AD. Rather, AD has a single medium intensity mode at 460 cm^{-1} which is absent from PA. These differences indicate that the normal mode description of some of the modes are different for the two species. The relative intensities are also quite different for the two species, reflecting these changes in the normal mode description and/or indicating differences in the excited charge-transfer state.

A previous study has suggested that the mode with the greatest intensity is likely to have the greatest Cu–S stretching character and its frequency is an indicator of the Cu–S bond length.[7] The most intense modes are 412 cm^{-1} (AD) and 408 cm^{-1} (PA) while the x-ray crystal structures show that the bond lengths are 2.15 and 2.26 Å for AD and PA, respectively. The frequency of the most intense mode decreases as the bond length increases, which is expected. Due to the number of peaks in the resonance Raman spectra it is expected that the normal mode description of this vibration must contain other internal coordinates in addition to the Cu–S bond stretch.

As stated above, there are also differences in the absorption spectra. The experimental absorption band maximum changes from 16000 to 16155 cm^{-1} (625 to 619 nm) going from PA to AD. However, analysis of the absorption spectra and the resonance Raman spectra (above) indicate that the S(Cys)→Cu charge transfer transition has the same frequency for both AD and PA, and is not blue-shifted in AD. The absorption bands, composed of ligand field and other charge transfer transitions[27] in addition to the Cu→S charge transfer transition, have been shown to be sensitive to the copper site coordination geometry,[7,23] which becomes slightly more tetrahedral on going from PA to AD. A survey of blue copper proteins does not reveal a clear relationship between the λ_{max} and the geometry of the copper site[7,23] indicating that other electronic transitions within the absorption band influence λ_{max}. The change in copper coordination geometry can cause changes in the intensity of other electronic transitions by modulating the coupling between these transitions. In azurin there is a weak σS→Cu charge transfer band at 526 nm[27] overlapping the πS→Cu charge

transfer transition in the ~620 nm band. An increase of the relative intensity of this band can shift the absorption band λ_{max} to the blue. The intensity of the $\sigma S \rightarrow Cu$ charge transfer band in three blue copper proteins increases in the order: azurin < plastocyanin < stellacyanin,[27] corresponding to increasing tetrahedral geometry.[23] The more tetrahedral geometry of AD azurin is expected to lead to a blue-shift of the band as a result of increased dipole strength of the $\sigma S \rightarrow Cu$ charge transfer transition, and this is what is observed. This change in coordination geometry to a more tetrahedral geometry should also result in an increase of the A_{470}/A_{620} intensity ratio[23] and that is what is seen (0.098 in AD vs. 0.090 in PA).

3.4.3 Proposed Model

To determine the origin of these spectral differences, a comparison of the chromophore structure and protein environment was performed. The copper metal sits in an environment which can be divided into two components: the structural environment imposed by the protein, and the electrostatic environment created by the protein. These two factors influence the properties of the excited charge-transfer state. A detailed examination of the spectra in Figure 3.7 and the Δ's in Table 3.3 can be useful in discriminating structural and electronic effects on the resonance Raman intensities. Table 3.3 shows that the total intensity of modes involving the Cu–N bond are larger in AD (212, 251 and 274 cm^{-1}) than in PA (216 and 263 cm^{-1}). The combined intensity of the 401 and 408 cm^{-1} modes in PA is approximately the same as the combined intensity of the 399 and 412 cm^{-1} modes of AD within experimental error. Also, the intensity of the mode at 460 cm^{-1} in AD is roughly equal to the intensity of both the 454 and 474 cm^{-1} modes in PA. For the 401/408 cm^{-1} and the ca. 460 cm^{-1} modes, the resonance Raman intensity simply seems to be redistributed among vibrations with similar frequencies. However, the changes in the intensity in the Cu-N modes is much more dramatic, suggesting a larger perturbation of the vibrations by the structural and/or electrostatic differences between the two azurins.

To understand these intensity changes, a comparison of the structures was performed. Since the resonance Raman intensities are dependent on Δ, the difference

between ground- and excited-state geometry along each normal mode, the properties of both the ground- and excited-state must be considered. The structure of the azurin molecule for *P. aeruginosa* and *A. denitrificans* can be compared by overlapping the protein backbone of the two species. Figure 3.9A shows a histogram of the RMS (Root Mean Square) deviations for each residue and shows that most of the residues have a low RMS difference with a median value of 0.56 Å. In addition, the overall RMS deviation is 0.83 Å using 1026 atoms indicating that the overall structures for the two species are similar. Figure 3.9B shows that the differences in structure tend to increase further from the copper site. However, a detailed comparison of the structure around the copper metal shows that it is somewhat different for the two proteins (Figure 3.1).[6,20] In AD the copper is slightly further above the NNS plane compared with PA. The copper moves further from Gly45 (3.13 Å vs. 2.93 Å), and closer to Cys112 (2.15 Å vs. 2.26 Å) in AD azurin. This results in a slightly more tetrahedral geometry of the copper site in AD azurin. These differences in the coordination geometry may change the normal mode descriptions.

In a previous study of plastocyanin it was found that structural changes result in a redistribution of Raman intensity among two or more vibrational modes.[11] For AD and PA azurins, a similar mechanism may be operating because these two azurins differ much more substantially in the copper site structure than the two plastocyanins. These slight differences in the coordinating residue distances of the two azurins may change how the internal coordinates of cysteine couple to the S_γ–Cu stretch, resulting in a change in the normal mode description. These structural differences would be observed as a redistribution of Raman intensity among the vibrational modes between 320 cm^{-1} and 500 cm^{-1} as seen for the 401/408 cm^{-1} bands and the ca. 460 cm^{-1} band.

Further support for this intensity redistribution comes from a comparison of the Raman spectra and x-ray crystal structures of the two species of azurin. The crystal structures suggest that the Cu–S(Cys) bond lengthens from 2.15 Å in AD azurin to 2.26 Å in PA azurin. Badger's rule[30] is an empirical relationship between the bond length and vibrational frequency, assuming no changes in the normal mode description, and can be used to calculate the expected frequency shift with bond

Figure 3.9: RMS histogram and plot as a function of distance.

(A) RMS per residue histogram comparing structures of *A. denitrificans* and *P. aeruginosa* azurin.

(B) RMS per residue vs. distance from the copper center. The distance of each residue was calculated using the α carbons only. The solid line through the plot is the same data after fast Fourier transform filtering to show RMS trend with distance.

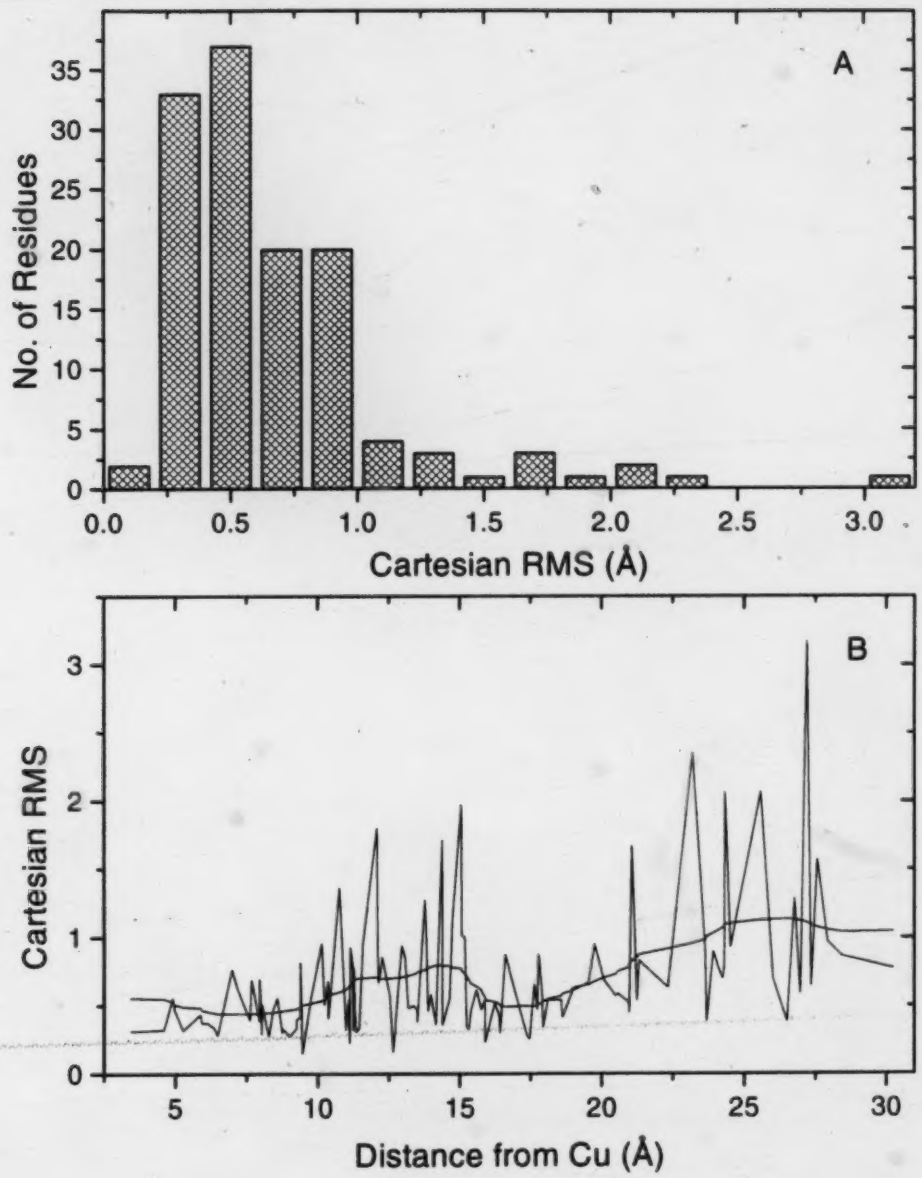
A
No. of Residues
0
5
10
15
20
25
30
35
0.0
0.5
1.0
1.5
2.0
2.5
3.0
Cartesian RMS (Å)
B
Cartesian RMS
0
1
2
3
5
10
15
20
25
30
Distance from Cu (Å)

length change. Using the Badger's rule relationship, $(r_1-d)/(r_2-d) = (\nu_2/\nu_1)^{2/3}$, with[7] r_1 = 2.15 Å, r_2 = 2.26 Å, d = 1.5, and ν_1 = 412 cm^{-1} yields ν_2 = 325 cm^{-1}, a downshift of 87 cm^{-1}. Only a 4 cm^{-1} downshift is observed, in the predicted direction, but with a very different magnitude. This serious deviation from Badger's rule supports intensity redistribution via an amino acid-dependent rotation of the normal modes, as proposed earlier for the plastocyanins.[11]

The modes at 212, 251 and 274 cm^{-1} in AD azurin and at 216 and 263 cm^{-1} in PA azurin which involve the Cu–N bonds require further comment. There is a lack of conservation of resonance Raman intensity in these modes (Table 3.3); in AD azurin, the reorganization energy along these modes is 40% greater than in PA azurin. The higher intensity of Cu–N(His) modes in AD azurin may reflect a different electrostatic environment near the histidines. Changes in the electrostatic environment provide new repulsive or attractive forces which may result in a new equilibrium geometry of the excited state and a new excited-state displacement. Different vibrational modes may be affected differently and independently, depending on the relative positions of dipoles and charges within the two azurins. There are several changes in the electrostatic environment within 15 Å of the copper site. There are four amino acid changes which involve a change in charge: Gln8 changes to Glu, Asn16 changes to Asp, Ser34 changes to Lys and Met56 changes to Lys going from PA to AD. The first three are closest to His46 and may be the origin of the increased Raman intensity of the Cu–N modes in AD. The last change is closest to the Cys112 and may influence Cu–S modes. In addition to the charge changes, there are five dipole changes: Gly9 changes to Ser, Gln12 changes to Ala, Ser89 changes to Gly, Ser118 changes to Trp and Asn42 changes to Ser going from PA to AD. The first three of these dipole changes are closest to His46, the fourth is closest to His117 and the fifth is closest to Gly45. Again, these changes are expected to have an overall greater effect on the Cu–N modes due to their proximity to the histidines. Work is in progress to further separate the contributions of the structural and electrostatic factors to the mode specific excited-state dynamics.

3.5 Conclusions

Self-consistent analysis of the resonance Raman excitation profiles and absorption spectrum of AD azurin demonstrates that the azurins have an inner-sphere reorganization energy of 0.26 eV. A comparison of the results for PA and AD azurin indicate that the observed spectral changes are due to a complex relationship between chromophore structure and protein environment at the copper site. The most important factors affecting the excited-state properties of the copper site appear to be the immediate geometry, and to a lesser degree, the electrostatic environment of the protein. In particular, the different frequencies and intensities observed in the resonance Raman spectra of the two azurins suggests the protein tunes the charge transfer dynamics in these two azurins via structurally-induced changes in the normal mode descriptions and selective distribution of charges and dipoles in the protein environment.

3.6 References

[1] Sykes, A. G. *Adv. Inorg. Chem.* **1991**, *36*, 377.

[2] Adman, E. T. *Adv. Protein Chem.* **1991**, *42*, 145.

[3] Hyun, Y.-L.; Davidson, V. L. *Biochemistry* **1995**, *34*, 12249.

[4] van Pouderoyen, G.; Cigna, G.; Rolli, G.; Cutruzzola, F.; Malatesta, F.; Silverstrini, M. C.; Brunori, M.; Canters, G. W. *Eur. J. Biochem.* **1997**, *247*, 322.

[5] Zumft, W. G.; Gotzmann, D. J.; Kroneck, P. M. H. *Eur. J. Biochem.* **1987**, *168*, 301.

[6] Baker, E. N. *J. Mol. Biol.* **1988**, *203*, 1071.

[7] Andrew, C. R.; Yeom, H.; Valentine, J. S.; Karlsson, B. G.; Bonander, N.; van Pouderoyen, G.; Canters, G. W.; Loehr, T. M.; Sanders-Loehr, J. *J. Am. Chem. Soc.* **1994**, *116*, 11489.

[8] Andrew, C. R.; Sanders-Loehr, *Acc. Chem. Res.* **1996**, *29*, 365.

[9] Han, J. H.; Adman, E. T.; Beppu, T.; Codd, R.; Freeman, H. C.; Huq, L.; Loehr, T. M.; Sanders-Loehr, J. *Biochemistry* **1991**, *30*, 10904.

[10] Fraga, E.; Webb, M. A.; Loppnow, G. R. *J. Phys. Chem.* **1996**, *100*, 3278.

[11] Loppnow, G. R.; Fraga, E. *J. Am. Chem. Soc.* **1997**, *119*, 896.

[12] Webb, M. A.; Kwong C. M.; Loppnow, G. L. *J. Phys. Chem. B* **1997**, *101*, 5062. This is Chapter 2 in this thesis.

[13] St. Clair, C. S.; Ellis, W. R. J.; Gray, H. B. *Inorg. Chim. Acta* **1992**, *191*, 149.

[14] Albrecht, A. C.; Hutley, M. C. *J. Chem. Phys.* **1971**, *55*, 4438.

[15] Loppnow, G. R.; Mathies, R. A. *Biophys. J.* **1988**, *54*, 35.

[16] Ferraro, J. R.; Nakamoto, K. In *Introductory Raman Spectroscopy*; Academic Press Inc: San Diego, **1994**.

[17] Myers, A. B.; Mathies, R. A. In *Biological Applications of Raman Spectroscopy*; T. G. Spiro, Ed.; Wiley: New York, **1988**; *Vol. 2*; pp 1.

[18] Lee, S-Y.; Heller, E. J. *J. Chem. Phys.* **1979**, *71*, 4777.

[19] Bernstein, F. C.; Koetzle, T.F.; Williams, G. J. B.; Meyer, E. F. Jr.; Brice, M. D.; Rodgers, J. R.; Kennard, O.; Shimanouchi, T.; Tasumi, M. *J. Mol. Biol.* **1977**, *112*, 535.

[20] Nar, H.; Messerschmidt, A.; Huber, R.; van de Kamp, M.; Canters, G. W. *J. Mol. Biol.* **1991**, *221*, 765.

[21] Blair, D. F.; Campbell, G. W.; Schoonover, J. R.; Chan, S. I.; Gray, H. B.; Malmstrom, B. G.; Pecht, I.; Swanson, B. I.; Woodruff, W. H.; Cho, W. K.; English, A. M.; Fry, H. A.; Lum, V.; Norton, K. A. *J. Am. Chem. Soc.* **1985**, *107*, 5755.

[22] Dave, B. C.; Germanas, J. P.; Czernuszewicz, R. S. *J. Am. Chem. Soc.* **1993**, *115*, 12175.

[23] Han, J.; Loehr, T. M.; Lu, Y.; Valentine, J. S.; Averill, B. A.; Sanders-Loehr, J. *J. Am. Chem. Soc.* **1993**, *115*, 4256.

[24] Qiu, D.; Dong, S.; Ybe, J. A.; Hecht, M. H.; Spiro, T. G. *J. Am. Chem. Soc.* **1995**, *117*, 6443.

[25] Grundler, H.; Schumann, H. D.; Steger, E. *J. Mol. Struct.* **1974**, *21*, 149.

[26] Vansant, F. K.; van der Veken, B. J.; Herman, M. A. *Spectrochim. Acta* **1974**, *30A*, 69.

[27] Solomon, E. I; Hare, J. W., Dooley, D. M., Dawson, J. H.; Stephens, P. J.; Gray, H. B. *J. Am. Chem. Soc.* **1980**, *102*, 168.

[28] Hemley, R. J.; Dawson, J. I.; Vaida, V. *J. Chem. Phys.* **1983**, *78*, 2915.

[29] Morris, D. E.; Woodruff, W. H. *J. Phys. Chem.* **1985**, *89*, 5795.

[30] Herschbach, D. R.; Laurie, V. W. *J. Chem. Phys.* **1961**, *35*, 458.

Chapter 4: A Structural Basis for Long-Range Coupling in Azurins from Resonance Raman Spectroscopy

Material previously published:

M. Adam Webb and Glen R. Loppnow

J. Phys. Chem. A **1999**, 103, pp. 6283-6287.

4.1 Introduction

Previous resonance Raman studies of plastocyanins,[1-3] blue copper proteins involved in photosynthesis in plants, have indicated that the spectra are sensitive to amino acid changes up to ~12Å from the copper metal ion and suggest that resonance Raman spectroscopy may be a powerful probe of coupling in these electron transport proteins. The frequencies of the resonance Raman modes are expected to be sensitive to the structure of the coordination sphere of the copper metal ion chromophore, while the resonance Raman intensities are influenced primarily by the excited-state dynamics. Little to no changes in frequency were observed in all the plastocyanins studied, suggesting the copper site geometry is very similar. However, the intensities appear to be much more sensitive to long-range interactions in the blue copper proteins. Two mechanisms have been suggested by which the resonance Raman intensities are influenced by the amino acid composition within 12 Å of the copper site.[1-3] The first is a short range (<8 Å) through-bond kinetic coupling of internal coordinates of nearby amino acids. The second is electrostatic interactions over distances of up to 13 Å from the copper site. Changes of amino acids >15 Å from the copper site did not appear to affect the resonance Raman spectra.

Although these previous studies indicated two possible long-range coupling mechanisms, they suffered from a lack of known plastocyanin crystal structures; only the x-ray crystal structure of poplar *a*,[4] and recently, spinach plastocyanin[5] are known. Instead, the interpretation of these results has rested on the crystal structure of poplar *a* plastocyanin alone, coupled with molecular modeling. Although the crystal structure of a spinach plastocyanin mutant, G8D, has recently become available[5] and supports this approach, the resolution of the structure is low. In an effort to understand the structural determinants of electron and charge transfer in protein environments from a more well-defined structural basis, we report here the resonance Raman spectra of four structurally characterized azurins, an analogous blue copper protein, from three species of bacteria, *Alcaligenes denitrificans* (AD), *Pseudomonas aeruginosa* (PA), and *Alcaligenes xylosoxidans* (AXI and AXII). The results presented here provide a strong structural basis for the interpretation of observed

resonance Raman intensity differences and frequency shifts as due to coupling between the active site and the surrounding protein matrix. This long-range coupling may explain the efficient electron transfer seen in these proteins.

4.2 Experimental

Azurin from *A. denitrificans* (AD) and *P. aeruginosa* (PA) was isolated and purified by methods described previously.[6] Azurin from *A. xylosoxidans* (NCIMB 11015, AXI and AXII) was isolated and purified by literature methods with slight modifications in the cell rupture and column chromatography steps (Figure 2.2).[7-9] Column chromatography was performed using Whatman CM-52 and Sephadex G-50 columns until the purity ratio (A_{280}/A_{620}) for azurin was ≤ 3.8 for AD, ≤ 2.1 for PA, 2.0-4.9 for AXI and 3.1-4.7 for AXII. Typical yields were 13-56 mg for AD, 46-58 mg for PA, 4-24 mg for AXI and 4-8 mg for AXII per 100 g of cell paste.

Samples were prepared for resonance Raman experiments by quantitative dilution with a cacodylate buffer solution (0.5-1.0 M cacodylate, 0.01 M Tris-HCl, pH 8.7). Room-temperature resonance Raman spectra were taken with 300 μL aqueous solutions (0.01 M Tris-HCl, 0.38-0.45 M cacodylate, pH 8.7) having an absorbance of 4-5 OD/cm at 620 nm. The addition of cacodylate did not have a noticeable effect on the absorption or resonance Raman spectra. Resonance Raman spectra were collected using a single monochromator with a CCD detector.[3,6] Laser excitation at 568.2 nm was obtained with a Kr ion laser (Coherent, Santa Clara, CA). The laser was spherically focused onto a 5-mm (o.d.) NMR tube containing the sample in a 135° backscattering geometry and with a typical power of 100-130 mW. Only the frequencies have been calibrated in the spectra presented, by measuring solvents of known frequencies (benzene, carbon tetrachloride and chloroform). Reported frequencies are accurate to ±2 cm^{-1}.

4.3 Results and Discussion

The azurin x-ray crystal structure from each species has been previously determined,[10-13] and the structure for *Pseudomonas aeruginosa* azurin with selected amino acids in the vicinity of the copper active site is shown in Figure 4.1. The copper has five coordinating atoms in a distorted trigonal bipyramidal geometry. Two nitrogens from His46 and His117 and a sulfur from Cys112 form a trigonal plane around the copper and are strongly bound. A sulfur from Met121 and an oxygen from Gly45 are weakly bound axial ligands. Figure 4.2 shows the resonance Raman spectra of the four species of azurin. Vibrational bands less than 300 cm^{-1} and bands near 800 cm^{-1} are not shown. The vibrational frequencies are generally similar for the four azurins. Strong modes occur between 330-500 cm^{-1} which have been interpreted to arise from the Cu–S(Cys) stretch mixed with other internal coordinates.[14] Weak Cu–N stretches are present at ~212, 250, and 274 cm^{-1} and a weak C–S stretch is present at 748 cm^{-1}(data not shown).[14] There is also an unassigned weak mode at 654 cm^{-1} (not shown). Although the spectra in Figure 4.2 are similar and exhibit similar frequencies, the relative intensities of the modes vary significantly between the species; these relative intensity differences were observed reproducibly with different excitation wavelengths within the S→Cu charge-transfer transition and from different preparations of each protein.

To interpret the observed resonance Raman spectral intensity differences from a sound structural basis, a number of correlations of the known protein structures[10-13] and sequences with the resonance Raman spectra were attempted. Each pair of spectra can be quantitatively compared by calculating the χ^2 values between the spectra. The reduced chi-squared value between the two resonance Raman spectra is calculated from: $\chi^2 = (1/f)\Sigma(I_1-I_2)^2$ where f is the number of degrees of freedom, I_1 and I_2 are resonance Raman spectral intensities for two species being compared, and the sum is carried out over the frequencies from 300-500 cm^{-1}. The χ^2 values are normalized so that the AD/AXII pair gives χ^2=1.0. These χ^2 values reflect both the intensity differences and the slight frequency shifts observed in Figure 4.2. As expected from Figure 4.2, the spectra for AD and AXII are the most similar and

Figure 4.1: Partial structure of *Pseudomonas aeruginosa* azurin near the copper site.[13] Amino acid differences among the four azurins within 10 Å of the copper site are shown. One-letter codes are given for the amino acids for each of the species *Alcaligenes denitrificans* (AD[10]), *Alcaligenes xylosoxidans* (AXII[11] and AXI[12]), and *Pseudomonas aeruginosa* (PA[13]). Structures are taken from the Brookhaven Data Bank.[15]

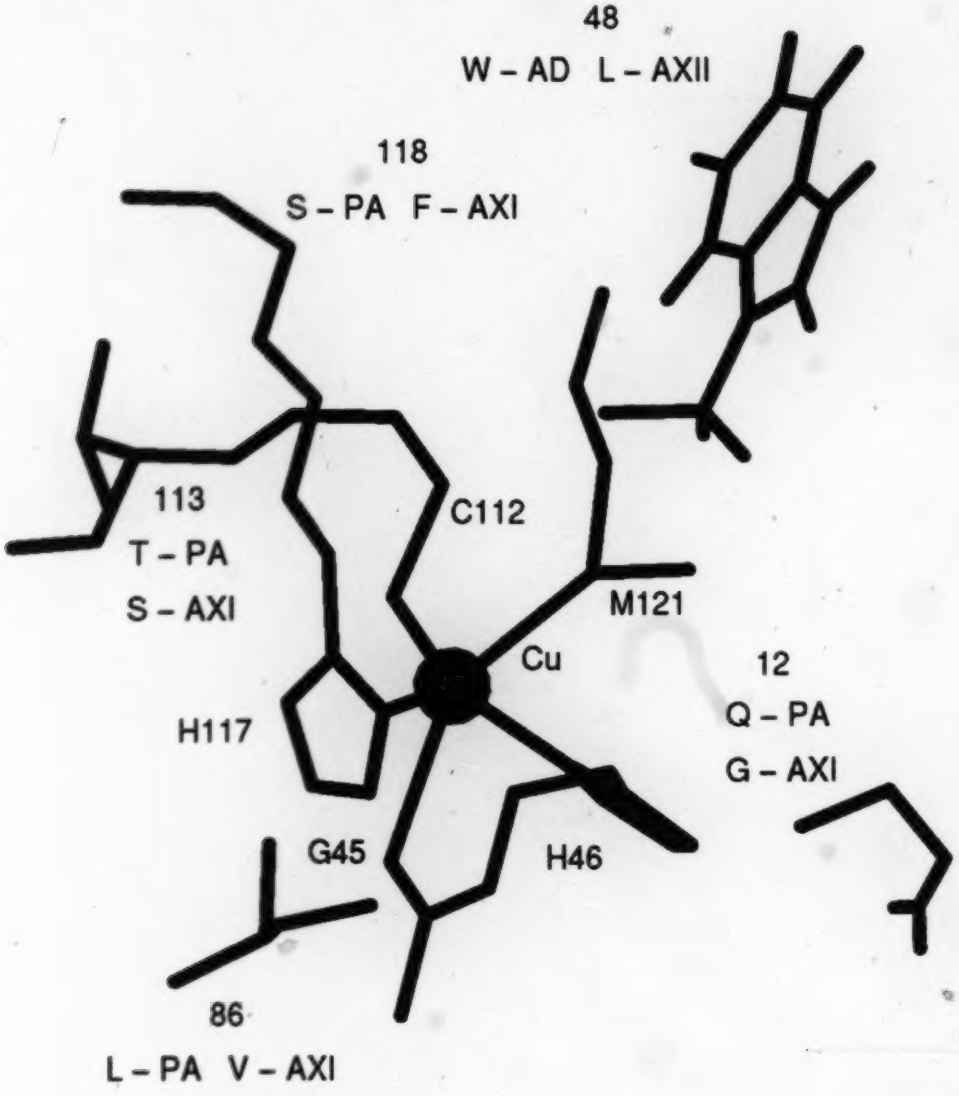
48
W – AD L – AXII
118
S – PA F – AXI
113
T – PA
S – AXI
C112
M121
Cu
12
Q – PA
G – AXI
H117
G45
H46
86
L – PA V – AXI

Figure 4.2: Resonance Raman spectra of azurins using an excitation wavelength of 568.2 nm. The spectra are labeled as in Figure 4.1. Vertical lines indicate species-dependent spectral changes. The spectra have been normalized to the highest-intensity peak and have been displaced along the y-axis for clarity.

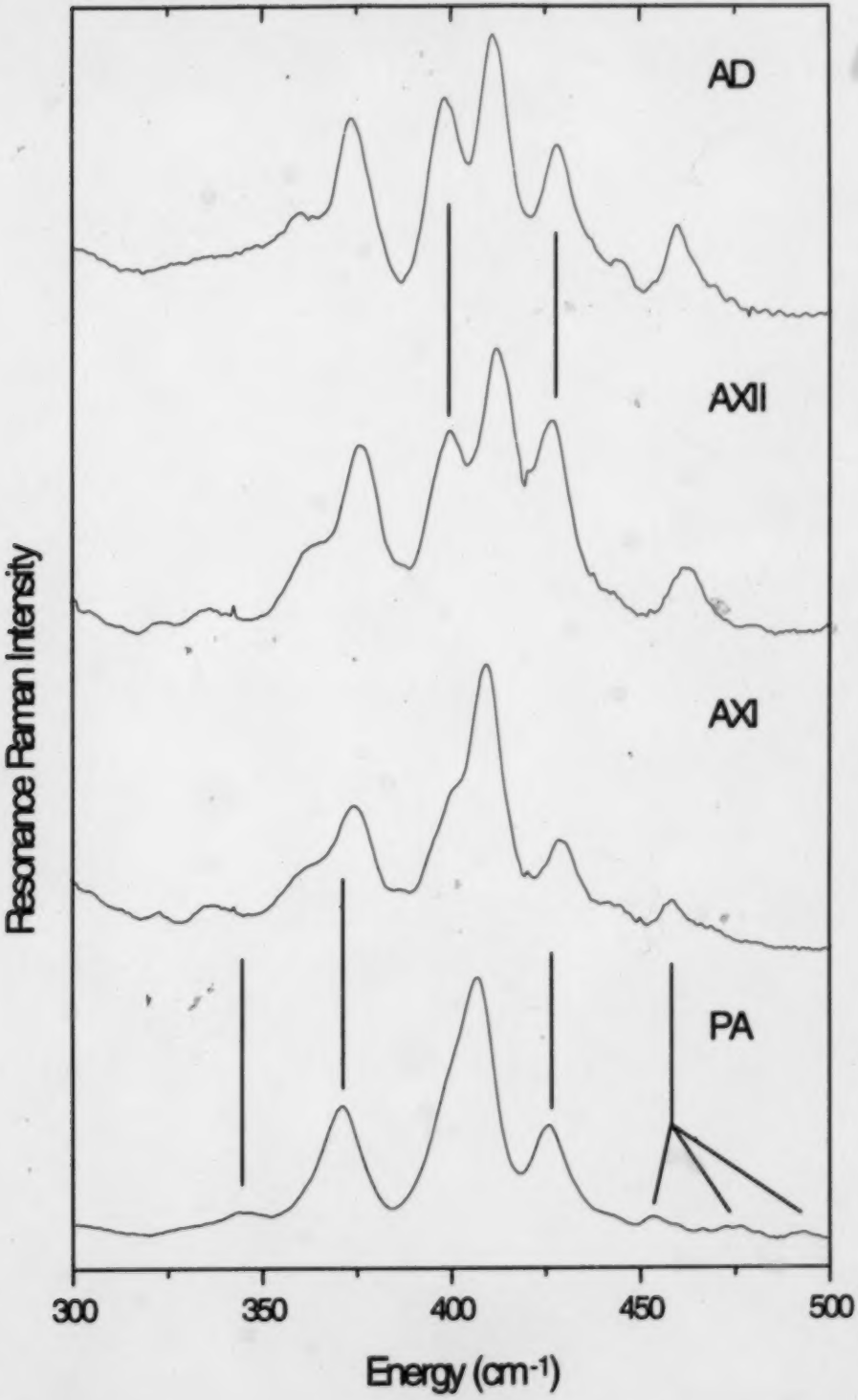
AD
AXII
AXI
PA
Resonance Raman Intensity
300
350
400
450
500
Energy (cm-1)

exhibit the smallest χ^2 (χ^2 = 1.0). Also, the spectrum of PA is most dissimilar with AD and AXII (χ^2 of 3.7 and 5.9, respectively), and is closest to AXI (χ^2 = 1.6).

The resonance Raman spectra are expected to be influenced by the structure of he coordination sphere and the protein environment around the copper metal ion. These two factors can be separated and examined independently to a certain extent. The x-ray structures of these four azurins show nearly identical secondary and tertiary structures and the protein backbones can be very closely superimposed. The root mean square (RMS) deviation between different pairs of azurins provides a convenient, quantitative means of comparing the azurin structures. The RMS deviation is calculated from the x, y and z coordinates over N atoms using RMS = $(\Sigma[(x_1-x_2)^2+(y_1-y_2)^2-(z_1-z_2)^2]/N)^{1/2}$ and the average x-ray crystal structures of each protein.[10-13] Two RMS deviations were calculated; one using only the copper atom and the five coordinating atoms (N, N, S, S, O), and the second using all the backbone and copper atoms (513 atoms per structure). The small RMS deviations using the entire protein backbone (RMS = 0.42-0.75 Å) indicates that the global structure of the four azurins are very similar to one another. The correlation coefficient of the resonance Raman difference parameter χ^2 vs. RMS deviation is 0.63 (Figure 4.3A), indicating a very rough relationship between overall protein backbone structure and the resonance Raman spectrum.

A similar examination of the copper center also shows few structural differences. The RMS deviation values are small (RMS = 0.12-0.22 Å), indicating that the azurin structures are also very similar at the copper center. Correlation of the resonance Raman spectral difference parameter χ^2 with the RMS deviation of the copper site is poor (Figure 4.3A), yielding a correlation coefficient of -0.45. Counter-intuitively, this suggests that the spectra tend to be more *similar* as the structural *differences* increase. A more detailed structural comparison of the copper center is given in Table 4.1. Because the most intense peaks near 400 cm^{-1} have been assigned to modes involving the Cu–S(Cys) bond,[14] it may be expected that the resonance Raman spectra would correlate with the Cu–S bond length. However, this is not what is observed, as the correlation coefficient of the resonance Raman spectral difference

Figure 4.3: Correlations of the azurin structures and sequences with resonance Raman spectral differences.

(A) Correlation of the spectral differences with the RMS deviation of the core atoms (R = -0.45, ■) and the protein backbone (R = 0.63, □).

(B) Correlation of the spectral differences with changes in Cu-S bond length (R = 0.41, ◆), and %identity (R = -0.88, ●). Note that the Raman spectral difference parameter χ^2 is expected to increase as the structural difference parameters, RMS deviation and ΔCu–S bond length, increase. However, χ^2 is expected to *decrease* as the %identity increases, as the %identity is a measure of environmental similarity.

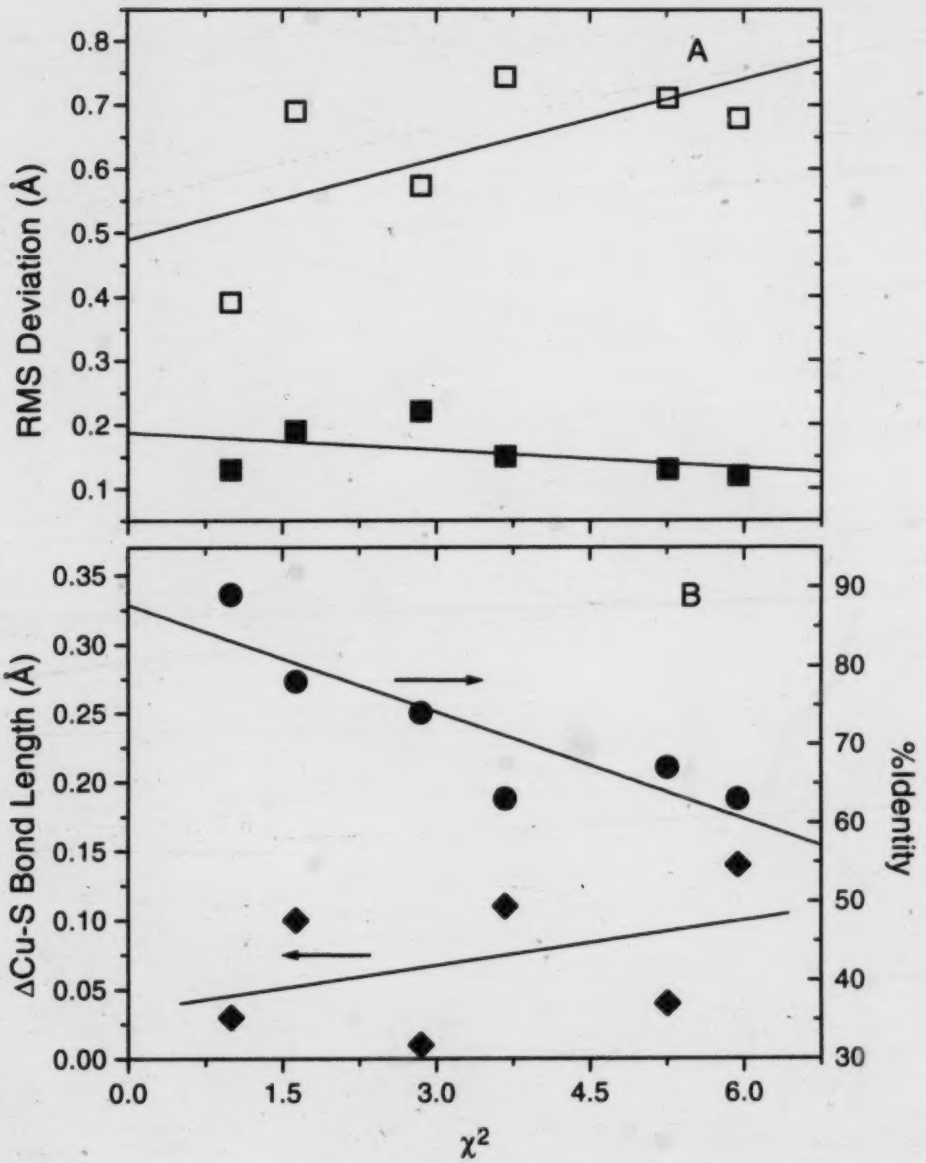
A
RMS Deviation (Å)
0.8
0.7
0.6
0.5
0.4
0.3
0.2
0.1
B
ΔCu-S Bond Length (Å)
0.35
0.30
0.25
0.20
0.15
0.10
0.05
0.00
%Identity
90
80
70
60
50
40
30
0.0
1.5
3.0
4.5
6.0
χ²

parameter χ^2 vs. ΔCu–S = $|d_{Cu\text{-}S,species1} - d_{Cu\text{-}S,species2}|$, where d is the bond length, is 0.41 (Figure 4.3B).

To determine if other copper site structural factors influence the resonance Raman spectrum, we compared the spectra of AD and AXII azurin, which have only two significant structural differences at the copper site. First, the Cu–O bond in AD azurin is 3.13 Å, similar to the 2.93 Å in PA azurin, and significantly different from the 2.75 Å in AXII azurin (Table 4.1). Second, in AD azurin the copper sits 0.13 Å above the NNS plane, as in AXI and PA azurin, while it is coplanar in AXII azurin (Table 4.1). These structural differences in the axial ligands do not qualitatively correlate well with the resonance Raman spectra, suggesting that differences in the copper site structure of this magnitude do not significantly influence the resonance Raman intensities. All of these results argue that the azurin resonance Raman spectra of these species do not correlate well with the structure of the copper site and suggest it is the protein environment, constructed by the amino acid side chains, which may be the determining factor in the resonance Raman spectrum and excited-state dynamics.

The protein forms the environment around the copper metal site via the amino acid side-chains. The microscopic local solvent properties, such as dielectric constant, polarity or hydrophobicity are determined by the amino acid side chains, while charged and dipolar amino acid residues create an electrostatic potential around the copper metal ion. To understand the effect of amino acid composition on the resonance Raman spectra, the %identity was calculated for each pair of azurins. The %identity is calculated from %identity = [1-(ΔAA/129)]×100%, where ΔAA is the number of amino acid changes. Only identical amino acids were used and sequence length differences were treated as amino acid changes. This method probably under-estimates the role of the amino acid environment, as the homology between these proteins is much higher than the identity. The %identity correlates well with the spectral difference parameter χ^2, with a correlation coefficient of -0.88 (Figure 4.3B). The negative sign indicates that the spectra become less different as the amino acid content becomes more similar, as expected. This good correlation supports the

Table 4.1: Distances around copper atom in azurins.

bond	AD	AXII	AXI	PA
Cu–N (H46)	2.08 Å	2.02 Å	1.97 Å	2.06 Å
Cu–N (H117)	2.00 Å	2.02 Å	1.92 Å	2.03 Å
Cu–S (C112)	2.15 Å	2.12 Å	2.16 Å	2.26 Å
Cu–S (M121)	3.11 Å	3.26 Å	3.18 Å	3.13 Å
Cu–O (G45)	3.13 Å	2.75 Å	2.51 Å	2.93 Å
Cu–NNS plane	0.13 Å	0.00 Å	0.13 Å	0.11 Å
ref.	10	11	12	13

X-ray crystal structures of each species were obtained from the Brookhaven Databank.[15] The Cu–NNS plane is the distance from the copper metal to the plane defined by the strongly ligated N, N, and S atoms.

hypothesis that the protein environment is the primary influence on the resonance Raman intensities in these proteins.

The ultimate goal of this work is to determine if specific resonance Raman spectral changes can be related to specific amino acid changes. In this way, it would be possible to look at specific interactions with distance to understand the long-range coupling in these electron transfer proteins. AD and AXII azurins have the highest number of identical amino acids and the most similar resonance Raman spectra. Within 16 Å of the copper metal there are only four amino acid changes (Table 4.2). The only difference within 10 Å of the copper site is a change in residue 48 from Trp in AD azurin to Leu in AXII azurin (Figure 4.1). This residue is also only two amino acids along the polypeptide strand from His46 and Gly45 which coordinate directly to the copper metal. In the plastocyanins,[1-3] changes in amino acids that are within a few amino acids of the copper center ligands along the same polypeptide strand were suggested to rotate the normal modes, resulting in a redistribution of intensity between two vibrational modes. This model is supported here by the observed changes in relative intensities of the modes at ~400 cm^{-1} and 428 cm^{-1}; in the spectrum of AD azurin the 428 cm^{-1} mode is less intense than the 400 cm^{-1} mode while it is more intense than the 400 cm^{-1} mode in the spectrum of AXII azurin. A second amino acid change is residue 16 from an Asp in AD azurin to an Asn in AXII azurin. This amino acid change removes a negative charge 13.4 Å from the copper, but leaves a dipole. A third amino acid change is residue 42 which changes from Ser in AD to Val in AXII and results in a loss of a dipole 12.8 Å from the copper. Note that the distance to the charges was measured from the copper to the atoms of the side chain which nominally carry the charge. In plastocyanin, dipole changes up to 12-13 Å from the copper site were seen to slightly affect the absolute intensities in resonance-enhanced modes.[1] In azurin, it appears that these two changes have a minimal effect on the resonance Raman spectrum. The fourth amino acid change is residue 7 changing from Ile in AD to Val in AXII. This is a minor, homologous change 10.5 Å from the copper and is unlikely to affect the spectrum. In plastocyanin it was found that homologous changes near the copper site on β-strands that are not

Table 4.2: Amino acid differences in azurin.

AD/AXII					AXI/PA				
residue change[a]			Å[b]	Δ[c]	residue change[a]			Å[b]	Δ[c]
7	Ile	Val	10.5	0/0	8	Ala	Gln	11.1	0/polar
16	Asp	Asn	12.6	-/polar	12	Gly	Gln	10.0	0/polar
42	Ser	Val	12.0	polar/0	16	Asp	Asn	12.1	-/polar
48	Trp	Leu	8.1	ϕ/0	34	Lys	Ser	11.4	+/polar
					40	Ala	Pro	10.7	0/0
					71	Asn	Asp	10.9	polar/-
					73	Val	Leu	11.3	0/0
					86	Val	Leu	6.3	0/0
					89	Gly	Ser	11.6	0/polar
					110	Tyr	Phe	10.5	polar, ϕ/ϕ
					113	Ser	Thr	7.6	polar/polar
					118	Phe	Ser	8.2	ϕ/polar

[a]The residue number is listed first followed by the amino acids for the two species to be compared. [b]This distance is measured from the copper site to the closest amino-acid side chain atom. Residues in bold are within 10 Å of the copper site and are shown in Figure 4.1. [c]Electrostatic changes are differences in charge or polarity of the amino acids. In the table, "0" is uncharged and non-polar, "ϕ" is aromatic, "polar" is uncharged and polar, "-" is negatively charged and "+" is positively charged.

directly covalently linked to the copper site have no effect on the resonance Raman spectra.[1]

The other pair of species which yield similar resonance Raman spectra is PA and AXI. The amino acid %identity is 78% and the resonance Raman spectra have a general similarity. A detailed examination of the spectra, however, reveals several significant changes (Figure 4.2). There are a total of 12 amino acid changes within 16 Å of the copper site and so it would be difficult to ascribe specific spectral changes to individual amino acid changes in this case. However, it may be possible to identify amino acid changes which are likely to be more important. There are three amino acid changes which occur within two amino acids along polypeptide strands ligated to the copper. Two conservative changes are Thr113 in PA azurin changing to Ser in AXI azurin and Phe110 in PA azurin is Tyr in AXI azurin, with Tyr adding a dipole 12.8 Å from the copper site in AXI. Both of these changes are on the same polypeptide strand as Cys112, although Tyr110 is physically closer to Met121. A significant change is Ser118 in PA azurin changing to Phe in AXI azurin. Ser has a dipole 8.8 Å from the copper site which is replaced by the aromatic ring of Phe in AXI azurin. This amino acid is adjacent to His117 and is expected to cause a significant redistribution of intensity in the spectra.

There are also three charge and three dipolar residue differences between AXI and PA azurin. AXI azurin has a negative charge (Asp16) 12.9 Å from the copper and a positive charge (Lys34) 15.1 Å from the copper, while PA azurin has a negative charge (Asp71) 11.8 Å from the copper metal (distance is from Cu to side chain atoms which nominally carry the charge). In each case, the charged amino acid is replaced by a dipole at a similar distance in the respective proteins; Asp16, Lys34, and Asn71 in AXI azurin becomes Asn, Ser and Asp in PA azurin, respectively. PA azurin has three additional dipoles compared to AXII. These are Gln8, Gln12 and Ser89 which replace Ala8, Gly12 and Gly89 in AXI. The distribution of charges and dipoles forms an electrostatic environment which may change the potential energy surface of the charge-transfer excited-state and/or the electronic coupling through the protein in its electron transfer function. The remaining three changes within 16 Å of

the copper site are homologous replacements. The first two are Leu86 and Leu73 in PA azurin changing to Val in AXI azurin. These are minor changes which are not likely to have much effect on the resonance Raman spectra. The third change is Pro40 in PA azurin to Ala in AXI azurin. Going from the conformationaly restricted Pro to Ala is likely to decrease the structural rigidity of AXI compared to PA and may have some structural effect on the copper site.

4.4 Conclusion

The results presented here demonstrate a sound structural basis for the correlation between protein environment and excited-state properties, as reflected in the resonance Raman intensities, by systematically examining the resonance Raman spectra of a series of homologous structurally-determined azurins. Confirmation of the two mechanisms by which the protein affects the excited-state dynamics, via a through-bond kinetic coupling of internal coordinates and through-space electrostatic interactions, is tentatively provided by the known structures of the four azurins presented here. Because the resonance Raman intensities and frequencies appear to be sensitive to these coupling mechanisms, resonance Raman spectroscopy could provide a uniquely powerful probe of long-range coupling in these proteins and provide a mechanistic insight in the efficient long-range electron transfer observed in these proteins. Clearly, probing the putative differential sensitivity of the resonance Raman intensities to electrostatic and kinetic coupling factors in the protein environment by using structurally-characterized site-directed azurin mutants is necessary. Such studies are in progress.

4.5 References

[1] Fraga, E.; Loppnow, G. R. *J. Phys. Chem. B* **1998**, *102*, 7659.

[2] Loppnow, G. R.; Fraga, E. *J. Am. Chem. Soc.* **1997**, *119*, 896.

[3] Fraga, E.; Webb, M.A.; Loppnow, G. R. *J. Phys. Chem.* **1996**, *100*, 3278.

[4] Guss, J. M.; Bartunik, H. D.; Freeman, H. C. *Acta Crystallogr.* **1992**, *B48*, 790.

[5] Xue, Y; Mats, Ö.; Hansson, Ö.; Young, S. *Protein Science* **1998**, *7*, 2099.

[6] Webb, M. A.; Kwong, M. C.; Loppnow, G. R. *J. Phys. Chem. B* **1997**, *101*, 5062. This is Chapter 2 in this thesis.

[7] Ambler, R. P. *Biochem. J.* **1963**, *89*, 341.

[8] Abraham, Z. H. L.; Lowe, D. J.; Smith, B. E. *Biochem. J.* **1993**, *295*, 587.

[9] Dodd, F. E.; Hasnain, S. S.; Hunter, W. N.; Abraham, Z. H. L.; Debenham, M.; Kanzler, H.; Eldridge, M.; Eady, R. R.; Ambler, R. P.; Smith, B. E. *Biochemistry* **1995**, *34*, 10180.

[10] Baker, E. N. *J. Mol. Biol.* **1988**, *203*, 1071.

[11] Dodd, F. E.; Hasnain, S. S.; Abraham, Z. H. L.; Eady, R. R.; Smith, B. E. *Acta Cryst* **1995**, *D51*, 1052.

[12] Li, C.; Inoue, T.; Gotowda, M.; Suzuki, S.; Yamaguchi, K.; Kai, K.; Kai, Y. *Acta. Cryst.* **1998**, *D54*, 347.

[13] Nar, H.; Messerschmidt, A.; Huber, R.; van de Kamp, M.; Canters, G. W. *J. Mol. Biol.* **1991**, *221*, 765.

[14] Blair, D. F.; Campbell, G. W.; Schoonover, J. R.; Chan, S. I.; Gray, H. B.; Malmstrom, B. G.; Pecht, I.; Swanson, B. I.; Woodruff, W. H.; Cho, W. K.; English, A. M.; Fry, H. A.; Lum, V.; Norton, K. A. *J. Am. Chem. Soc.* **1985**, *107*, 5755.

[15] Bernstein, F. C.; Koetzle, T.F.; Williams, G. J. B.; Meyer, E. F. Jr.; Brice, M. D.; Rodgers, J. R.; Kennard, O.; Shimanouchi, T.; Tasumi, M. *J. Mol. Biol.* **1977**, *112*, 535.

Chapter 5: Evidence for Anisotropic Long-Range Coupling Between the Active Site and Protein in Four Azurins

5.1 Introduction

Blue copper proteins, such as azurin, are involved in electron transport chains.[1] These proteins exhibit efficient and rapid long-range intramolecular electron transfer. Understanding electron transfer and the role of distance, medium, orientation and protein structure has been the subject of much work.[2-6] The electron transfer rate constant is dependent on the electronic coupling, H_{DA}, between electron donor and acceptor at the transition state by the Marcus equation as follows:[2]

$$k = \frac{2\pi}{\hbar} \frac{H_{DA}^2}{(4\pi\lambda RT)^{1/2}} e^{-(\Delta G^\circ + \lambda)^2/4\lambda RT} \qquad (5.1)$$

where ΔG° is the standard free energy of reaction and λ is the nuclear reorganization energy. For large separation of donor and acceptor H_{DA} is expected to decay exponentially as follows:[2]

$$H_{DA} = H_{DA}^0 e^{-\beta(r - r_0)} \qquad (5.2)$$

where H_{DA}^0 is the coupling at r_0, r_0 is the van der Waals separation between electron donor and acceptor, r is the actual distance between electron acceptor and donor, and β is an empirical decay constant. The value of β is thought to depend on the specific electron transfer pathway.[2,5-7]

Electron transfer rates can be measured by using an electron donor which can be triggered by a laser pulse to transfer an electron from the donor to copper(II). One method to measure intramolecular electron transfer rate constants has been to use Ru-modified azurin.[5,8,9] $Ru(bpy)_2(im)^{3+}$ (bpy = 2,2'-bipyridine, im = imidazole) is attached to an existing histidine[10,11] or to a histidine introduced into the protein using site-directed mutagenesis.[6,12] Electron transfer to the copper site from ruthenium is initiated using a laser pulse. A second method is to use electron transfer from the existing disulfide bridge (Cys3-Cys26) to the copper site, which provides a different pathway.[13,14] In this method, pulse radiolysis experiments are used to measure electron transfer rates for wild type protein and mutants.[4,15] A third method is to use photoexcitation of 1-thiouredopyrene-3,6,8-trisulfonic (TUPS) adducts of amino acids.[16] Lysine-TUPS derivatives of azurin are prepared chemically and the transient

absorption kinetics of the copper(II) reduction and copper(I) reoxidation are measured.[17,18] This method provides new pathways for electron transfer. Electron transfer can be measured using these various methods for wild type and mutant azurin to evaluate the kinetics for various pathways. These measurements yield the dependence of the H_{DA} and β on protein composition and structure.

Resonance Raman spectroscopy may provide information about electronic and vibronic coupling, which are important for electron transfer, along electron transfer pathways. In Chapters 2 and 3, the absorption spectra and the resulting resonance Raman excitation profiles of azurin from *P. aeruginosa*[19] and *A. denitrificans*[20] have been analyzed. This chapter continues with a similar analysis of two *A. xylosoxidans* azurins. In Chapter 4 it was seen that AXI and AXII azurin have high homology to azurin from *Alcaligenes denitrificans* (AD) and *Pseudomonas aeruginosa* (PA), respectively, and the resonance Raman spectra of AXI and AXII azurin are quite similar to PA and AD azurin, respectively. The good correlation of spectral differences with protein composition indicates that resonance Raman is sensitive to the coupling of the copper to the protein environment. In this chapter, a quantitative analysis of the four azurin species is done to test the qualitative ideas of Chapter 4 and to more closely examine the relationship between electron transfer and the resonance Raman intensities. The total inner sphere reorganization energy was found to be the same for the four azurin species. However, there are significant differences in the parameters found, most prominently in the mode-specific reorganization energies, and this will be discussed in greater detail below. Surprisingly, the resonance Raman spectra seem to be more sensitive to amino acid changes in one direction than in others. This result suggests an anisotropic long-range coupling between the copper active site and the protein, and that resonance Raman spectroscopy may be sensitive to hard-wired electron transfer pathways.

5.2 Methods

5.2.1 Experimental

The two azurins from *Alcaligenes xylosoxidans* (AXI and AXII) were isolated and purified as described previously in Chapters 2 and 4 using modified literature procedures.[21-24] Column chromatography was used to obtain a purity ratio A_{280}/A_{620} of 2.0-4.9 for AXI and 3.1-4.7 for AXII. Typical yields were 4.24 mg of AXI and 4-8 mg of AXII per 100 g of cell paste.

Samples were prepared for resonance Raman experiments by quantitative dilution with a cacodylate buffer solution (0.5-1.0 M cacodylate, 0.01 M TRIS-HCl, pH 8.7). Addition of cacodylate buffer did not have a noticeable effect on the absorption or resonance Raman spectra of azurin. Room-temperature resonance Raman spectra were taken as described previously[19] using 250-300 μL aqueous samples (0.01 M TRIS-HCl, pH 8.7, 0.45-0.83 M and 0.34-0.75 M cacodylate for AXI and AXII, respectively) having an absorbance of 1-11 OD/cm and 2-5 OD/cm for AXI and AXII, respectively. Bleaching of the sample was accounted for by measuring the absorption at 560 nm (ε_{560} = 2720 $M^{-1}cm^{-1}$ (AXI), ε_{560} = 2710 $M^{-1}cm^{-1}$ (AXII)). The average absorbance was used to calculate the concentration of azurin.

Absolute resonance Raman cross sections of azurin were found using the relative integrated intensities of azurin and cacodylate as previously described in Chapter 2.[19] Absolute Raman cross sections of cacodylate were calculated from the A-term expression.[19,25] The calculated Raman cross sections for cacodylate are 113, 110, 96.7, 96.0 and 87.1 × 10^{-14} $Å^2$/molecule at 579.7, 582.1, 599.6, 600.6 and 613.7 nm, respectively.

5.2.2 Intensity Analysis

The resonance Raman and absorption cross sections in the Condon approximation can be written using the time dependent equations of Lee and Heller.[19,26-28] The implementation of these equations has been described in detail.[26,27,29,30] Self-consistent analysis of the absorption spectrum and the resonance Raman excitation profiles was done in the same manner as previously described for

plastocyanin[27,29] and azurin.[19] The resonance Raman excitation profiles provided the primary constraints on the simulated spectral band shape and bandwidth. The scaling of the Δ's was determined by the width of the resonance Raman excitation profiles and the relative Δ's were determined by the relative intensities. The reorganization energy in a mode, λ_i, is related to Δ_i by $\lambda_i=(\Delta_i^2\omega_i)/2$ where ω_i is the frequency in cm^{-1}. The total inner-sphere reorganization energy is the sum of the reorganization energy of the individual modes.

5.3 Results and Discussion

5.3.1 Analysis of *A. xylosoxidans* I and II

The resonance Raman spectra were taken for the two azurins throughout the S→Cu charge transfer absorption band. Figure 5.1 and Figure 5.2 show the resonance Raman spectra of AXI and AXII, respectively. In Chapter 4 it was noted that the spectrum of AXII is comparable to that of azurin from *A. denitrificans*. Similarly, the resonance Raman spectra of AXI and PA azurin are comparable. Analysis of the absorption spectra and the resulting resonance Raman excitation profiles with Equations 2.4 and 2.5 gave the results given in Table 5.1 and Table 5.2. The fits to the absorption spectra are given in Figure 5.3. The deviations of the fit are due to the presence of electronic transitions which are not modeled and do not contribute resonance enhancement. The fits to the resonance Raman excitation profiles are shown in Figure 5.4 and Figure 5.5 for AXI and AXII, respectively. The resulting parameters can be compared to the results obtained previously for AD and PA azurin.

In Chapter 4 the spectra were compared to each other to test for correlation between spectral intensity differences and structure and sequence.[21] For these comparisons the spectra were normalized to the intensity of the most intense mode. This analysis compared changes of relative intensities and frequencies while ignoring absolute intensity. In this work, the absolute resonance Raman cross sections of both *A. xylosoxidans* azurins have been measured and so the spectra can be scaled to

Figure 5.1: Resonance Raman spectra of *A. xylosoxidans* I azurin. Spectra shown are typical scans and have been divided by a tungsten-halogen lamp spectrum (Eppley Laboratory, Inc.). The cacodylate internal standard appears at 605 and 638 cm^{-1}.

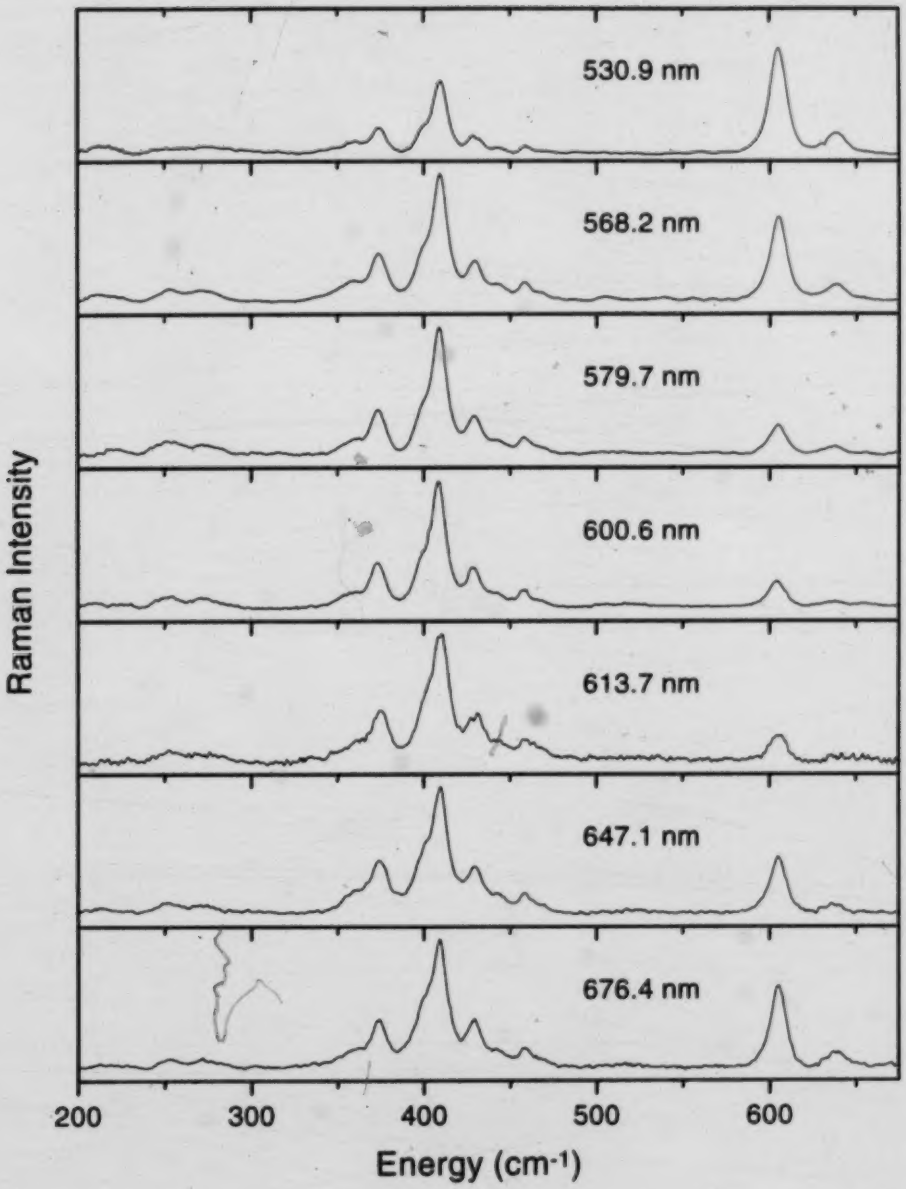
530.9 nm
568.2 nm
579.7 nm
600.6 nm
613.7 nm
647.1 nm
676.4 nm
Raman Intensity
200
300
400
500
600
Energy (cm-1)

Figure 5.2: Resonance Raman spectra of *A. xylosoxidans* II azurin. Spectra shown are typical scans and have been divided by a tungsten-halogen lamp spectrum (Eppley Laboratory, Inc.). The cacodylate internal standard appears at 605 and 638 cm^{-1}.

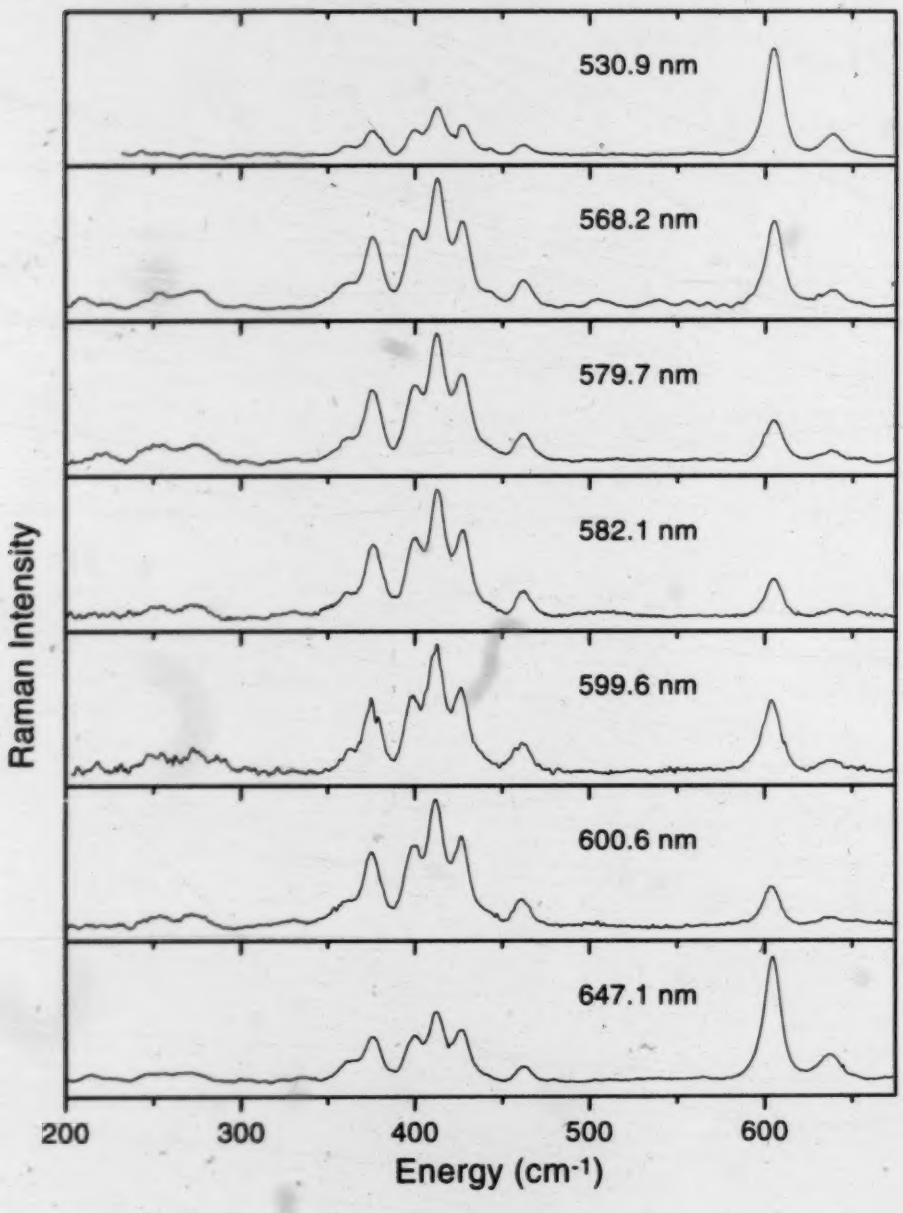
530.9 nm
568.2 nm
579.7 nm
582.1 nm
599.6 nm
600.6 nm
647.1 nm
Raman Intensity
200
300
400
500
600
Energy (cm-1)

Table 5.1: Absolute resonance Raman cross sections of *A. xylosoxidans* I azurin.

		Excitation wavelength/nm										
$\bar{\nu}$	$\lvert\Delta\rvert$	530.9	568.2	579.7	580	582.1	599.6	600.6	613.7	618.5	647.1	676.4
252	0.92	0.56/0.34	0.66/1.07	2.19/1.33	---/1.34	1.54/1.38	1.56/1.66	1.54/1.67	1.68/1.70	1.27/1.68	0.86/1.21	0.28/0.57
271	0.97	0.49/0.44	1.27/1.38	2.17/1.71	---/1.72	1.87/1.77	2.15/2.12	1.91/2.13	2.37/2.17	1.76/2.14	0.90/1.53	0.52/0.72
360	0.96	0.89/0.80	2.14/2.43	2.82/3.00	2.99/3.01	2.84/3.11	2.65/3.65	3.12/3.67	4.02/3.70	2.67/3.62	1.91/2.52	0.80/1.15
374	1.29	1.26/1.58	3.09/4.81	6.14/5.92	3.87/5.94	6.58/6.12	5.58/7.18	6.05/7.21	8.41/7.25	6.46/7.10	3.18/4.91	1.62/2.24
398	1.29	1.21/1.79	2.82/5.42	7.02/6.65	6.96/6.68	7.19/6.88	6.65/8.04	7.75/8.07	8.68/8.09	7.05/7.92	3.22/5.43	2.45/2.46
410	1.81	3.15/3.79	6.77/11.4	16.2/14.0	13.9/14.1	17.0/14.5	13.5/16.9	14.9/17.0	19.3/17.0	15.5/16.6	6.42/11.3	3.88/5.12
429	1.16	1.09/1.72	2.72/5.15	6.90/6.30	6.41/6.33	7.02/6.52	5.77/7.57	6.64/7.59	9.47/7.58	6.40/7.40	3.00/5.03	2.06/2.26
444	0.50	0.19/0.34	0.60/1.01	1.61/1.24	1.45/1.24	1.49/1.28	1.47/1.48	1.55/1.49	2.47/1.48	0.77/1.44	0.56/0.98	0.48/0.44
458	0.56	0.25/0.47	0.74/1.39	1.94/1.70	1.75/1.70	1.88/1.75	2.04/2.02	1.93/2.03	2.58/2.02	1.04/1.97	0.74/1.32	0.55/0.59
468	0.36	0.11/0.20	0.33/0.58	0.79/0.71	0.70/0.71	0.63/0.73	0.87/0.85	0.67/0.85	1.50/0.84	0.55/0.82	0.28/0.55	0.23/0.24

The resonance Raman cross sections are shown as experimental/calculated in units of $Å^2$/molecule $\times 10^{10}$. A --- indicates no signal was observed above the baseline noise and no cross section was measured. The errors in cross sections are ±10% for strong lines and ±20% for weak lines. The observed Raman shifts, $\bar{\nu}$, are in units of cm^{-1} and Δ's are in dimensionless normal coordinates. The cross sections were calculated using Equation 2.4 and the following parameters: zero-zero energy, E_0 = 14,150 cm^{-1}, transition length, M = 0.81 Å, temperature, T = 0 K, refractive index, n = 1.33, Lorentzian homogeneous linewidth, Γ_L = 500 cm^{-1}, Gaussian homogeneous linewidth, Γ_G = 150 cm^{-1}, inhomogeneous linewidth, Θ = 0 cm^{-1}.

Table 5.2: Absolute resonance Raman cross sections of *A. xylosoxidans* II azurin.

		Excitation wavelength/nm						
$\bar{\nu}$	$\|\Delta\|$	530.9	568.2	579.7	582.1	599.6	600.6	647.1
251	0.94	---/0.34	0.74/1.11	1.99/1.35	1.22/1.39	1.50/1.52	1.04/1.52	0.80/0.68
270	0.99	---/0.44	1.00/1.45	1.72/1.76	1.43/1.81	2.46/1.98	1.15/1.97	0.83/0.87
362	0.90	0.53/0.69	2.26/2.20	2.50/2.62	2.68/2.69	1.68/2.88	2.54/2.87	1.57/1.19
376	1.24	1.08/1.42	3.22/4.49	5.23/5.35	5.69/5.48	5.43/5.85	4.65/5.84	3.04/2.40
399	1.31	1.11/1.81	3.96/5.70	6.51/6.76	6.93/6.93	6.71/7.35	6.11/7.33	3.41/2.96
413	1.42	2.13/2.30	4.97/7.19	8.73/8.52	8.81/8.72	8.55/9.22	7.06/9.19	4.00/3.68
426	1.25	1.27/1.89	3.97/5.89	7.16/6.96	7.19/7.13	6.71/7.51	5.75/7.48	3.51/2.97
440	0.52	0.41/0.35	0.69/1.09	1.48/1.28	1.24/1.31	1.13/1.38	0.99/1.37	0.43/0.54
462	0.69	0.40/0.69	1.17/2.11	2.54/2.49	2.06/2.54	2.85/2.66	1.77/2.64	0.93/1.03

The resonance Raman cross sections are shown as experimental/calculated in units of $Å^2$/molecule $\times 10^{10}$. A --- indicates no signal was observed above the baseline noise and no cross section was measured. The errors in cross sections are ±10% for strong lines and ±20% for weak lines. The observed Raman shifts, $\bar{\nu}$, are in units of cm^{-1} and Δ's are in dimensionless normal coordinates. The cross sections were calculated using Equation 2.4 and the following parameters: zero-zero energy, E_0 = 14,800 cm^{-1}, transition length, M = 0.63 Å, temperature, T = 0 K, refractive index, n = 1.33, Lorentzian homogeneous linewidth, Γ_L = 285 cm^{-1}, Gaussian homogeneous linewidth, Γ_G = 0 cm^{-1}, inhomogeneous linewidth, Θ = 250 cm^{-1}.

Figure 5.3: Absorption spectra of *A. xylosoxidans* I/II azurin.

(A) Experimental (solid) and calculated (dashed) absorption spectra of *A. xylosoxidans* I azurin. The dashed line was calculated using Equation 2.5 and the parameters in Table 5.1.

(B) Experimental (solid) and calculated (dashed) absorption spectra of *A. xylosoxidans* II azurin. The dashed line was calculated using Equation 2.5 and the parameters in Table 5.2.

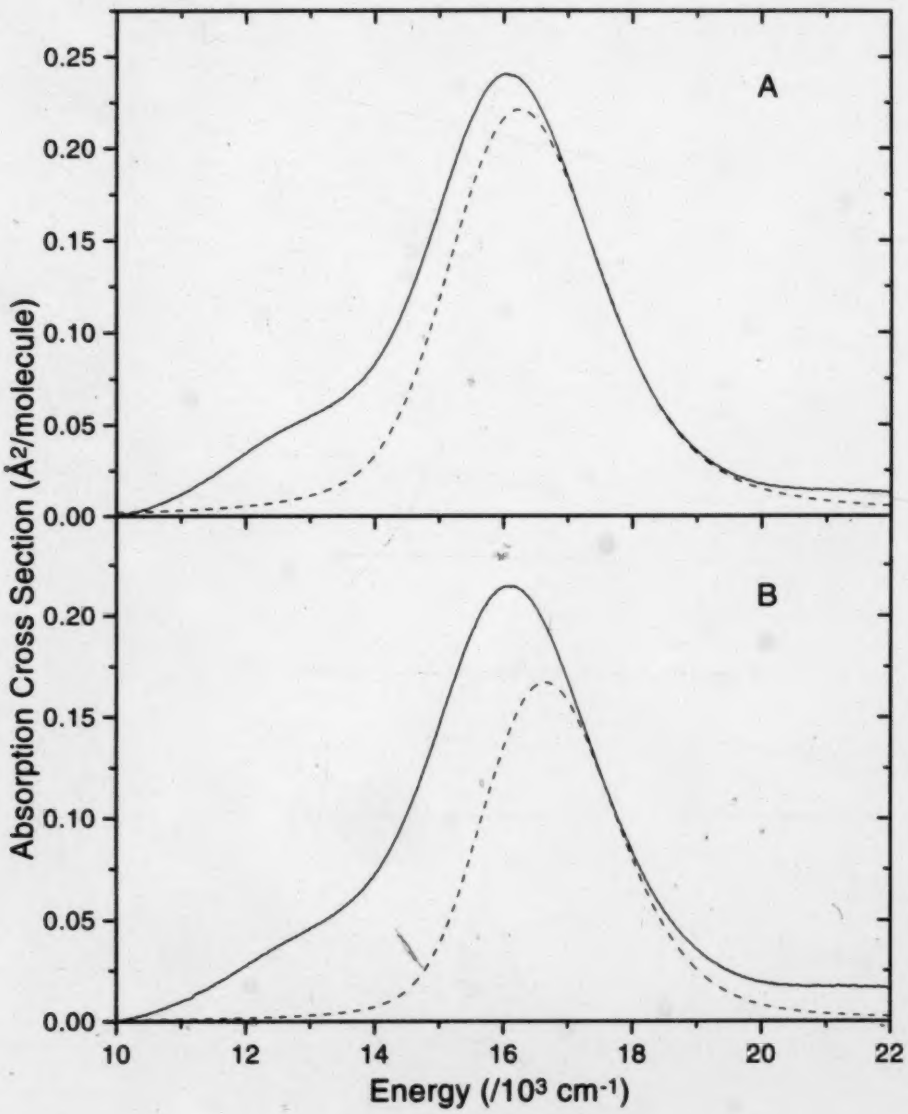
A
B
0.25
0.20
0.15
0.10
0.05
0.00
Absorption Cross Section (Å²/molecule)
10
12
14
16
18
20
22
Energy (/10³ cm⁻¹)

Figure 5.4: Resonance Raman excitation profiles of *A. xylosoxidans* I azurin. The solid lines were calculated using Equation 2.4 with the parameters in Table 5.1.

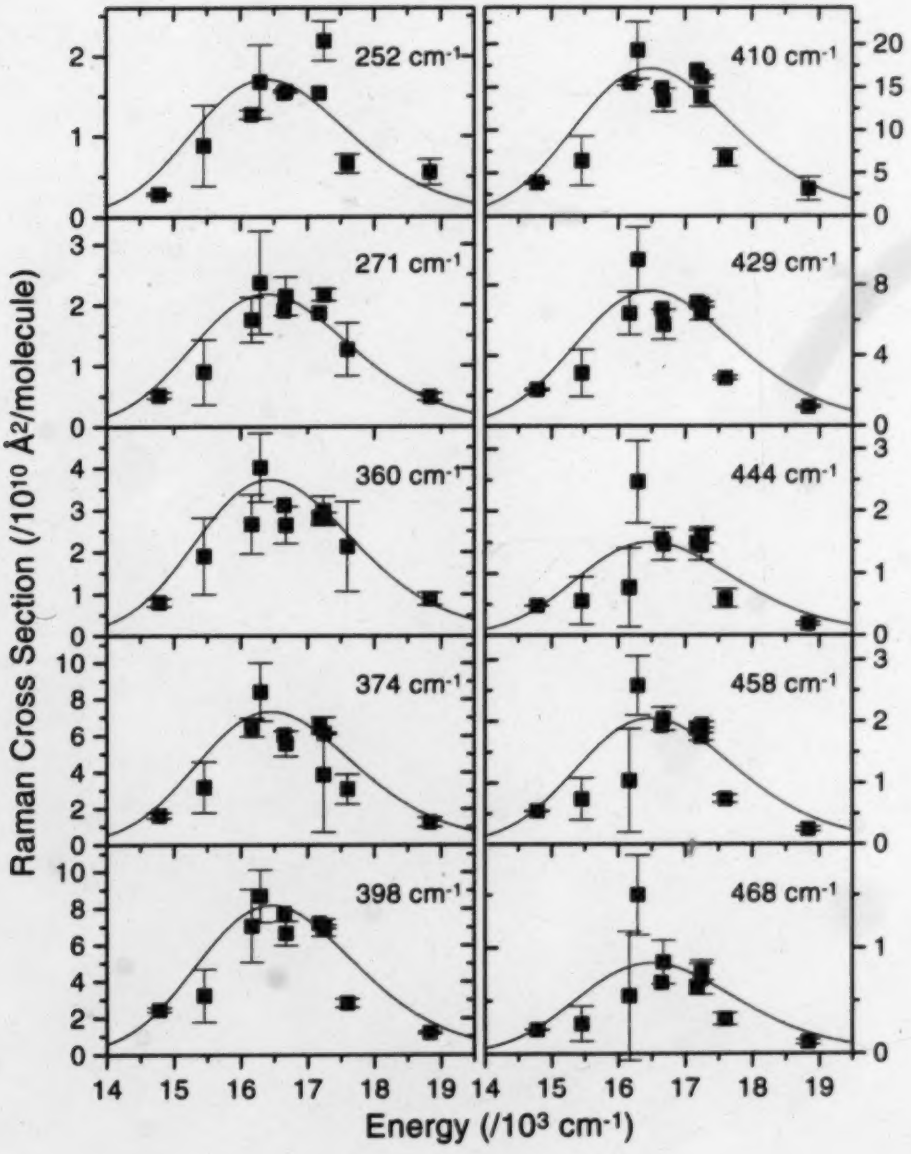
252 cm-1
410 cm-1
271 cm-1
429 cm-1
360 cm-1
444 cm-1
374 cm-1
458 cm-1
398 cm-1
468 cm-1
Raman Cross Section (/10^10 Å^2/molecule)
Energy (/10^3 cm-1)

Figure 5.5: Resonance Raman excitation profiles of *A. xylosoxidans* II azurin. The solid lines were calculated using Equation 2.4 with the parameters in Table 5.2.

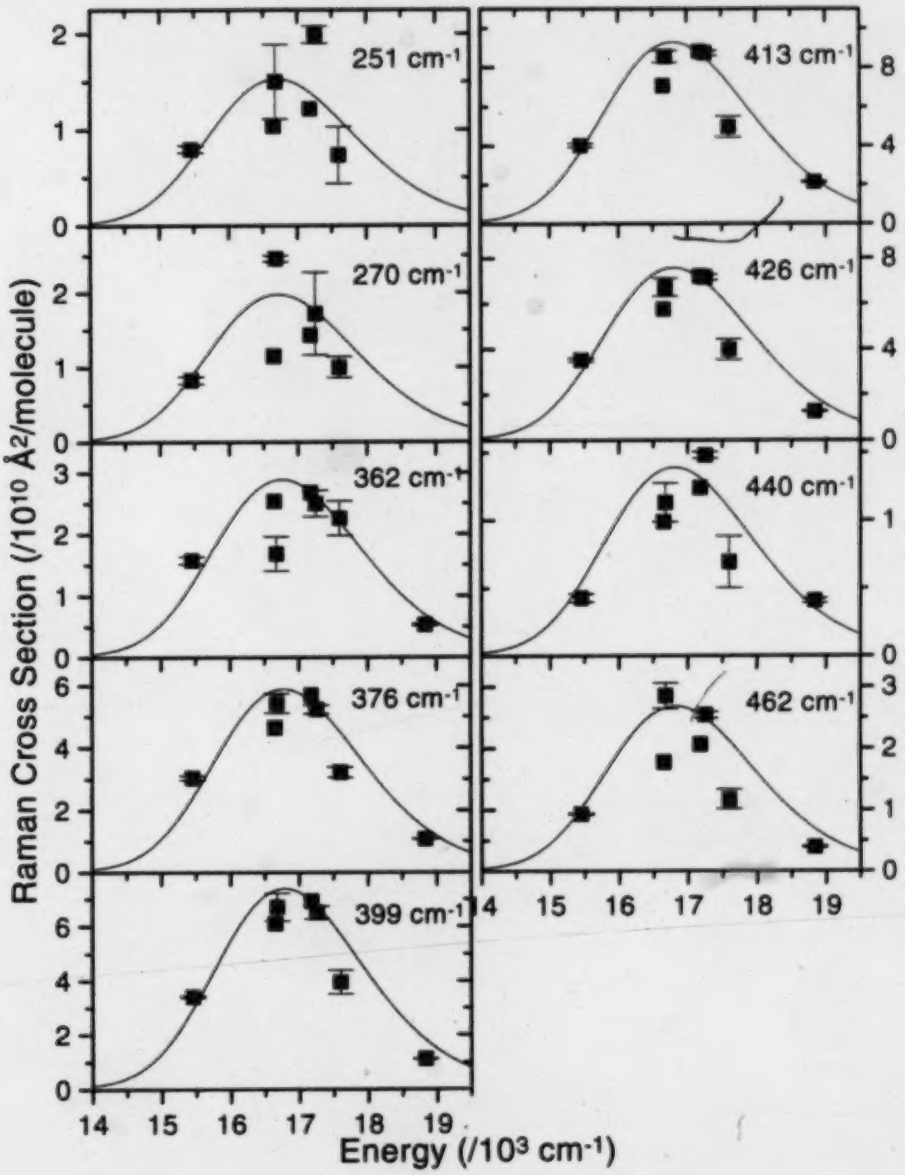
251 cm-1
413 cm-1
270 cm-1
426 cm-1
362 cm-1
440 cm-1
376 cm-1
462 cm-1
399 cm-1
Raman Cross Section (/10^10 Å^2/molecule)
Energy (/10^3 cm^-1)

reflect the true cross section. This process will reveal more accurate relationships between the spectroscopic results and molecular structure and composition. The spectra of the four azurins at 568.2 nm were scaled to the cross sections and χ^2 values calculated as before.[21] The χ^2 values are normalized so that the AD/AXII pair gives χ^2=1.0. The most similar spectra are AD and AXII (χ^2 = 1.0). The spectrum of PA is most dissimilar with AD and AXII (χ^2 = 2.4 and χ^2 = 3.1) and is closest with AXI (χ^2 = 1.2). AXI is closer to AD than AXII (χ^2 = 1.6 and χ^2 = 2.1). Figure 5.6 is the analogous graph to Figure 4.3 and shows the correlations of the spectral differences to structure and sequence. The values of RMS difference and %identity are taken from Chapter 4.[21] The relatively poor correlation of the spectra with structure, as reflected by the RMS difference of the backbone (0.63) and copper center (-0.43), has not changed. Therefore, the resonance Raman spectra show a very weak correlation with overall protein structure and no correlation to the copper site geometry. However, the correlation to the Cu–S bond length has increased from 0.41 to 0.64 and suggests a very weak correlation, of similar magnitude as the correlation with the protein backbone. The correlation with %identity increases slightly from –0.88 to –0.91 supporting the hypothesis of Chapter 4 that the protein environment is the primary influence on the resonance Raman intensities.

5.3.2 Molecular Parameters

The absorption spectra and the resulting resonance Raman excitation profiles have been analyzed for four azurin species. Analysis of the AXI and AXII azurin spectra was straightforward and yields important quantitative information that may be otherwise overlooked. A full analysis, as performed here, is needed to get accurate results in cases where the assumptions used to simplify the calculation fail. For example, some methods for calculating reorganization energy make the assumption that the absorption bandwidth is determined solely by the Frank-Condon vibronic progression in the resonance Raman active modes.[31,32] This was not the case for azurin[19,20] and plastocyanin[27] in previous studies. It was found that the charge transfer transition did not correspond to the absorption maximum as might be

Figure 5.6: Correlations of the azurin structures and sequences with resonance Raman spectral differences.

(A) Correlation of the spectral differences with the RMS deviation of the core atoms (R = -0.43, ■) and the protein backbone (R = 0.63, □).

(B) Correlation of the spectral differences with changes in Cu-S bond length (R = 0.64, ◆), and %identity (R = -0.91, ●). Note that the Raman spectral difference parameter χ^2 is expected to increase as the structural difference parameters, RMS deviation and ΔCu–S bond length, increase. However, χ^2 is expected to *decrease* as the %identity increases, as the %identity is a measure of environmental similarity.

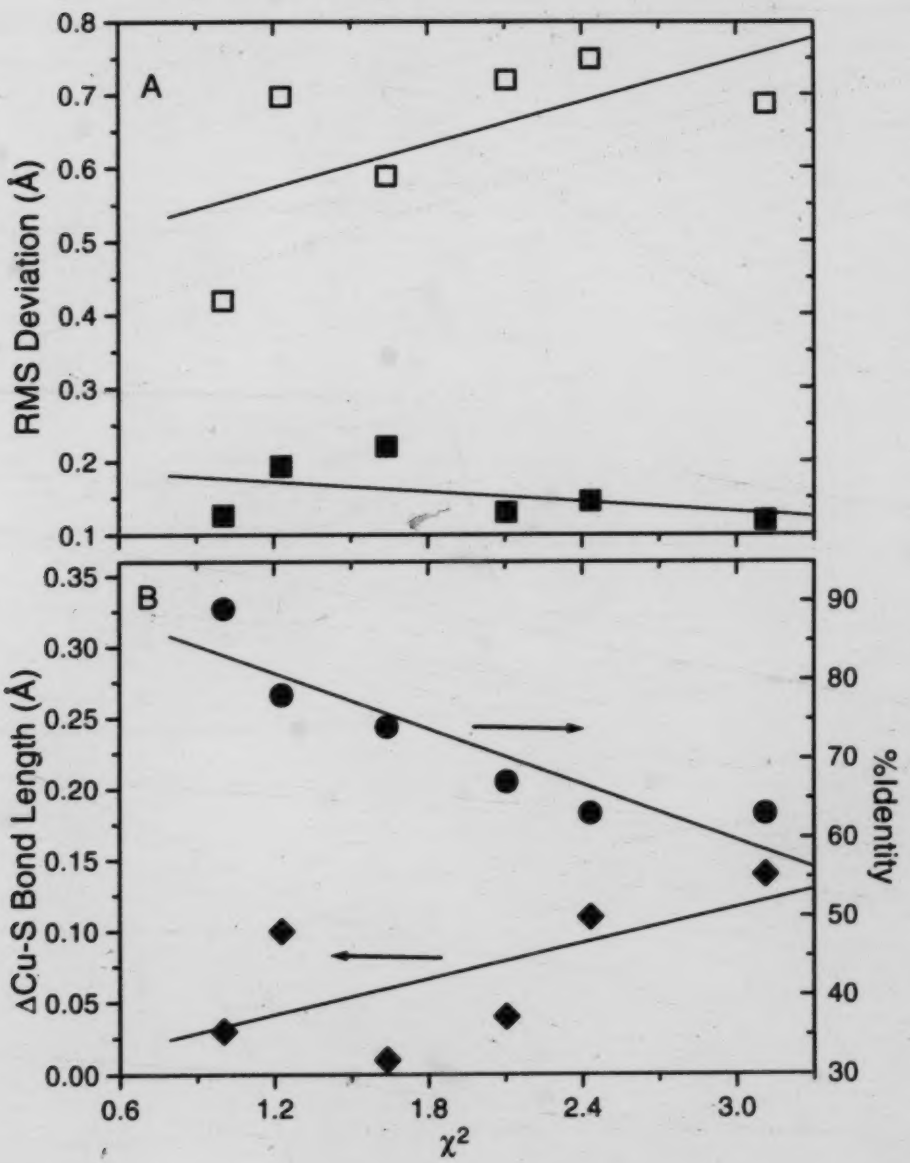
A
B
RMS Deviation (Å)
ΔCu-S Bond Length (Å)
%Identity
χ²
0.8
0.7
0.6
0.5
0.4
0.3
0.2
0.1
0.35
0.30
0.25
0.20
0.15
0.10
0.05
0.00
90
80
70
60
50
40
30
0.6
1.2
1.8
2.4
3.0

expected and that there was significant contribution to the absorption spectrum by other electronic transitions. Self-consistent analysis of the absorption spectrum and the resulting resonance Raman excitation profiles gives a number of molecular parameters. Some of the results of the four azurins are summarized in Table 5.3. There are both similarities and significant differences, and these are discussed below. The absorption spectrum of each species varies in ν_{max} and ε_{max} which may be consistent with small changes in the electronic structure. Changes in amino acids (i.e. charges/dipoles) and in structure around the copper may result in perturbations in the electronic structure. Perturbation of the electronic structure is further examined in Chapter 6. The mutant azurin Met121Glu is used to alter the structure of and introduce a charge at the copper site, resulting in large changes in the absorption spectrum. Among the four wild-type azurins, the absorption spectra are fairly similar. This is likely due to the highly conserved nature of the copper metal site. Although the absorption spectrum changes, the calculated ligand-to-metal charge transfer energy is more similar in each species (Table 5.3). This is also likely a result of the highly conserved nature of the copper active site and may be linked to the protein's function.

The rate of electron transfer, k, is related to the standard free energy of reaction, $\Delta G°$, and the nuclear reorganization energy, λ as shown in Equation 5.1.[2] The nuclear reorganization energy can be divided into inner- and outer-sphere contributions where the inner-sphere roughly refers to nuclear reorganizations of the donor and acceptor and the outer-sphere roughly refers to reorganization of the solvent or protein environment. One route of electron transfer passes through Cys112[4] and the reorganization energy of the S→Cu charge transition may be a contribution to the inner-sphere reorganization energy of electron transfer. In Chapters 2 and 3, the total inner-sphere reorganization energy for charge transfer was measured for PA and AD azurin (Table 5.3). Total reorganization energy of AX I and II are the same as for PA and AD (Table 5.3). This result is expected and may show how these proteins have similar properties in order to serve similar functions in each species. The sum of the experimental cross sections are all very similar for the four azurins. Since the total reorganization energy is proportional to the sum of the

Table 5.3: Comparison of parameters for four species of azurin.

	AD[a]	PA[b]	AXI[c]	AXII[c]
E_0 (cm^{-1})	14300	14200	14150	14800
M (Å)	0.73	0.63	0.81	0.63
Γ_L (cm^{-1})	450	160	500	285
Γ_G (cm^{-1})	75	0	150	0
θ (cm^{-1})	150	280	0	250
ν_{max} (cm^{-1})	16150	16000	16150	16100
LMCT (cm^{-1})	16500	16300	16500	16800
ε_{max} ($M^{-1}cm^{-1}$)	5200	4800	6270	5730
λ_{tot} (eV)	0.25	0.26	0.27	0.24

[a]Values from ref 20.

[b]Values from ref 19.

[c]Values from this work.

In this table E_0 is the zero-zero energy for the resonant state, M is the transition length, Γ_L is the Lorentzian homogeneous linewidth, Γ_G is the Gaussian homogeneous linewidth, θ is the inhomogeneous linewidth, ν_{max} is the location of the absorption band maximum, LMCT is the ligand-to-metal charge transfer energy, ε_{max} is the extinction coefficient at the absorption maximum and λ is the total inner-sphere reorganization energy.

intensity it would be expected that the total reorganization energy would be similar. The distribution of reorganization energy among the vibrational modes is different among the species due to variations in the amino acids which alter the environment of the copper metal ion. This last result will be described in more detail below.

Parameters such as E_0, M and broadening vary significantly between species and do not follow any easily discernable pattern. There are two possible reasons for this seemingly randomness of the parameters between species. The first possibility is that the observed differences are related in a complex manner to the properties of the azurin species. The amino acid sequences (Figure 1.1) and geometry (Table 4.1) are different for each species. The amino acid changes reflect the separate evolution of each species and are related to function. The differences in the protein environment could be expected to influence the excited-state structure and dynamics. A second possibility is that the analysis does not yield unique answers. A significant limitation on the restraint of the parameters is the complexity of the absorption spectrum. It is known that there are other transitions in this region with the band at ~620 being assigned to the S→Cu charge transfer.[33] Solomon and co-workers locate the charge transfer band of *P. aeruginosa* at 16,220 cm^{-1} which compares well with a value of 16,300 cm^{-1} obtained in Chapter 2.[19] However, ligand field transitions may contribute more than we allow for in the analysis. However, this does not mean all parameters are in doubt. The scaling of the Δ's is restrained by the width of the resonance Raman excitation profiles which are the same for the four species. Ligand-to-metal charge transfer energy (LMCT) and E_0 are well constrained since they are determined by the maxima of the resonance Raman excitation profiles. The transition length and the total broadening are sensitive to the absorption spectrum intensity and width. These values are going to depend greatly on how the absorption spectrum is interpreted and on how much of the absorption band is due to charge transfer. The calculated spectrum was constrained to fill the maximum area allowed by the measured absorption band. It may be appropriate to look at these values as an upper limit as defined by the absorption spectrum. Work is underway using Stark spectroscopy to more definitively determine the ligand-to-metal charge transfer contribution to the 620 nm absorption band.[34]

5.3.3 Electron Transfer

Previous studies have shown that the charge-transfer is strongly coupled to the electron transfer[10,35] and could provide a good model for understanding the electron transfer pathway. One goal of this work is to tie the charge transfer results we have obtained to electron transfer. Electron transfer studies measuring electron transfer rates through different pathways[4,10,17] have found more efficient coupling through Cys112 This result suggests that the protein has preferred pathways for electron transfer.

Surprisingly, when comparing the four azurin species, an anisotropic response was observed. When comparing AD and AXII, there is one amino acid change ≤10Å from the copper metal (Figure 4.1). This is in contrast to four amino acids changes between PA and AXI. However, the observed spectral changes between the azurin pairs are comparable. Trp48 is replaced by Leu going from AD to AXII. This is a significant change only three amino acids from the copper metal. There are two similar differences between PA and AXI. Phe118 is replaced by Ser and Ser113 is replaced by Thr going from PA to AXI. Both of these changes are adjacent to strongly-bound copper ligands. However, they do not seem to have the same magnitude of influence on the spectra as the Trp48Leu change. For plastocyanin, it was found that changes in amino acids that are chemically connected can affect the distribution of intensity of the observed normal modes.[36] The other two amino acid changes going from PA to AXI are Gly12Gln and Val86Leu, and are not on the same peptide strand as the copper ligands. Gln12 might be expected to have some effect through the introduction of a dipole. The introduction of charges and dipoles have been observed to result in intensity changes of vibrational modes.[36] The magnitude of the intensity change will decrease with distance of the dipole. The Val86Leu change is a conservative substitution and not expected to have an effect on the spectrum. In plastocyanin, it was found that there are few amino acid changes ≤12 Å from the copper.[29,36] The spectral differences could be obtained in the same manner as was done for azurin and correlated with distance of the amino acid changes to obtain a relationship of the magnitude of spectral change with distance. This can not be done with azurin because of the number of changes between azurin species.

Intramolecular electron transfer has been studied with azurin as the disulfide bridge provides a convenient source of an electron and the electron transfer can be easily triggered.[13] Two electron transfer routes were calculated starting at Cys3 and ending at the copper.[4] One route starts with a through-space jump from Cys3 to Thr30. The electron goes to Val31 and a second through-space jump to Trp48. The electron continues through Val49 and a third through-space jump to Phe111. The electron passes through Cys112 and finally reaches the copper.[4] The other pathway follows the peptide chain from Cys3 to Asn10 before a through-space jump to His46 and then to the copper.[4] Note that of the above mentioned amino acid changes, only Trp48 is part of these electron transfer paths. In Figure 5.6, the point corresponding to AD vs. AXII deviates significantly more from the best fit line than the other points and the correlation increases to –0.93 if this point is left out. This suggests that the spectral difference for this pair is greater than what is expected from %identity alone and is consistent with greater coupling of the copper to Trp48.

An intriguing interpretation of the anisotropic effect of amino acid composition on the resonance Raman spectra is that the spectra are sensitive to long-range vibronic coupling, probably modulation of the electron transfer electronic coupling matrix element by vibrational coordinates. The amino acid sequence and structure of the protein is thought to be related to the electron transfer function of the protein. Research has shown that the electron transfer properties of PA azurin[10,11] depend on the composition and secondary structure of the protein along the electron transfer pathway.[5,6] In the simplest description of long-range electron transfer, the electron transfer rate decays exponentially with distance, modulated by some distance-decay constant. The predicted distance-decay constants are 1.26 $Å^{-1}$ for an α-helix and 1.00 $Å^{-1}$ for a β-strand.[5,6] The intramolecular electron transfer rates of five Ru-modified derivatives of azurin were measured giving a decay-constant for azurin of 1.10 $Å^{-1}$, which is close to the predicted value for β-strand[5,6] and consistent with the secondary structure of azurin. The electron transfer rate may also be affected by the properties of specific amino acids but this has not been well characterized. In azurin, it appears that the peptide backbone may be more important than the amino acid side chains.[4,37] Calculations using a tight-binding extended Hückel type method

show that the aromatic groups do not promote electron transfer.[37] However, measurements of intramolecular electron transfer of *P. aeruginosa* mutants show significant rate changes in some Trp48 mutants.[4] Changing Trp48 to Phe or Try increased the electron transfer rate constant, k_{ET}, from 44 s^{-1} to 80 and 85 s^{-1}, respectively.[4] Amino acids such as Ala and Met decreased the rate slightly (k_{ET} = 35 s^{-1} and 33 s^{-1}, respectively), while Ser slightly increased rate (k_{ET} = 50 s^{-1}).[4] These results are consistent with the significant effect this residue has on the resonance Raman spectra, and suggest the resonance Raman spectrum may be a uniquely sensitive probe of electronic coupling in these proteins. When Trp48 is replaced with Leu in PA, analogous to the change in AD/AXII azurin, the intramolecular electron transfer rate is not significantly changed.[4] This suggests that the electronic coupling has not changed and the resonance Raman spectrum may reflect changes in vibronic coupling. The conflicting evidence makes the contextual interpretation of the resonance Raman spectroscopy difficult. Clearly, concurrent measurement of electron transfer rates and resonance Raman spectra for particular mutants of azurin should clarify the relationship between amino acid composition, electron transfer kinetics, and the resonance Raman spectra. Such studies are currently in progress (See Chapter 7).

5.4 Conclusion

The absorption spectra and the resulting resonance Raman excitation profiles have been analyzed for four species of azurin. The total inner-sphere reorganization energy was found to be the same for four species of azurin. This may be related to the function of the protein with the low value facilitating rapid electron transfer. Quantitative comparison of the resonance Raman spectra of four azurins confirms the qualitative conclusions of Chapter 4. It was found that although there is a very weak correlation of spectral differences with protein structure, the primary influence on the resonance Raman spectra is the protein environment. Anisotropic coupling was observed with extended vibronic coupling along a proposed electron transfer route. The results are consistent with greater coupling of the copper through Cys112

suggesting that resonance Raman may be sensitive to electronic/vibronic coupling which is needed for efficient long-range intramolecular electron transfer.

5.5 References

[1] See chapter 1 for background on azurin and blue copper proteins.

[2] Marcus, R. A.; Sutin, N. *Biochim. Biophys. Acta* **1985**, *811*, 265.

[3] Holten, D.; Windsor, M. W.; Parson, W. W.; Thornber, J. P. *Biochim. Biophys. Acta* **1978**, *501*, 112.

[4] Farver, O.; Skov, L. K.; Young, S.; Bonander, N.; Karlsson, G. B.; Vänngård, T.; Pecht, I. *J. Am. Chem. Soc.* **1997**, *119*, 5453.

[5] Gray, H. B.; Winkler, J. R. *Annu. Rev. Biochem.* **1996**, *65*, 537.

[6] Langen, R.; Chang, I-J.; Germanas, J. P.; Richards, J. H.; Winkler, J. R.; Gray, H. B. *Science* **1995**, *268*, 1733.

[7] Gray, H. B.; Winkler, J. R. *J. Electroanal. Chem.* **1997**, *438*, 43.

[8] Margalit, R.; Kostic, N. M.; Che, C.-M.; Blair, D. F.; Chiang, H.-J.; Pecht, I.; Shelton, J. B.; Shelton, J. R.; Schroeder, W. A.; Gray, H. B. *Proc. Natl. Acad. Sci. USA* **1984**, *81*, 6554.

[9] Bjerrum, M. J.; Casimiro, D. R.; Chang, I-J.; Di Bilio, A. J.; Gray, H. B.; Hill, M. G.; Langen, R.; Mines, G. A.; Skov, L. K.; Winkler, J. R.; Wuttke, D. S. *Journal of Bioenergetics and Biomembranes* **1995**, *27*, 295.

[10] Regen, J. J.; Di Bilio, A. J.; Winkler, J. R.; Richards, J. H.; Gray, H. B. *Inorg. Chim. Acta* **1998**, *275-276*, 470.

[11] Skov, L. K.; Pascher, T.; Winkler, J. R.; Gray, H. B. *J. Am. Chem. Soc.* **1998**, *120*, 1102.

[12] Gray, H. B.; Winkler, J. R. *J. Electroanal. Chem.* **1997**, *438*, 43.

[13] Farver, O.; Pecht, I. *Proc. Natl. Acad. Sci. USA* **1989**, *86*, 6968.

[14] Farver, O.; Pecht, I. *J. Am. Chem. Soc.* **1992**, *114*, 5764.

[15] Farver, O.; Skov, L. K.; Gilardi, G.; van Pouderoyen, G.; Canters, G. W.; Wherland, S. Pecht, I. *Chem. Phys.* **1996**, *204*, 271.

[16] Kotlyar, A. B.; Borovok, N.; Hazani, M. *Biochemistry* **1997**, *36*, 15827.

[17] Borovok, N.; Kotlyar, A. B.; Pecht, I.; Skov, L. K.; Farver, O. *FEBS Letters* **1999**, *457*, 277.

[18] Kotlyar, A. B.; Borovok, N.; Hazani, M. *Biochemistry* **1997**, *36*, 15828.

[19] Webb, M. A.; Kwong, C. M.; Loppnow, G. R. *J. Phys. Chem. B* **1997**, *101*, 5056. This is Chapter 2 in this thesis.

[20] Webb, M. A.; Loppnow, G. R. *J. Phys. Chem. B* **1998**, *102*, 8923. This is Chapter 3 in this thesis.

[21] Webb, M. A.; Loppnow, G. R. *J. Phys. Chem. A* **1999**, *103*, 6283. This is Chapter 4 in this thesis.

[22] Ambler, R. P. *Biochem. J.* **1963**, *89*, 341.

[23] Abraham, Z. H. L.; Lowe, D. J.; Smith, B. E. *Biochem. J.* **1993**, *295*, 587.

[24] Dodd, F. E.; Hasnain, S. S.; Hunter, W. N.; Abraham, Z. H. L.; Debenham, M.; Kanzler, H.; Eldridge, M.; Eady, R. R.; Ambler, R. P.; Smith, B. E. *Biochemistry* **1995**, *34*, 10180.

[25] Albrecht, A. C.; Hutley, M. C. *J. Chem. Phys.* **1971**, *55*, 4438.

[26] Myers, A. B.; Mathies, R. A. In *Biological Applications of Raman Spectroscopy*; Spiro, T. G., Ed.; Wiley: New York, **1988**; Vol 2, p 1.

[27] Fraga, E.; Webb, M. A.; Loppnow, G. R. *J. Phys. Chem.* **1996**, *100*, 3278.

[28] Lee, S-Y.; Heller, E. J. *J. Chem. Phys.* **1979**, *71*, 4777.

[29] Loppnow, G. R.; Fraga, E. *J. Am. Chem. Soc.* **1997**, *119*, 896.

[30] Loppnow, G.R.; Mathies, R. A. *Biophys. J.* **1988**, *54*, 35.

[31] Blackbourn, R. L.; Johnson, C. S.; Hupp, J. T.; Bryant, M. A.; Sobocinski, R. L.; Pemberton, J. E. *J. Phys. Chem.* **1991**, *95*, 10535.

[32] Wootton, J. L.; Zink, J. I. *J. Phys. Chem.* **1995**, *99*, 7251.

[33] Solomon, E. I.; Hare, J. W.; Dooley, D. M.; Dawson, J. H.; Stephens, P. J.; Gray, H. B. *J. Am. Chem. Soc.* **1980**, *102*, 168.

[34] Chowdury, A.; Peteanu, L. A.; Webb, M. A.; Loppnow, G. R. Paper in preparation

[35] Dong, S.; Spiro, T. G. *J. Am. Chem. Soc.* **1998**, *120*, 10434.

[36] Fraga, E.; Loppnow, G. R. *J. Phys. Chem. B* **1998**, *102*, 7659.

[37] Broo, A.; Larsson, S. *J. Phys. Chem.* **1991**, *95*, 4925.

Chapter 6: Electronic Structure of *Pseudomonas aeruginosa* M121E Mutant Azurin

A version of this chapter has been submitted as an article to the *Journal of Physical Chemistry* with the following authors:

M. Adam Webb,[a] Cynthia N. Kiser,[b] John H. Richards,[b] Angel J. Di Bilio,[b] Harry B. Gray,[b] Jay R. Winkler,[b] and Glen R. Loppnow.[a]

[a]*Department of Chemistry, University of Alberta, Edmonton, Alberta* Canada T6G 2G2

[b]*Beckman Institute, California Institute of Technology, Pasadena, California* USA 91125

6.1 Introduction

Blue copper proteins exhibit a number of interesting spectral and redox properties. The proteins have a strong S→Cu charge transfer absorption band at ~600 nm, giving them a distinctive blue color.[1] The electron spin resonance (ESR) spectrum is characterized by an unusually narrow hyperfine splitting ($A_{\parallel} < 90 \times 10^{-4}$ cm^{-1}) in the $g_{\parallel}$ region and varying degrees of rhombicity.[1] The reduction potential ranges from 184 mV for *Rhus vernicifera* stellacyanin to 680 mV for *Thiobacillus ferrooxidans* rusticyanin, which is much higher than 115 mV for aqueous $Cu_{2+/+}$.[2] It is proposed that these properties originate from the unusual geometry imposed on the copper metal ion by the protein.[3,4] The structure of the copper metal site of *P. aeruginosa* is shown in Figure 6.1. Azurin has one Type 1 copper ion in a distorted trigonal bipyramid geometry with three strongly coordinated planar ligands (Cys112, His46 and His117) and two weakly coordinating axial ligands (Met121 and Gly45). The role of structure and the ligands has been probed by absorption[5], resonance Raman[6] and ESR[7] studies of site-specific mutants of azurin. For example, it has been found that the methionine is not needed in order to get the blue copper site, as evident from the absorption[5] spectrum and the lack of methionine in stellacyanin[8]. However, methionine has been suggested to play an important role in the fine tuning of the reduction potential to produce the large range of potentials seen.[9]

In this work, we further probe the role of methionine in fine-tuning the electronic properties of the copper metal ion by studying the M121E mutant of *P. aeruginosa* azurin at two different pH's using resonance Raman spectroscopy. Resonance Raman intensities provide detailed information about excited-state structure and dynamics on an extremely fast time scale.[10] By exciting at a wavelength within an electronic absorption band, enhancement of the normal modes which are coupled to the electronic transition occurs and the intensities reflect the conformational distortion of the molecule in the excited-state.[10] The absorption and resonance Raman results presented here suggest that replacing Met121 with Glu results in a significant perturbation to the electronic structure, which increases upon deprotonation of Glu. Surprisingly, the resonance Raman spectrum excited within the

Figure 6.1: Copper metal site of *P. aeruginosa* azurin for wild type and M121E mutant. Structure of the copper metal site from x-ray structures for *P. aeruginosa*[29] wild type (purple) at pH 5.5 and M121E[30] (green) mutant azurin at an approximately similar pH.

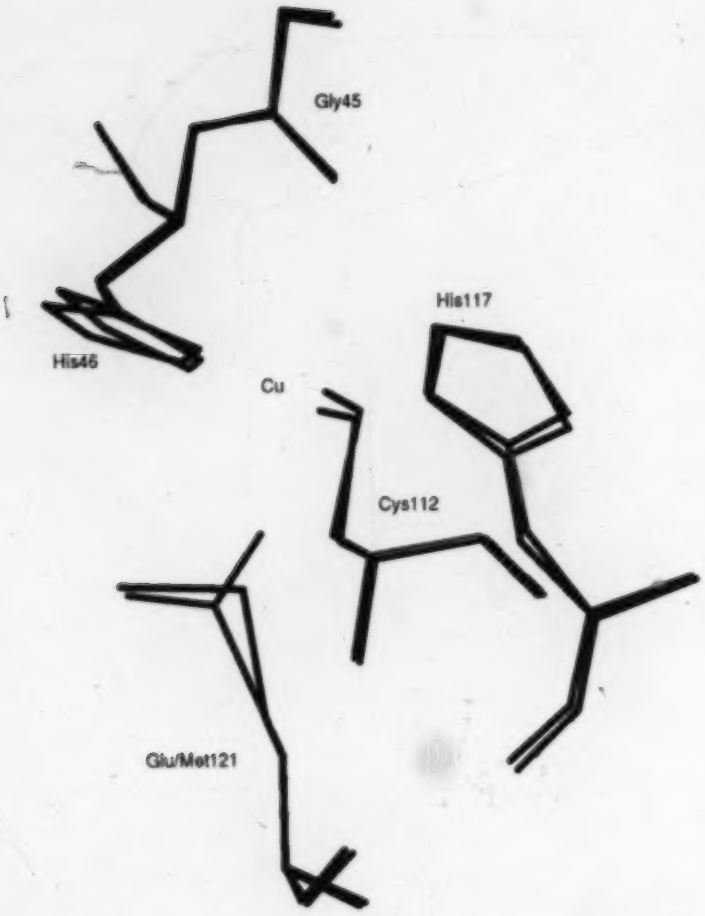
Gly45
His117
His46
Cu
Cys112
Glu/Met121

~600 nm band is mostly independent of pH. This suggests that the introduction of Glu121 has altered the electronic character of the absorption bands. This is consistent with the strong pH dependence of the absorption spectrum. The total inner sphere reorganization energy was measured for M121E azurin to be much smaller at both pH's than for the wild type. This is presumably due to the same perturbations in the electronic structure as evident in the absorption spectrum and the resonance Raman excitation profiles. The results are discussed in terms of a two state model of the electronic and molecular structure of the copper metal site of azurin.

6.2 Methods

6.2.1 Experimental

Azurin mutant M121E was generously provided by H. Gray and was prepared as previously described.[11,12] Samples were prepared for resonance Raman experiments by quantitative dilution with a cacodylate buffer solution (0.5–1.0 M cacodylate, 0.01 M acetate, pH 7.0) or sulfate (1.5-2.0 M, 0.1 M phosphate, pH 3.5). Addition of cacodylate buffer or sulfate did not have a noticeable effect on the absorption or resonance Raman spectra of azurin. Sulfate was used when addition of cacodylate buffer caused precipitation of the protein at pH 3.5. Room-temperature resonance Raman spectra were taken as described previously[13] using 250-300 μL aqueous samples having an absorbance of 2.2-4.9 OD/cm at 572 nm at pH 7.0 or 3.8-4.6 OD/cm at 612 nm at pH 3.5. Bleaching of the sample was accounted for by measuring the absorption at 500 nm (ε_{500} = 509 $M^{-1}cm^{-1}$) at pH 7.0 and at 560 nm (ε_{560} = 2170 $M^{-1}cm^{-1}$) at pH 3.5. The absorbance at 500/560 nm was used because at the absorption maximum of this band, the absorbance is too large. The average absorbance was used to calculate the concentration of azurin.

6.2.2 Intensity Analysis.

The resonance Raman and absorption cross sections in the Condon approximation can be written using the time dependent equations of Lee and

Heller.[10,14,15] These equations and the implementation of these equations has been described in detail.[10,14-18] Self-consistent analysis of the absorption spectrum and the resonance Raman excitation profiles was done in the same manner as previously described for plastocyanin[14,16] and azurin.[18]

6.2.3 Molecular Modeling.

For any given configuration of atoms, it is possible to calculate a potential energy. Calculation of the potential energy and its first and second derivatives with respect to the atomic coordinates is used for geometry minimization, harmonic vibration analysis and molecular dynamics simulations. A complete mathematical description of a molecule starts with the Schrödinger equation:

$$H\Psi(R,r) = E\Psi(R,r). \qquad (6.1)$$

where H is the Hamiltonian for the system, Ψ is the wavefunction and E is the energy. Ψ is a function of the nuclei (R) and the electrons (r) positions. The Born-Oppenheimer approximation separates the nuclear and electron motions into two separate equations. The equation for the motion of the electrons is:

$$H_{elec}\psi(r;R) = E_{elec}\psi(r;R) \qquad (6.2)$$

The motions of the electrons and the electronic energy, E_{elec}, depend explicitly on the electronic coordinates and parametrically on the nuclear coordinates. The nuclear coordinates do not appear explicitly in ψ. This equation, along with nuclear repulsion, defines the potential energy surface, $E_{tot}(R)$, which depends only on the positions of the nuclei. *Ab initio* programs directly solve Equation 6.2 given fixed nuclear coordinates. The equation for the motion of the nuclei on this potential energy surface is given by:

$$H_{nucl}\Phi(R) = E_{tot}\Phi(R). \qquad (6.3)$$

To solve Equation 6.3, it is necessary to first solve Equation 6.2 to get the potential energy, $E_{tot}(R)$. However, this is generally not practical and it is desirable to devise an empirical fit to the potential surface using a forcefield approximation. Also, since the nuclei are relatively large objects and the quantum mechanical effects are

generally insignificant, Equation 6.3 can be replaced with Newton's equation of motion:

$$-\frac{dV}{dR} = m\frac{d^2R}{dt^2} \qquad (6.4)$$

where V is the potential energy, m is the mass and R gives the position of the atoms. Molecular dynamics calculations involve solving Equation 6.4 to describe the motions of the system with time whereas molecular mechanics calculations focus on the properties of a static geometry. An empirical forcefield consists of the expression and the parameters needed to fit the potential energy surface.[19,20] The form of the potential energy expression and the values of the parameters are developed to model specific classes of compounds and are crucial to the molecular model. This work uses the AMBER[21,22] forcefield which was parameterized for proteins and DNA. This forcefield has been extended to include polysaccharides.[23] The functional form of the potential energy terms are given by:[24]

$$E_{pot} = \sum_b K_2(b-b_0)^2 + \sum_\theta H_\theta(\theta-\theta_0)^2 + \sum_\phi \frac{V_n}{2}[1+\cos(n\phi-\phi_0)]$$
$$+\sum \varepsilon\left[(r^*/r)^{12} - 2(r^*/r)^6\right] + \sum q_i q_j/\varepsilon_{ij} r_{ij} + \sum\left[\frac{C_{ij}}{r_{ij}^{12}} - \frac{D_{ij}}{r_{ij}^{10}}\right] \qquad (6.5)$$

The first three terms handle the internal coordinates of bonds, angles and dihedrals. The fourth and fifth terms represent the van der Waals and electrostatic interactions, respectively. The final term augments the electrostatic description of hydrogen bonds. In the Discover program, there are two special considerations. The first is that the 1-4 non-bonded interactions are scaled by 0.5. The second is that a distance-dependent dielectric is assumed where $\varepsilon = 4r$. A distance-dependent dielectric has been shown to model the bulk solvent and dielectric effects in proteins.[25-27]

Calculations of the geometries at pH 3.5 and 7.0 were performed on an Indigo^2 workstation (Silicon Graphics Inc. Palo Alto, CA) using the InsightII molecular modeling environment software (Molecular Simulations Inc., Palo Alto, CA). The x-ray crystal structures of the proteins were obtained from the Brookhaven protein data bank[28] (5azu[29] and 1etj[30] for PA and M121E azurin, respectively). Hydrogen was added using the Biopolymer module and the acidic/basic residues were

protonated/deprotonated as pH warranted. Atom types and charges are defined in the AMBER residue library in the InsightII software. Geometry minimization was done with the Discover module of InsightII using the crystal structure as the initial starting point. Energy minimization was done using the conjugated gradient algorithm until the calculated gradient was ≤0.0001 kcal mol^{-1} along each coordinate. It was found that the geometry did not change appreciably for a gradient ≤0.001 to a gradient ≤0.0001.

6.3 Results

The resonance Raman spectra were measured for M121E at various wavelengths throughout the S→Cu charge transfer band. The spectra for M121E azurin are shown in Figure 6.2 at pH 3.5 and in Figure 6.3 at pH 7.0. The vibrational modes can be assigned using the wild type as a guide.[31] The modes between 345 and 425 cm^{-1} can be assigned to modes involving the Cu–S(Cys) stretch mixed with other internal coordinates. The modes between 261 and 273 cm^{-1} involve the Cu–N(His) stretch. The 300 cm^{-1} mode found at pH 7.0 could be due to a Cu–O(Glu) bond which can form upon deprotonation. The intensity standards are visible in the spectra at 605 and 638 cm^{-1} for cacodylate at pH 7.0 and 981 cm^{-1} for sulfate at pH 3.5.

The spectra for M121E azurin at pH 3.5 (Figure 6.2) are similar to those found earlier.[6] The resonance Raman spectra were found to not vary with excitation wavelength in the 568-676 nm region, which is the same as what is found for the wild type azurin.[18,32,33] This indicates that all the measured vibrational modes are coupled to the same electronic transition, namely the S→Cu charge transfer. The observed frequencies between 263-424 cm^{-1} are very similar to those seen in the wild type[18] (Table 6.1). The absolute intensity of the mutant spectrum is ~10 times less than the wild type and the relative intensities of the modes are significantly different than what is measured in the wild type (see Chapter 2). The intensity of a mode is proportional to both Δ^2 and its reorganization energy.

The resonance Raman spectra of the two pH's excited within the ~600 nm band show the same frequencies (Figure 6.2 and Figure 6.3) which would seem to

Figure 6.2: Resonance Raman spectra of M121E azurin at pH 3.5. Azurin concentration was 0.8-1.0 mM. Spectra were taken as two overlapping windows and pieced together using overlapping peaks. The spectra have had a baseline subtracted and have been divided by a tungsten-halogen lamp spectrum (Eppley Laboratory, Inc.). The sulfate internal standard appears at 981 cm^{-1}. The feature marked ++ is a stray light artifact.

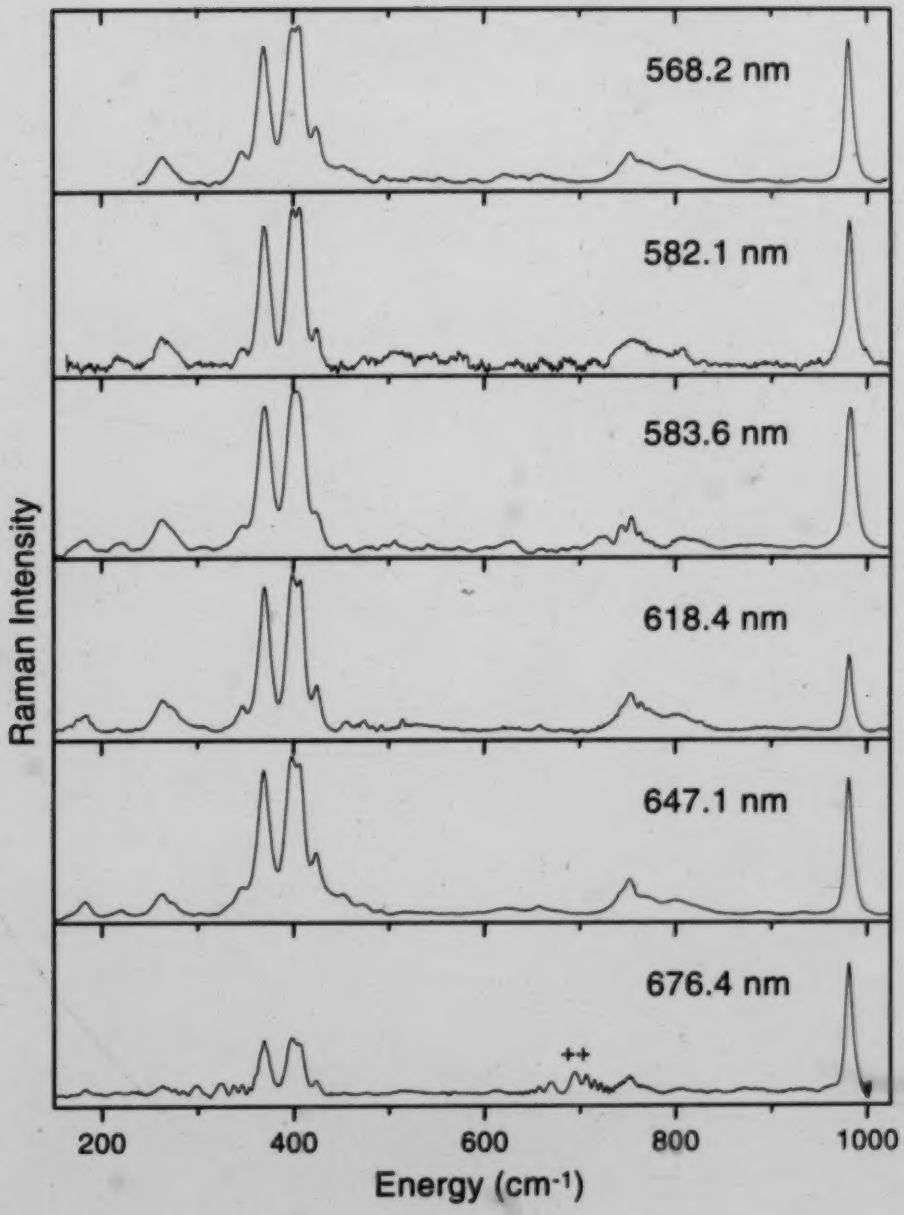
568.2 nm
582.1 nm
583.6 nm
618.4 nm
647.1 nm
676.4 nm
++
Raman Intensity
200
400
600
800
1000
Energy (cm-1)

Figure 6.3: Resonance Raman spectra of M121E azurin at pH 7.0. Azurin concentration was 2.0-4.5 mM. Spectra shown are typical scans. The spectra have had a baseline subtracted and have been divided by a tungsten-halogen lamp spectrum (Eppley Laboratory, Inc.). The cacodylate internal standard appears at 605 and 638 cm^{-1}.

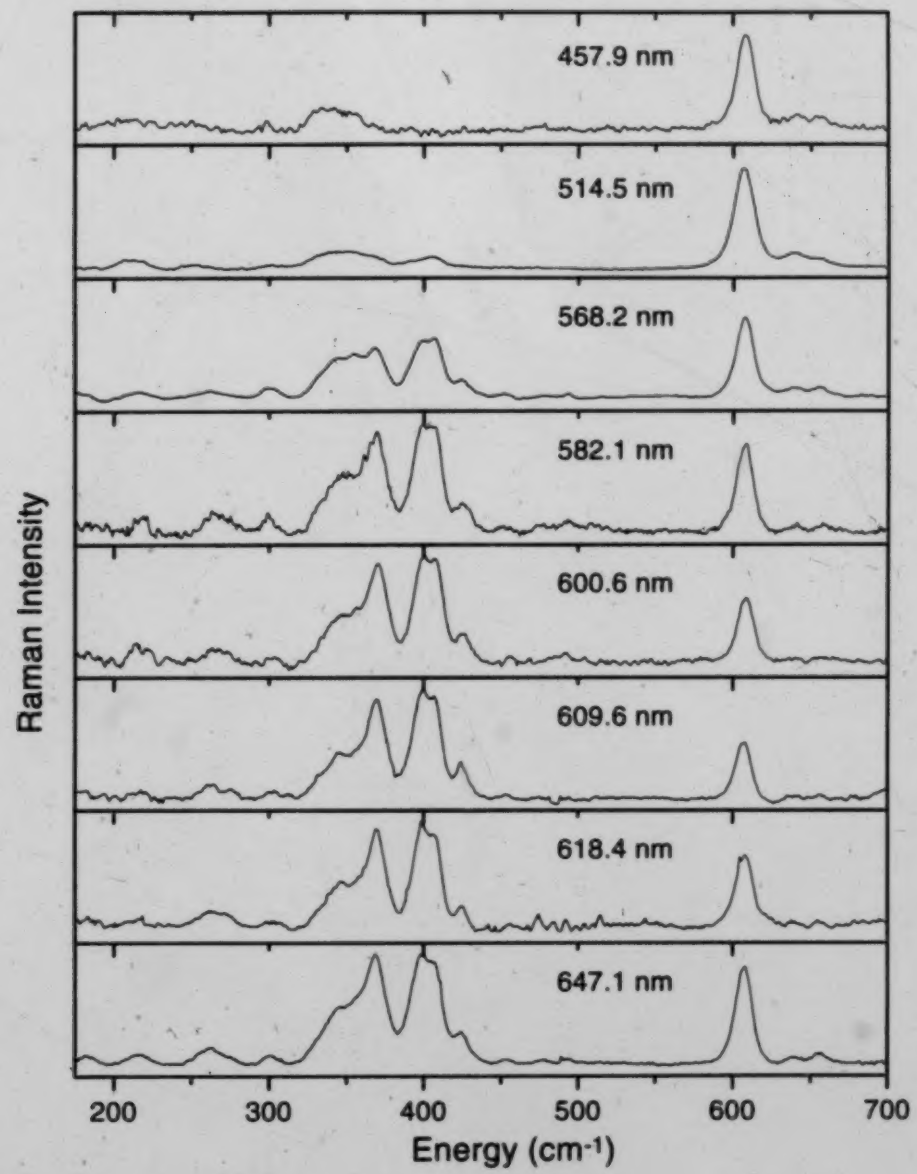
457.9 nm
514.5 nm
568.2 nm
582.1 nm
600.6 nm
609.6 nm
618.4 nm
647.1 nm
Raman Intensity
200
300
400
500
600
700
Energy (cm-1)

Table 6.1: Mode specific reorganization energies of azurin.

	PA[a]		M121E (pH 5.5)[b]			M121E (pH 7.0)[b]		
$\bar{\nu}$/cm^{-1}	|Δ|	λ/cm^{-1}[c]	$\bar{\nu}$/cm^{-1}	|Δ|	λ/cm^{-1}[c]	$\bar{\nu}$/cm^{-1}	|Δ|	λ/cm^{-1}[c]
216	0.85	78						
263	1.30	220	261	0.34	15	263	0.24	8
			273	0.36	18			
						300	0.16	4
344	0.75	100	345	0.18	5	345	0.71	87
						355	0.23	9
371	1.60	470	369	0.66	80	369	0.86	136
401	1.20	290	396	0.49	48	396	0.71	101
408	1.60	520	407	0.48	46	407	0.72	106
426	1.30	360	424	0.22	10	425	0.36	27
439	0.23	12						
454	0.31	22						
476	0.27	17						
493	0.13	4						
654	0.18	11						
Total/cm^{-1}		2100			220			478
Total/eV		**0.26**			**0.03**			**0.06**

[a] Values taken from ref 18.
[b] From this work.
[c] Reorganization energy is calculated as $\lambda_i = \bar{\nu}_i \Delta_i^2/2$.

indicate that the structure of the copper center is similar at the two pH's. However, there is evidence of structural change, which is discussed in detail below. The spectrum at pH 7.0 also shows a weak band at 300 cm^{-1}, which is possibly due to a Cu–O stretch. This mode is not visible at pH 3.5, further suggesting it arises upon deprotonation of the Glu oxygen. Several modes also show significant increase in relative intensity. In previous work with plastocyanin[34], increases in intensity of specific modes were attributed to the presence of charges in the vicinity of the copper. The spectrum of M121E azurin at pH 7.0 was also measured at 457.9 nm (Figure 6.3) and is comparable to the reported spectrum at 413.1 nm.[6] The resonance Raman spectrum of M121E azurin at pH 7.0 shows a wavelength dependence (Figure 6.3) as the excitation line is tuned to lower energies, indicating the presence of two different electronic states being responsible for the absorption bands at 572 and 416 nm.

The absorption spectrum of M121E azurin shows a large pH dependence (Figure 6.4). The absorption spectrum at pH 3.5 is typical of blue copper proteins. The spectrum undergoes blue-shifting of the bands and intensity redistribution from the 612 nm band into the 416 nm band as the pH changes from 3.5 to 7.0, resulting in a color change from blue to brown. This has been previously interpreted as resulting from a large structural change.[5-7] The change in the absorption band at pH 7.0 is likely due to coordination of an electron pair of the Glu oxygen with the copper ion, coupled with the introduction of a negative charge at the copper site. Table 6.2 and Table 6.3 summarize the experimental resonance Raman cross sections of M121E azurin at pH 3.5 and 7.0, respectively. Figure 6.5 shows the calculated fit to the absorption spectra at both pH's using Equation 2.5. Two calculations are done at pH 3.5 using two models. The first calculation was done in the same manner as pH 7.0 and wild type azurin.[18,32,33] The other ("alternative") model used is described below. Figure 6.6 and Figure 6.7 show the good agreement between the calculated and experimental resonance Raman excitation profiles. Table 6.2 and Table 6.3 give the parameters used for the calculations and list the calculated cross sections at the excitation wavelengths found in this work by using Equation 2.4. Deviations of the calculated absorption spectra from the experimental spectra are due to the presence of other electronic transitions that were not modeled. Because of the presence of other

Figure 6.4: Comparison of absorption spectra of M121E azurin at pH 3.5 (solid) and pH 7.0 (dotted). The absorption bands are labeled with the peak positions in nm.

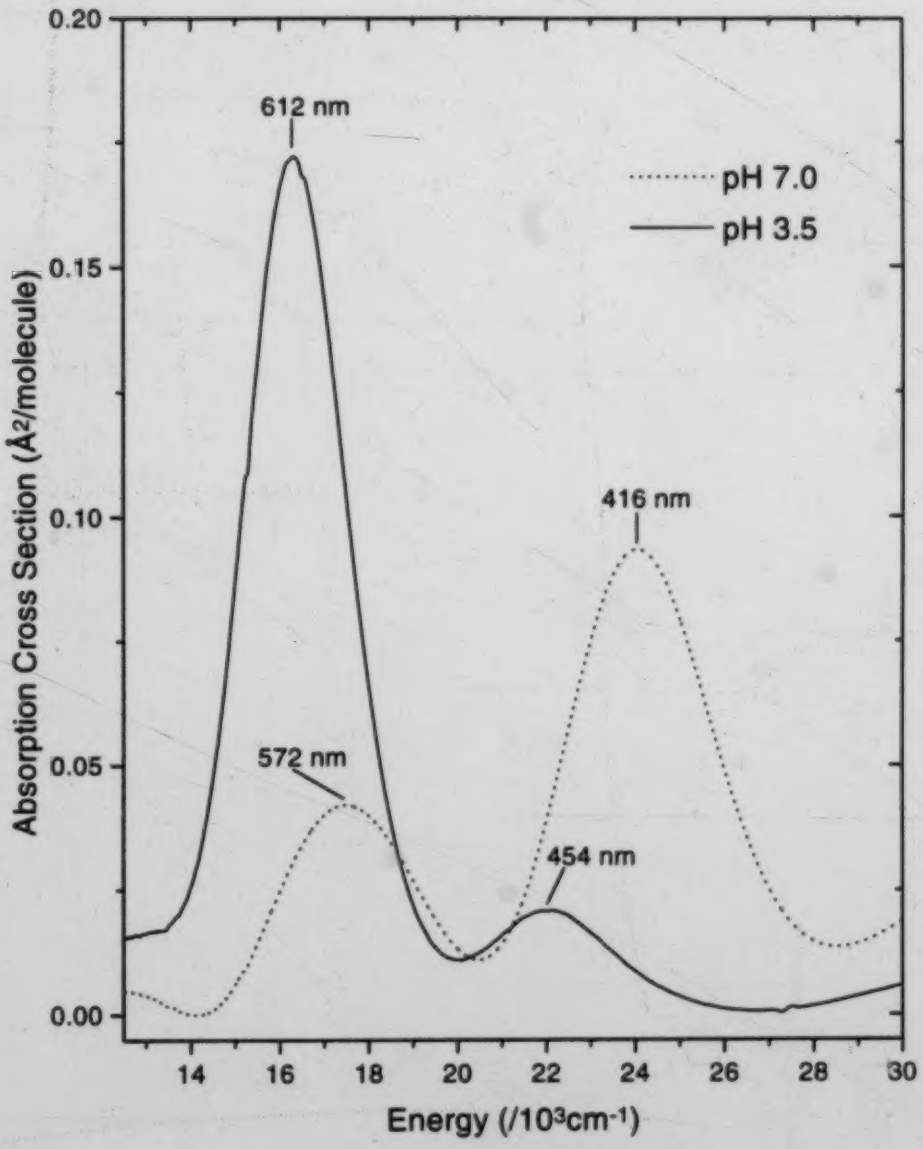
0.20
0.15
0.10
0.05
0.00
612 nm
416 nm
572 nm
454 nm
pH 7.0
pH 3.5
Absorption Cross Section (Å²/molecule)
14
16
18
20
22
24
26
28
30
Energy (/10³cm⁻¹)

Table 6.2: Absolute resonance Raman cross sections of M121E at pH 3.5.

		Excitation wavelength/nm					
$\bar{\nu}$	$\lvert\Delta\rvert$	568.2	582.1	583.6	618.4	647.1	676.4
261	0.34(0.21)	1.38/1.15	1.36/1.88	1.63/1.96	2.97/2.94(3.04)	1.20/1.91	---/0.73
275	0.36(0.24)	0.35/1.45	0.83/2.37	0.80/2.48	3.72/3.68(3.80)	0.42/2.38	---/0.91
345	0.18(0.16)	1.02/0.56	0.65/0.91	0.80/0.94	1.35/1.34(1.32)	1.12/0.84	---/0.31
369	0.66(0.66)	9.56/9.22	6.61/14.7	10.5/15.3	21.9/21.5(21.1)	10.3/13.4	2.62/4.95
396	0.49(0.53)	7.22/6.06	6.50/9.62	7.47/10.0	14.0/13.8(13.5)	7.77/8.48	2.31/3.11
407	0.48(0.52)	7.95/6.02	6.78/9.53	7.67/9.91	13.8/13.6(13.4)	7.42/8.30	2.00/3.04
424	0.22(0.24)	1.55/1.37	0.72/2.16	0.88/2.24	3.10/3.03(3.02)	1.64/1.84	0.27/0.67

The observed Raman shifts, $\bar{\nu}$, are in units of cm^{-1} and Δ's are in dimensionless normal coordinates. The resonance Raman cross sections are shown as experimental/calculated(alternative) in units of $Å^2$/molecule $\times 10^{11}$. A --- indicates no signal was observed above the baseline noise and no cross section was measured. The errors in cross sections are ±10% for strong lines and ±20% for weak lines. The cross sections were calculated using Equation 2.4 and the following parameters: zero-zero energy, E_0 = 15,800 cm^{-1}, transition length, M = 0.63 Å, temperature, T = 0 K, refractive index, n = 1.33, Lorentzian homogeneous linewidth, Γ_L = 500 cm^{-1}, Gaussian homogeneous linewidth, Γ_G = 330 cm^{-1}, inhomogeneous linewidth, Θ = 520 cm^{-1}. The alternative model was used to calculate the cross sections (see text). This model used the following parameters: zero-zero energy, E_0 = 16,000 cm^{-1}, transition length, M = 0.20 Å, temperature, T = 0 K, refractive index, n = 1.33, Gaussian homogeneous linewidth, Γ_G = 50 cm^{-1}, Lorentzian homogeneous linewidth, Γ_L = 0 cm^{-1} inhomogeneous linewidth, Θ = 700 cm^{-1}.

Table 6.3: Absolute resonance Raman cross sections of M121E at pH 7.0.

		Excitation wavelength/nm						
$\bar{\nu}$	$\|\Delta\|$	514.5	568.2	582.1	600.6	609.6	618.4	647.1
263	0.24	0.78/0.02	1.18/2.39	4.50/3.72	3.38/4.34	3.61/3.98	2.94/3.35	2.16/1.10
300	0.16	0.48/0.01	0.99/0.81	1.40/1.25	1.43/1.47	1.13/1.37	0.82/1.17	0.57/0.40
345	0.71	5.32/0.16	8.78/9.87	17.6/15.2	18.5/18.6	16.9/17.8	9.80/15.7	9.60/6.08
355	0.23	0.60/0.02	1.27/0.92	1.14/1.40	1.78/1.74	1.43/1.68	0.57/1.49	0.67/0.59
369	0.86	2.43/0.25	7.41/12.5	16.9/19.1	23.5/23.8	22.9/23.1	12.7/20.7	11.3/8.33
396	0.71	1.11/0.21	5.21/9.18	12.5/13.7	16.7/16.7	17.0/16.2	9.20/14.4	7.98/5.79
407	0.72	1.72/0.23	7.12/10.3	14.5/15.2	17.4/18.2	18.6/17.5	8.93/15.5	7.79/6.09
425	0.36	0.26/0.06	1.85/3.04	3.03/4.40	5.00/5.10	4.76/4.80	1.73/4.17	2.23/1.57

The observed Raman shifts, $\bar{\nu}$, are in units of cm^{-1} and Δ's are in dimensionless normal coordinates. The resonance Raman cross sections are shown as experimental/calculated in units of $Å^2$/molecule $\times 10^{11}$. The errors in cross sections are ±10% for strong lines and ±20% for weak lines. The cross sections were calculated using Equation 2.4 and using the following parameters: zero-zero energy, E_0 = 16,200 cm^{-1}, transition length, M = 0.24 Å, temperature, T = 0 K, refractive index, n = 1.33, Lorentzian homogeneous linewidth, Γ_L = 0 cm^{-1}, Gaussian homogeneous linewidth, Γ_G = 50 cm^{-1}, inhomogeneous linewidth, Θ = 700 cm^{-1}.

Figure 6.5: Absorption spectrum of M121E azurin.

A. Experimental (solid) and calculated (dashed/dotted) absorption spectra of M121E at pH 3.5. The dashed and dotted lines were calculated using Equation 2.5 and the parameters in Table 6.2, and correspond to the two models used for the data at this pH (see text).

B. Experimental (solid) and calculated (dashed) absorption spectra of M121E at pH 7.0. The dashed line was calculated using Equation 2.5 and the parameters in Table 6.3.

Note the difference in y-axis scales for the two absorption spectra.

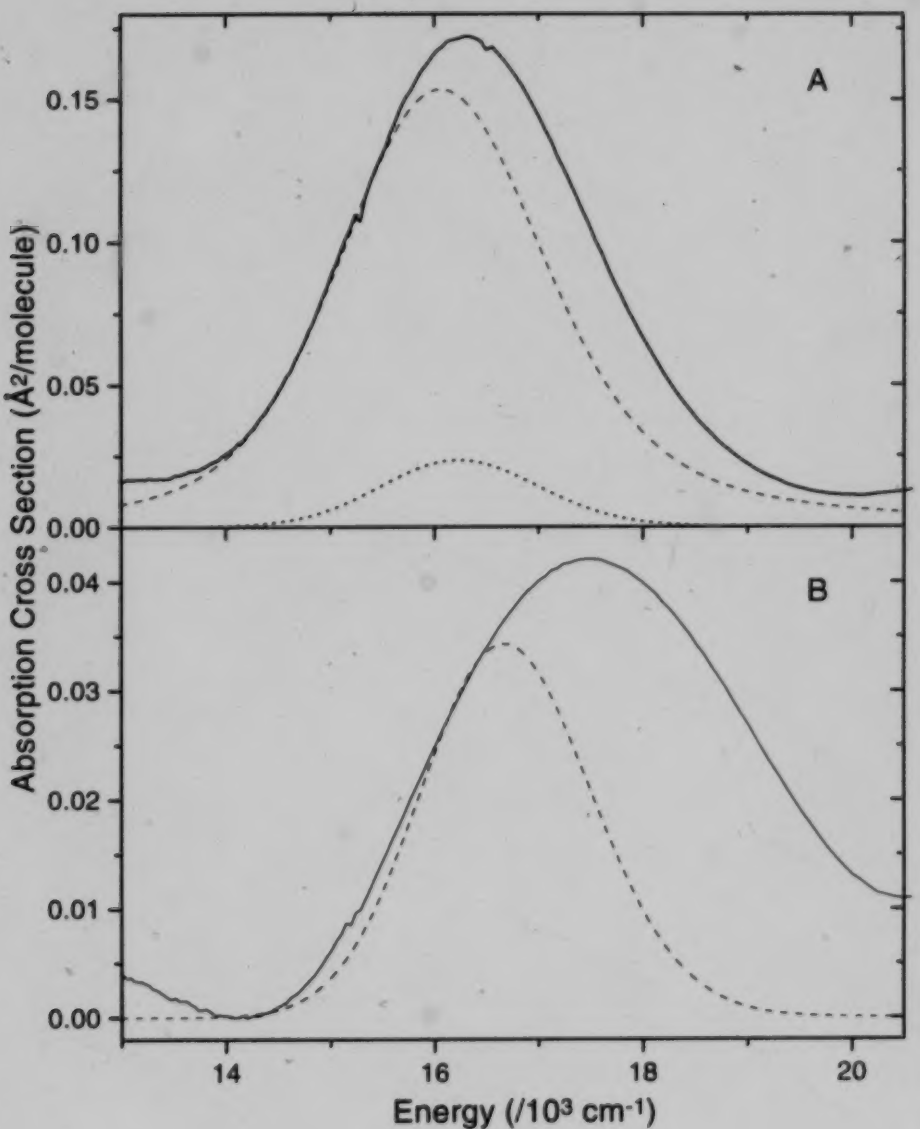
A
B
0.15
0.10
0.05
0.00
0.04
0.03
0.02
0.01
0.00
Absorption Cross Section (Å²/molecule)
14
16
18
20
Energy (/10³ cm⁻¹)

Figure 6.6: Resonance Raman excitation profiles of M121E, pH 3.5. The solid lines were calculated using Equation 2.4 with the parameters in Table 6.2. Due to the small amount of sample available and progressive bleaching of the sample, only one spectrum was obtained at each wavelength. The error in each point is expected to be similar to those at pH 7.0.

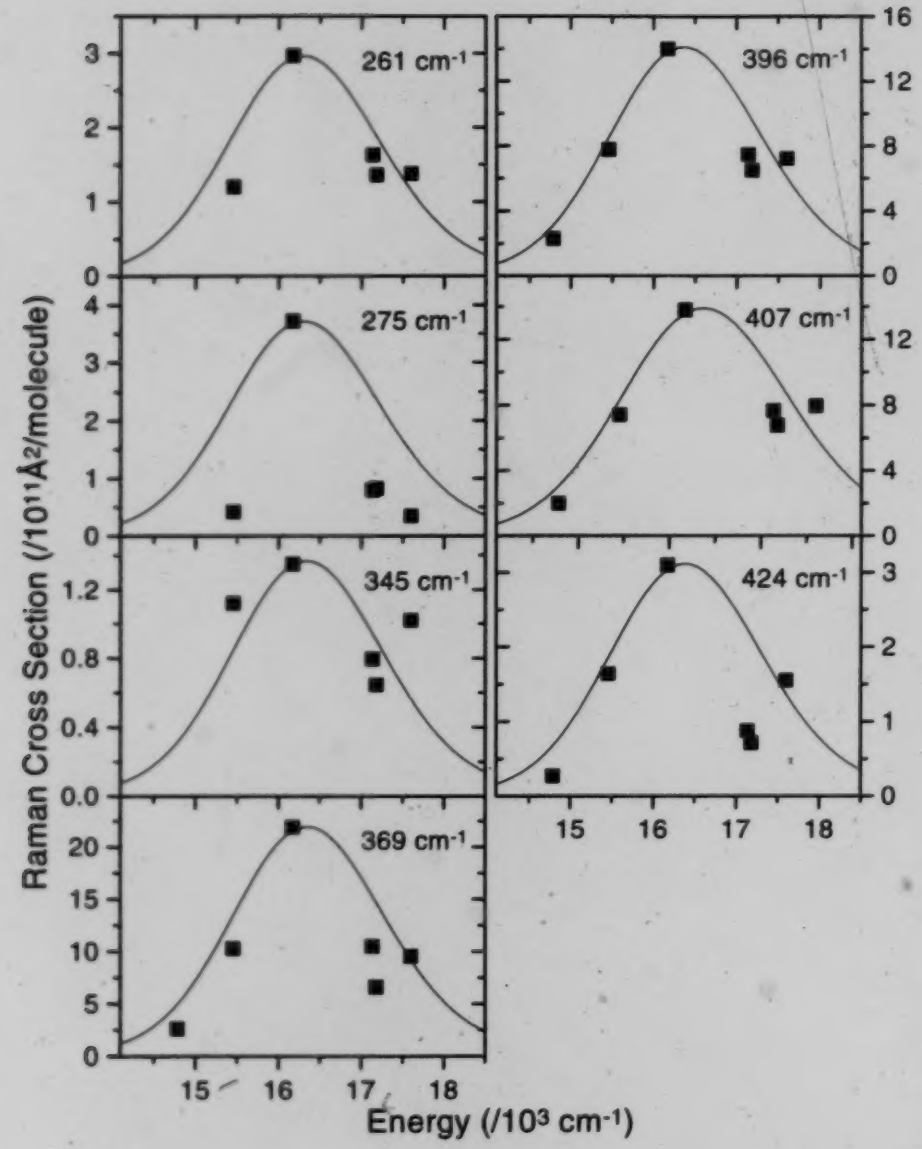
261 cm-1
396 cm-1
275 cm-1
407 cm-1
345 cm-1
424 cm-1
369 cm-1
Raman Cross Section (/10¹¹Å²/molecule)
Energy (/10³ cm-1)

Figure 6.7: Resonance Raman excitation profiles of M121E, pH 7.0. The solid lines were calculated using Equation 2.4 with the parameters in Table 6.3. Error bars represent the uncertainties in the experimental resonance Raman cross sections (■).

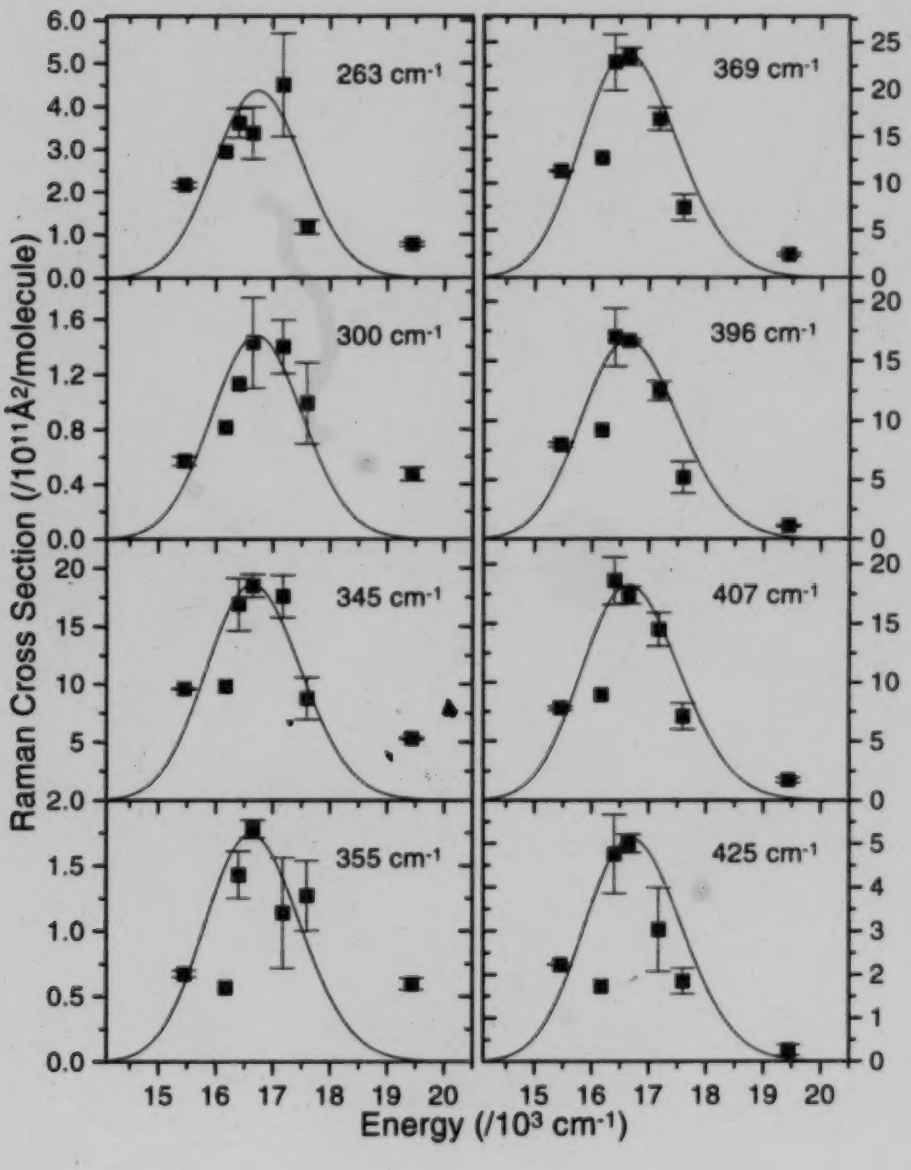
263 cm-1
369 cm-1
300 cm-1
396 cm-1
345 cm-1
407 cm-1
355 cm-1
425 cm-1
Raman Cross Section (/10^11 Å^2/molecule)
Energy (/10^3 cm-1)

electronic transitions, the resonance Raman excitation profiles were used as the primary constraint on the spectral band shape, position and bandwidth. The intensities of the resonance Raman excitation profiles were used to partition the broadening into homogeneous and inhomogeneous components.

The parameters for M121E azurin at pH 3.5 were found to be significantly different than those at pH 7.0. The large change in the parameters seems to be a result of empirically damped resonance Raman intensities and increased extinction in the absorption band. The large change in parameters such as broadening is not expected. We can use the parameters found for pH 7.0 as a guide and, if we assume that the broadening at pH 3.5 is the same as that at pH 7.0, we can recalculate the resonance Raman excitation profiles ("alternative" model). In order to fit the profiles, the transition length was decreased to 0.20 Å and E_0 increased to 16,000 cm^{-1}. The absorption spectrum of pH 7.0 was used as a guide for the intensity of the calculated absorption spectrum. The relative deltas were adjusted to fit the resonance Raman excitation profiles and scaled to maintain the same total reorganization energy. The parameters and a sample fit at 618.4 nm are given in Table 6.2. The resulting calculated absorption spectrum is much less intense and is shown as the dotted line in Figure 6.5. This would suggest that the electronic transition to which the vibrations are coupled is very small. These two set of parameters for M121E azurin at pH 3.5 represent lower and upper limits to the somewhat ambiguous fit of the absorption and resonance Raman excitation profiles. The lower value of the transition length is more consistent with the value found for pH 7.0 and is consistent with an altered electronic structure. The sum of the overtone and combination bands between 750 and 900 cm^{-1} at an excitation wavelength at 647.1 nm were measured as a check on the low values of Δ obtained for this azurin mutant and to test the resonance Raman excitation profile models used at pH 3.5. The calculated sum was 3.14×10^{-12} and 2.07×10^{-11} $Å^2$/molecule for the standard and alternative models, respectively. Comparison of these calculated values to the experimental value of 2.83×10^{-11} $Å^2$/molecule shows that the standard model predicts values much smaller than obtained experimentally. However, the alternative model predicts values close to those obtained

experimentally, within the experimental error. Thus, the alternative model appears to be more consistent with the overtone/combination bands.

To fully examine the effect of Glu121 on the copper site it would be ideal to look at the crystal structure at pH's where Glu121 is in different ionization states. Unfortunately, the available crystal structure is only at one somewhat ill-defined pH.[30] The mutant protein was crystallized at pH 6.0 in the presence of 25%PEG, which alters the pH of the resulting crystals. The crystals were blue-green in color indicating the presence of the protonated protein.[30] The pH is probably close to the pK_a of 5.0[30] of the Glu121 side chain. To examine the probable structure of the copper site as a function of pH, molecular modeling was performed to calculate two structures, one for protonation on each oxygen, for azurin at pH 3.5. The two structures were calculated separately and then averaged. It was found that the position of the Glu121 side chain was significantly different for the two structures, with the structure changing if the hydrogen is between the oxygen and the copper.

6.4 Discussion

6.4.1 Structure

The structure of the M121E mutant azurin has been examined by ESR,[7] EXAFS,[7] x-ray crystallography[30] and molecular modeling. The similarity of the absorption spectrum of M121E azurin at pH 3.5 to the wild type suggests a structural similarity whereas the large change in the absorption spectrum of M121E azurin at pH 7.0 suggests a large structural change. The change of Met121 to Glu may be expected to cause significant changes in the copper site geometry resulting in the observed spectral changes. A good knowledge of the structure of M121E azurin at both pH's is needed to build a structurally consistent model.

Figure 6.1 compares the x-ray crystal structure of M121E[30] azurin to the wild type. Figure 6.1 shows the copper has moved slightly toward the glutamic acid side chain in the mutant resulting in a Cu–O(Glu) bond of 2.21 Å.[30] The Glu side chain also appears to approach the copper. As a result, the copper sits 0.36 Å above the NNS plane compared to 0.1 Å for the wild type.[29] The short Cu–S and Cu–N bonds

are similar to those of the wild type.[29] The Cu–O(Gly) bond is increased to 3.4 Å by the movement of the copper and slight rotation of the peptide backbone.[30] Unfortunately, the exact pH is not known and there is only the structure at one pH. To look at how the structure varies with pH, molecular modeling will be described below.

Figure 6.8 shows the results of Discover calculations of protein structures of copper- and apoprotein at pH 3.5 and 7.0. The structures are consistent with a pH dependent extended X-ray absorption fine structure (EXAFS) study[7] and give the same qualitative trends. The EXAFS parameters show the bond lengths of Cu to the three strongly bond ligands (NNS) to be very similar at the two pH's.[7] The Cu–O(Glu) bond changes from 2.86 to 1.90 Å going from pH 3.5 to 7.0.[7] The Discover calculations give the same trend with the Cu–O bond changing from 2.68 to 2.06 Å. This is expected due to the stronger attraction of the negatively charged oxygen to the copper at higher pH. This been interpreted as the Cu moving towards the axial position.[6,7] An alternative interpretation is that the copper, being strongly bound within the NNS plane, does not move significantly but rather the oxygen moves toward the copper. In Figure 6.8 it appears that Glu121 moves the most upon pH change. The structures of the corresponding apoproteins are also shown in Figure 6.8 as lighter colored structures. At pH 3.5 there are smaller differences between the structures than at pH 7.0. This seems to imply a greater flexibility at pH 7.0 but it is not clear what the mechanism would be. The largest changes in structure with pH or removal of copper appear to be in the orientation of the histidine rings and in the position of the Glu121 side chain. This is consistent with the Glu121 side chain being more flexible than the other ligands as indicated by the higher average temperature factor of Glu121compared to the other ligands.[30] When the structures of four molecules are superimposed, the greater mobility of the Glu121 side chain is visible as a greater variability in the Glu121 position among the four molecules.[30] The Glu side chain is slightly longer than that of Met allowing the oxygen to get closer to the copper (Figure 6.1) resulting in the observed differences in the ESR and EXAFS data.

The ESR spectrum of M121E azurin at pH 4 is similar to that of stellacyanin whereas the ESR parameters at pH 8.0 are similar to the tetrahedral type 2 copper

Figure 6.8: Structure of the copper metal site of M121E azurin at pH 3.5 (dark blue), pH 7.0 (dark red) and the x-ray structure[30] (green). Structures of apoprotein are also plotted for pH 3.5 (light blue) and pH 7.0 (light red). Structures at pH 3.5 and 7.0 are calculated using Discover module of InsightII software as described in text.

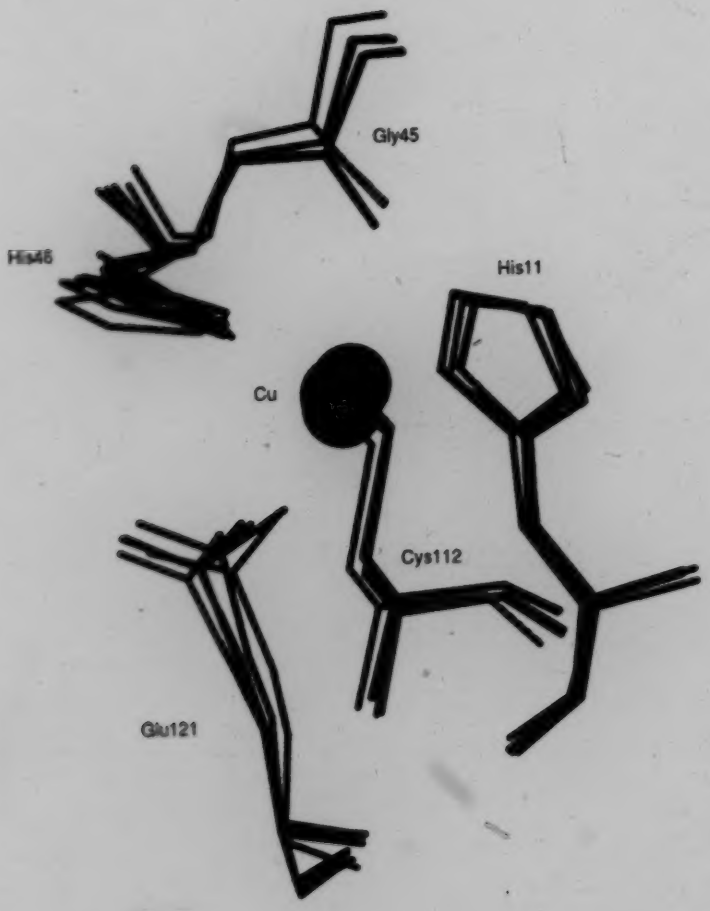
Gly45
His46
His11
Cu
Cys112
Glu121

center of nitrite reductase from *A. xylosoxidans*.[7] This would appear to indicate a large geometry shift with pH change to a more tetrahedral geometry. However, ESR results should be interpreted in the context of other data. Studies of cobalt and nickel-substituted azurin and cobalt-substituted horse liver alcohol dehydrogenase have shown that ESR can give seemingly contradictory results compared to x-ray crystal structures.[35,36] In azurin, the ESR spectrum can indicate an interaction with a fifth ligand whereas the crystal structure shows a large distance to the supposed fifth ligand.[35] Johnson and co-workers found that the magnitude of the zero-field splitting does not always provide a reliable method of distinguishing between tetra- and pentacoordinate metal atoms in low-symmetry environments.[36] They suggest that the cryogenic temperatures used for the ESR measurement may stabilize and/or promote the formation of the pentacoordinate species. The flexibility of the Glu121 side chain may facilitate the formation of the pentacoordinate species, resulting in a larger change in the rhombicity of the ESR spectrum.

The x-ray structure may also be affected by crystal packing forces. However, these forces would more likely pack the atoms closer, resulting in a shorter axial bond in better agreement with the ESR results. An alternative way to look at structure is to do NMR studies of the protein in solution at room temperature. This removes possible packing and cryogenic temperature effects. A NMR study of *P. aeruginosa* azurin[37] measured the secondary structure of azurin and compared it to the x-ray structure. They found that the structure was almost identical with that of the x-ray structure. The largest differences were in the loops, which are expected to be the floppiest part of the structure and the least structurally defined. This is consistent with minimal packing in the crystals. The strong hydrogen bonding involving the peptide backbone NHs of Cys112, Thr113, Phe114 and Asn47 increases the rigidity of this portion of the copper site. However, there appears to be a lack of strong hydrogen bonding involving the NHs of residues 117-120 as indicated by their faster exchange rates.[37] The aromatic rings of Phe15 and Phe114, which flank Met121 and His117, are flipping rapidly on the NMR time scale.[37] This suggests that the copper site might not be uniformly rigid and allows for the axial Met121 to be slightly more flexible than the other ligands.

6.4.2 Reorganization Energy

Table 6.1 lists the mode-specific reorganization energies for *Pseudomonas aeruginosa* azurin and M121E at the two pH's. The total inner sphere reorganization energy of PA azurin was found to be 0.26 eV[18] compared to 0.03 eV and 0.06 eV for M121E at pH 3.5 and 7.0, respectively. Unfortunately, the overtone/combination bands were too small to measure and could not be used as a check on the Δ's. The reorganization energy of M121E is much lower that of the wild type suggesting that the difference in ground- and excited-state geometry is small in the mutant compared to the wild type. The higher reorganization energy at pH 7.0 may be due to coordination to O of Glu121. Increasing the number of coordinating atoms increases the reorganization energy needed upon charge transfer. This is seen when comparing plastocyanin and azurin where the number of ligands increases from four to five.[18] However this only predicts an increase of 0.03/4 eV to 0.04 eV and leaves 0.02 eV unaccounted for. This additional energy may be due to strong coordination of oxygen to copper.

One explanation for the low reorganization energy of M121E azurin is that the copper center is more rigid, resulting in less structural rearrangement upon charge transfer. However, EXAFS[7], x-ray crystal structure[30], NMR[37], and Discover calculations done here suggest that the Glu121 side chain is more flexible than the other ligands (see above).

Another possible explanation is that there is little structural change upon charge transfer. This may be consistent with a perturbation in the electronic structure of the mutant due to the change of residue 121 from Met to Glu121. This mutation may result in the ~600 nm band having more ligand field type character. The transition would then be more localized on the copper metal ion and therefore the structural distortion in the excited state is reduced. The absorption spectrum at pH 7.0 may show this altered electronic mixing. The absorption spectrum at pH 3.5 is much more similar to the wild type. However, the absorption spectrum of M121E azurin is blue shifted from 625 to 612 nm and the extinction coefficient decreases from 4.8 to

4.5 $mM^{-1}cm^{-1}$ compared to the wild type (Table 1.1). Note that these differences are of similar size as the differences between species of wild type azurin. This suggests the electronic structure may be alike. Another possible reason for little structural change with charge transfer is that very little charge is transferred. For plastocyanin, Solomon found that only ~25% of an electron transferred[38] and this amount seems to be smaller in M121E azurin as indicated by the low intensity of the charge transfer absorption band at pH 7.0. However, the band is still due to the same type of electronic transition with the subsequent nuclear reorganization. The transition length was found to be 0.24 Å for M121E azurin at pH 7.0 compared to 0.63 Å for PA azurin. Although the transition length was found to be 0.63 Å for M121E azurin at pH 3.5, there is some doubt in this result. The broadening parameters and transition length of M121E azurin at pH 3.5 are much larger than at pH 7.0. This is due to an order of magnitude decrease of the resonance Raman cross sections compared to wild type along with a large apparent increase in the absorption band. It was assumed that the band at 612 nm in M121E azurin at pH 3.5 was due mainly to the S→Cu charge transfer and the parameters were fit accordingly. However, it is known that the absorption band contains several charge transfer and ligand field transitions[39] and it is not possible to distinguish the exact contribution of the charge transfer transition. The altered electronic mixing could result in the 612 nm band having much less charge transfer character than in the wild type. The total intensity of the 600 nm and 416 nm bands is the same at both pH's. This may indicate that the same transitions are present with one transition being very sensitive to the ionization state of Glu121. The introduction of a charge could greatly blue shift the ligand field transition contribution of the 612 nm band leaving behind a much smaller charge transfer band. It is also consistent with a redistribution of intensity due to changes in the mixing of the orbitals which give rise to the electronic transitions. The expected weak ligand field transitions involve the $3d_{z^2}$, $3d_{xz}$, $3d_{yz}$ and $3d_{x^2-y^2}$ copper orbitals.[39,40] Glu121 is located close to the defined z-axis and will have the most influence on orbitals with large components along the z-axis. The introduction of a charge could stabilize an orbital and lower its energy and cause a red-shifting of the absorption band. For a plastocyanin model, it was found that the second most intense absorption involved

$3d_{xz}$, which gains intensity by mixing with S(Cys) 3pπ.[40] Changing the geometry of the copper site can alter the mixing of copper and sulfur orbitals and alter the resulting intensities of the transitions. Although it is not clear how the electronic structure of the copper site is changing, it is apparent that changing Met121 to Glu has had a significant influence on the electronic structure reflected in the absorption spectrum.

6.5 Conclusion

The results presented here suggest that the replacement of Met121 with Glu results in a large perturbation in the electronic structure. The absorption and resonance Raman spectra seem to point to a two state model with two ionization states of Glu121. At low pH, Glu121 is protonated resulting in a blue-copper like coordination, yet still perturbed from wild-type M121E azurin. At higher pH, Glu121 is deprotonated introducing a negative charge close to the copper metal center. This charge may introduce a strong electronic perturbation which results in blue-shifting and redistribution of intensity of absorption bands. This model could be tested using mutants, which introduce charge at various distances from the copper site and do not alter the copper site geometry, to examine the electronic perturbation separately from the structural perturbation. These results illustrate that the axial ligands may play a significant role in tuning the electronic structure of blue copper proteins.

6.6 References

[1] Malkin, R.; Malmström, B. G. *Adv. Enzmol.* **1970**, *33*, 177.

[2] Adman, E. T. In *Metalloproteins – Part I: Metal Proteins with Redox Roles*; Harrison, P. M., Ed.; Verlag Chemie: Florida, **1985**, p 413

[3] Broman, L.; Malmström, B. G.; Aasa, R.; Vanngard, T. *J. Mol. Biol.* **1962**, *5*, 301.

[4] Vallee, B. L.; Williams, R. J. P. *Proc. Natl. Acad. Sci. USA* **1968**, *59*, 498.

[5] Di Bilio, A. J.; Chang, T. K.; Malmström, B. G.; Gray, H. B.; Karlsson, B. G.; Nordling, M.; Pascher, T.; Lundberg, L. G. *Inorg. Chim. Acta* **1992**, *198-200*, 145

[6] Andrew. C. R.; Yeom, H.; Valentine, J. S.; Karlsson, B. G.; Bonander, N., van Pouderoyen, G.; Canters, G. W.; Loehr, T. M.; Sanders-Loehr, J. *J. Am. Chem. Soc.* **1994**, *116*, 11489.

[7] Strange, R. W.; Murphy, L. M.; Karlsson, B. G.; Reinhammer, B.; Hasnain, S. S. *Biochemistry* **1996**, *35*, 16391.

[8] Bergman, C.; Gandvik, E.-K.; Nyman, P.O.; Strid, L. *Biochem. Biophys. Res. Commun.* **1977**, *77*, 1052.

[9] Gray, H. B.; Malmström, B. G. *Comments Inorg. Chem.* **1983**, *2*, 203.

[10] Myers, A. B.; Mathies, R. A. *In Biological Applications of Raman Spectroscopy*; Spiro, T. G., Ed.; Wiley: New York, **1988**; Vol 2, p 1.

[11] Piccioli, M.; Luchinat, C.; Mizoguchi, T. J.; Ramirez, B. E.; Gray, H. B.; Richards, J. H. *Inorg. Chem.* **1995**, *34*, 737.

[12] Faham, S.; Day, M. W.; Connick, W. B.; Crane, B. R.; Di Bilio, A. J.; Schaefer, W. P.; Rees, D. R.; Gray, H. B. *Acta Cryst.* **1999**, *D55*, 379.

[13] Details of how resonance Raman spectra were taken are given in Chapter 2.

[14] Fraga, E.; Webb, M. A.; Loppnow, G. R. *J. Phys. Chem.* **1996**, *100*, 3278.

[15] Lee, S-Y.; Heller, E. J. *J. Chem. Phys.* **1979**, *71*, 4777.

[16] Loppnow, G. R.; Fraga, E. *J. Am. Chem. Soc.* **1997**, *119*, 896.

[17] Loppnow, G.R.; Mathies, R. A. *Biophys. J.* **1988**, *54*, 35.

[18] Webb, M. A.; Kwong, C. M.; Loppnow, G. R. *J. Phys. Chem. B* **1997**, *101*, 5056. This is Chapter 2 in this thesis.

[19] Ermer, O. *Structure and Bonding* **1976**, *27*, 161.

[20] Hagler, A. T. In *Conformation in Biology & Drug Design, The Peptides*; Meienhofer, J., Ed.; Academic Press: New York; **1985**, *Vol 7*, p 213.

[21] Weiner, S. J.; Kollman, P. A.; Case, D. A.; Singh, U. C.; Ghio, C.; Alagona, G.; Profeta, S. Jr.; Weiner, P. *J. Am. Chem. Soc.* **1984**, *106*, 765

[22] Weiner, S. J.; Kollman, P. A.; Nguyen, D. T.; Case, D. A. *J. Comp. Chem.* **1986**, *7*, 230.

[23] Homas, S. W. *Biochemistry* **1990**, *29*, 9110.

[24] *Insight II User Guide*, **1995**. Biosym/MSI, San Diego.

[25] Aqvist, J.; Leijonmark, M.; Tapia, O. *Eur. Biophys.* **1989**, *16*, 327.

[26] Levitt, M. *Annu. Rev. Biophys. Bioeng.* **1982**, *11*, 251.

[27] Makinen, M. W.; Troyer, J. M.; Van der Werff, H.; Berensden, H. J.; Van Gunsteren, W. F. *J. Mol. Biol.* **1989**, *207*, 210.

[28] Bernstein, F. C.; Koetzle, T.F.; Williams, G. J. B.; Meyer, E. F. Jr.; Brice, M. D.; Rodgers, J. R.; Kennard, O.; Shimanouchi, T.; Tasumi, M. *J. Mol. Biol.* **1977**, *112*, 535.

[29] Nar, H.; Messerschmidt, A.; Huber, R.; van de Kamp, M.; Canters, G. W. *J. Mol. Biol.* **1991**, *221*, 765.

[30] Karlsson, B. G.; Tsai, L.-C.; Nar, H.; Sanders-Loehr, J.; Bonander, N.; Langer, V.; Sjölin, L. *Biochemistry* **1997**, *36*, 4089.

[31] Blair, D. F.; Campbell, G. W.; Schoonover, J. R.; Chan, S. I.; Gray, H. B.; Malmstrom, B. G.; Pecht, I.; Swanson, B. I.; Woodruff, W. H.; Cho, W. K.; English, A. M.; Fry, H. A.; Lum, V.; Norton, K. A. *J. Am. Chem. Soc.* **1985**, *107*, 5755.

[32] Webb, M. A.; Loppnow, G. R. *J. Phys. Chem. B* **1998**, *102*, 8923. This is Chapter 3 in this thesis.

[33] Webb, M. A.; Loppnow, G. R. *J. Phys. Chem. A* **1999**, *103*, 6283. This is Chapter 4 in this thesis.

[34] Fraga, E.; Loppnow, G.R. *J. Phys. Chem. B* **1998**, *102*, 7659.

[35] Jiménez, H. R.; Salgado, J.; Moratel, J. M.; Morgenstern-Badarau, I. *Inorg. Chem.* **1996**, *35*, 2737.

[36] Werth, M. T., Tang, S.-F.; Formicka, G.; Zeppezauer, M.,; Johnson, M. K. *Inorg. Chem.* **1995**, *34*, 218.

[37] Van de Kamp, M.; Canters, G. W.; Wijmenga, S. S.; Lommen, A.; Hilbers, C. W.; Nar, H.; Messerschmidt, A.; Huber, R. *Biochemistry* **1992**, *31*, 10194.

[38] Solomon, E. I.; Lowery *Science* **1993**, *259*, 1575.

[39] Gewirth, A. A.; Solomon, E. I. *J. Am. Chem. Soc.* **1988**, *110*, 3811.

[40] Pierloot, K.; De Kerpel, J. O.; Ryde, U.; Roos. B. O. *J. Am. Chem. Soc.* **1997**, *119*, 218.

Chapter 7: Conclusions and Future Work

7.1 Conclusions and Future Work

The primary goal of this work was to examine the coupling of the copper metal active site of azurin to the protein environment and to quantify the important factors which influence the charge transfer excited-state dynamics. The method used was resonance Raman spectroscopy which provided a structurally sensitive probe of the chromophore. An homologous series of azurins was examined to build up a structurally-based model of the coupling of the copper metal active site and the protein environment.

Comparison of the resonance Raman spectra of four azurins obtained using excitation wavelengths throughout the S→Cu charge transfer absorption band at ~620 nm, demonstrated that the total inner-sphere reorganization energy is the same for all four azurins. However, the mode-specific reorganization energy, as reflected in the relative intensities of the individual vibrational modes, is sensitive to the protein environment in a complex manner. The spectral difference parameter, χ^2, was found to be a good measure for comparing spectra, particularly if the intensities were quantitated, and was found to correlate better with the protein composition than any parameter of protein or active site structure. This result was somewhat surprising and counterintuitive. Discussed below are some alternative models and experiments designed to test all these models.

The work with the azurin mutant Met121Glu suggested that the axial ligands may fine tune the electronic structure of the copper center. This can be investigated further using mutants of Met121 and Gly45. X-ray crystal structures are available for several Met121 mutants at the Research Collaboratory for Structural Bioinformatics Protein Data Bank.[1] Figure 7.1 shows the location of Met121 in the protein. Replacing Met with Gln creates a strong axial ligand[2] similar to that of Glu at pH 7.0. The advantage of this mutant is that there is no charge added which will help separate electrostatic effects from change in coordination geometry and strength of ligand binding. A second useful mutation is Met121Ala. In this case, the axial ligand is removed making the site more similar to stellacyanin which lacks methionine. The crystal structure of Met121Ala and the azide derivative are known.[3] The EPR

Figure 7.1: Selected azurin amino acids. Shown are selected amino acids which are mentioned in the text as possible locations of site-directed mutagenesis. The amino acids shown are Trp48, Val31 and Thr30, involved in intramolecular electron transfer to Cys3 (blue), Met 121 (orange) ligated to copper, Phe110 and His35 (purple) for which x-ray crystal structures are available for Phe110Ser and His35Gln mutant azurin, Thr113, Ser118, Gln12 and Leu86 (green) which are ≤ 10 Å from the copper and Val43, Phe114, Pro115, Ala119 and Gly123 (yellow) which are close to the copper along the peptide strands.

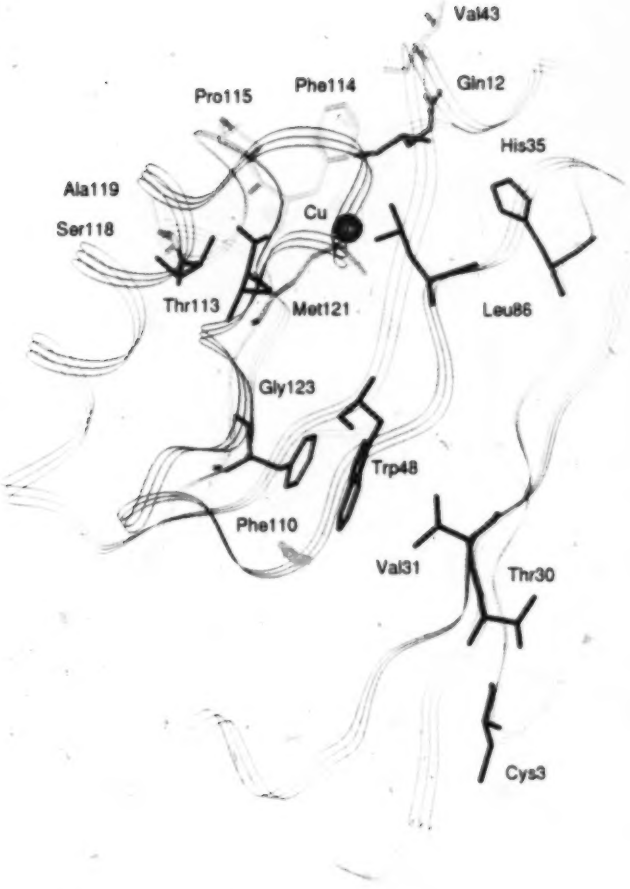
Val43
Gln12
Phe114
Pro115
His35
Ala119
Ser118
Cu
Thr113
Met121
Leu86
Gly123
Trp48
Phe110
Val31
Thr30
Cys3

spectrum shows that there is no water at the copper site of Met121Ala and the structure is very similar to wild type.[3] The absorption spectrum retains the appearance of a typical blue copper protein with a strong absorption band at ~620 nm.[3] The reduction potential has increased compared to the wild type (373 mV vs. 310 mV) which also confirms the lack of a water molecule in the cavity which lowers the reduction potential.[3] The addition of azide results in a decrease of the reduction potential to 330 mV.[3] The absorption band at 620 nm decreases and a band at 409 nm increases indicating a geometry change when the azide binds to copper.[3] This mutant gives a test of a weak axial ligand with Met121Ala alone and a strong axial ligand with the azide derivative. Replacing Met121 with Gln, Ala and Ala-azide allows for further testing of the role of the methionine in tuning the properties of the copper metal ion. A complete study of the role of Met121 might involve exchanging Met for all other 19 amino acids and measuring the absorption spectrum, resonance Raman spectrum and reduction potential. This would test the effect of hydrophobicity, charge, size and strong and weak ligands on the properties of the copper center.

The above mutants will also change the geometry of the copper site which can make interpretation of the data difficult. It may be useful to also examine mutations further from the copper center. For example, specific mutations can be made to introduce a charge or dipole at a fixed distance from the copper metal without perturbing the copper site geometry. Two possibilities, where crystal structures are available,[1] are Phe110Ser and His35Gln which introduce dipoles near the copper site (Figure 7.1). In the first case, Ser is only two amino acids from Cys112 and is at a similar distance as the Trp48Leu change upon going from *A. denitrificans* and *A. xylosoxidans* II azurin, as discussed in Chapters 4 and 5. In order to make an accurate comparison, it would be best to look at a Trp48Ser mutant as well. This will test the apparent anisotropic coupling seen by making a similar change at a similar distance but along a different peptide strand. It is hypothesized that changes made to amino acids that are not on an efficient electron transfer path will have a lesser effect on the resonance Raman spectrum and the effect should fall off quickly with distance. Replacing His35 with Gln gives a different change in that His35 is physically close to the copper through-space but is far from the copper as measured through the peptide

backbone. This gives a test of through-space interactions. His35 could also be replaced by a charged amino acid such as Lys or Glu to add a positive or negative charge, respectively, to test electrostatic interactions. In Table 4.2 amino acid changes between four species of azurin are listed. One possible strategy would be to make single mutations from the list such as Thr113Ser, Ser118Phe, Gln12Gly and Leu86Val. These are the amino acid changes within 10 Å of the copper for *P. aeruginosa* and *A. xylosoxidans* (Table 4.2, Figure 7.1) azurin. This would test the contribution of each amino acid change independently and differentiate between through-bond and through-space interactions. However, the crystal structures are not known for any of these variations.

The above proposed work will require structures to measure the distance of mutation from the copper and to check if the geometry of the copper site or protein has been altered due to the mutation. This is likely the most difficult aspect. Structures are typically obtained from x-ray crystallography and structures of a number of mutants are readily available.[1] However, a mutant may not crystallize as well as the wild type. Protein crystallization is controlled by solubility, protein stability and solution conditions such as concentration, temperature, pH and the presence of buffers, metals, solvents or other molecules.[4-7] Mutations can have numerous consequences,[4,8] including conformational changes, decreases in stability, loss of activity, incomplete folding, changes in solubility or unforeseen degradation.[9] Fortunately, mutant proteins will often crystallize under the same conditions used for the wild type protein.[4] One study found that over 80% of single site variants could be crystallized under conditions closely similar to those used for the native protein.[10] X-ray structures would be the best for the sort of analysis done here. However, crystal structures are not always done and may not be available for all desired mutants.

An alternative to using x-ray structures is NMR which has been used to measure the secondary structure of the reduced form of azurin.[11] The use of 2D and 3D NMR spectroscopy has enabled the determination of protein structures in solution.[7,12] The interproton distances are determined using nuclear Overhauser effect spectroscopy (NOESY) and/or correlated spectroscopy (COSY). One of the most difficult tasks is to separate and assign all the NOESY cross peaks. This has

become easier as computer programs allow the efficient assignment of the hundreds or even thousands of NMR peaks[13] and the use of 3D and 4D heteronuclear experiments can be used to resolve ambiguities.[14] The NMR experiment is very different from an x-ray experiment and the results are presented in a different manner. The analysis of x-ray diffraction data results in a crystallographic refinement that minimizes the R-factor, which is the deviation from ideal covalent geometry.[14] The analysis of NMR data results in distance restraints to which a group of structures which satisfy those constraints are built.[7,13,14] The final product of the x-ray analysis is a most probable structure that represents the electron density plot whereas the outcome of the NMR analysis is an ensemble of conformations lying within the spectroscopic bounds.[14] The NMR structures determined are of similar quality as that of moderately good X-ray crystal structures.[14] Differences arise at the surface of the protein and in peptide loops which are subject to crystal packing forces and may be more mobile in solution.[7,13,14] In the interior of the protein the resolution of the NMR structure approaches that of the best x-ray data.[14] The main advantage with using NMR is that it is not necessary to crystallize the protein. Also, since NMR has been done on azurin[11] the assignments can be used as a guide. One complication with azurin is the presence of Cu^{++} which is paramagnetic and causes broadening of the NMR signals by decreasing the longitudinal relaxation time (T_1) of protons.[12] This can be avoided by using the reduced protein since the structures of the reduced and oxidized protein have been found to be very similar.[15] However, there may be differences in the copper coordination which will be important in the case of mutants of the copper ligands, such as the Met121 mutations suggested above. Therefore NMR may be more suitable for mutations which are further from the copper and in cases where the exact geometry of the copper is not required.

A third possibility is to do a geometry minimization using programs such as InsightII[16] and MOE[17] utilizing a forcefield approach starting from the wild type crystal structure. These programs use an empirical fit to the potential energy surface in order to simplify the problem. Energy minimization is performed to find the geometry which minimizes the potential energy. This process is an iterative adjustment of the confirmation until the net force on each atom is close to zero.[18]

This does not give exact structures but would give reasonable distances from the copper to a mutation assuming that the protein structure is not disrupted by the mutation. However, it will not give accurate results of the copper geometry as the forcefield parameters for metals such as copper are limited. A higher level of theory may be needed to calculate accurate Cu–ligand bond lengths and angles. An *ab inito* calculation is not practical due to the number of atoms in the protein and even a small section of the protein would required tremendous computing resources. It may be feasible to use a semi-empirical method such MNDO, AM1 or PM3. These methods approximate many of the needed integrals using empirical functions. These methods are often quite successful in obtaining geometries for molecules which are close to crystal structures. However, most semiempirical methods lack functions for transition metals such as copper. The use of energy minimized structures may be somewhat limited depending on the needed accuracy.

A number of studies have looked at electron transfer rate dependence on protein structure and composition.[19-21] These studies measured intramolecular electron transfer along different pathways through the protein and found that the copper is more strongly coupled to Cys112 than to the other ligands.[19-21] The resonance Raman spectra also appears to show some directional sensitivity to amino acid changes. This result is consistent with the anisotropic coupling seen in the electron transfer studies.[19,21] Testing this apparent anisotropic response of the resonance Raman spectrum was mentioned above. The use of mutants close to the copper along each peptide strand would test if the resonance Raman spectrum is more sensitive in a particular direction. For example, amino acids Val43, Trp48, Phe110, Phe114, Pro115, Ala119 and Gly123 are all two amino acids from a copper ligand (Figure 7.1). Single mutations at all these positions can be tested. However, only Phe110Ser and Phe114Ala have crystal structures available and so are the best choices to examine.

Concurrent measurement of electron transfer rates and resonance Raman spectra for particular mutants of azurin is needed to clarify the relationship between amino acid composition, electron transfer kinetics, and the resonance Raman spectra. These experiments would involve using specific azurin mutants of individual amino

acids along a specific electron transfer route. One obvious choice is to use Trp48Leu of *P. aeruginosa* azurin. The electron transfer rate has been measured[19] and it provides the same amino acid change as *A. xylosoxidans* II to compare. A second change is the Val31Trp mutant which has a much higher electron transfer rate than the wild type (Figure 7.1).[19] It may also be desirable to change Thr30 as this is the last amino acid in the electron transfer route before Cys3 (Figure 7.1).[19] Changing the location of the mutation can be used to examine the distance from the copper over which the coupling can be observed. Trp48 has a through-bond distance of ~17 Å from the copper atom to the side chain, following the calculated electron transfer path[19] and it would be interesting to see if coupling can be seen from Val31 or Thr30 which are about 22 and 30 Å from the copper along the electron transfer path.[19]

Using different mutants makes it possible to study the effect of protein structure and composition and to further examine the apparent anisotropic coupling of the copper and the protein environment. The choice of mutant will be determined by the desired property that is to be tested and will also be greatly influenced by the availability of the mutant and knowledge of the structure.

7.2 References

[1] Berman, H. M.; Westbrook, J.; Feng, Z.; Gilliland, G.; Bhat, T. N.; Weissig, H.; Shindyalov, I. N.; Bourne, P. E. *Nucleic Acids Research* **2000**, *28*, 235. WWW address: http://www.rcsb.org/pdb/.

[2] Coremans, J. W. A.; Poluektov, O. G.; Groenen, E. J. J.; Warmerdam, G. C. M.; Canters, G. W.; Nar, H.; Messerschmidt, A. *J. Phys. Chem.* **1996**, *100*, 19706.

[3] Tsai, L.-C.; Bonander, N.; Harata, K.; Karlsson, G.; Vänngard, T.; Langer, V.; Sjölin, L. *Acta. Cryst.* **1996**, *D52*, 950.

[4] Ducruix, A.; Giegé, R. (Ed.) In *Crystallization of Nucleic Acids and Proteins; A Practical Approach*; Oxford Unifersity Press: New York, **1992**.

[5] Arakawa, T.; Timasheff, S. N. *Methods Enzymol.* **1985**, *114*, 49.

[6] McPherson, A. *Methods Enzymol.* **1985**, *114*, 112.

[7] Voet, D.; Voet, J. G. In *Biochemistry*, 2nd Ed.; John Wiley & Sons; Inc., New York, **1995**.

[8] Oxender, D. L.; Fox, C. F. (Ed.) In *Protein Engineering*; Alan R. Liss, New York, **1987**.

[9] Marston, F. A. O. *Biochem. J.* **1986**, *240*, 1.

[10] Wozniak, J. A.; Faber, H. R.; Dao-pin, S.; Zhang, X-J.; Matthews, B. W. *Methods, A Companion to Methods Enzymol.* **1990**, *1*, 100.

[11] Van de Kamp, M.; Canters, G. W.; Wijmenga, S. S.; Lommen, A.; Hilbers, C. W.; Nar, H.; Messerschmidt, A.; Huber, R. *Biochemistry* **1992**, *31*, 10194.

[12] Günther, H. In *NMR Spectroscopy; Basic Principles, Concepts and Applications in Chemistry*, 2nd Ed.; John Wiley and Sons., Chichester, England, **1995**.

[13] Wüthrich, K. *Science* **1989**, *243*, 45.

[14] Wagner, G.; Hyberts, S. G.; Havel, T. F. *Annu. Rev. Biophys. Biomol. Struct.* **1992**, *21*, 167.

[15] Shepard, W. E. B.; Anderson, B. F.; Lewandoski, D. A.; Norris, G. E.; Baker, E. N. *J. Am. Chem. Soc.* **1990**, *112*, 7817.

[16] Molecular Simulations Inc., Palo Alto, CA. WWW address: www.msi.com.

[17] Chemical Computing Group Inc., Montreal, Quebec. WWW address: www.chemcomp.com.

[18] *Insight II User Guide*, **1995**. Biosym/MSI, San Diego.

[19] Farver, O.; Skov, L. K.; Young, S.; Bonander, N.; Karlsson, G. B.; Vänngård, T.; Pecht, I. *J. Am. Chem. Soc.* **1997**, *119*, 5453.

[20] Gray, H. B.; Winkler, J. R. *Annu. Rev. Biochem.* **1996**, *65*, 537.

[21] Langen, R.; Chang, I-J.; Germanas, J. P.; Richards, J. H.; Winkler, J. R.; Gray, H. B. *Science* **1995**, *268*, 1733.